DESIGN MODIFICATION FOR THE MODULAR HELIUM REACTOR FOR HIGHER TEMPERATURE OPERATION AND RELIABILITY STUDIES FOR NUCLEAR HYDROGEN PRODUCTION PROCESSES

A Dissertation

by

S.M. MOHSIN REZA

Submitted to the Office of Graduate Studies of
Texas A&M University
in partial fulfillment of the requirements for the degree of

DOCTOR OF PHILOSOPHY

May 2007

Major Subject: Nuclear Engineering

DESIGN MODIFICATION FOR THE MODULAR HELIUM REACTOR FOR HIGHER TEMPERATURE OPERATION AND RELIABILITY STUDIES FOR NUCLEAR HYDROGEN PRODUCTION PROCESSES

A Dissertation

by

S.M. MOHSIN REZA

Submitted to the Office of Graduate Studies of
Texas A&M University
in partial fulfillment of the requirements for the degree of

DOCTOR OF PHILOSOPHY

Approved by:

Chair of Committee,	Kenneth L. Peddicord
Committee Members,	Marvin L. Adams
	William H. Marlow
	Karl T. Hartwig
	Edwin A. Harvego
Head of Department,	William E. Burchill

May 2007

Major Subject: Nuclear Engineering

ABSTRACT

Design Modification for the Modular Helium Reactor for Higher Temperature Operation and Reliability Studies for Nuclear Hydrogen Production Processes. (May 2007)

S.M. Mohsin Reza; B.S., Dhaka University of Engineering and Technology (DUET), Bangladesh;

M.S., Texas A&M University

Chair of Advisory Committee: Dr. Kenneth Lee Peddicord

Design options have been evaluated for the Modular Helium Reactor (MHR) for higher temperature operation. An alternative configuration for the MHR coolant inlet flow path is developed to reduce the peak vessel temperature (PVT). The coolant inlet path is shifted from the annular path between reactor core barrel and vessel wall through the permanent side reflector (PSR). The number and dimensions of coolant holes are varied to optimize the pressure drop, the inlet velocity, and the percentage of graphite removed from the PSR to create this inlet path. With the removal of ~10% of the graphite from PSR the PVT is reduced from 541 ^{0}C to 421 ^{0}C.

A new design for the graphite block core has been evaluated and optimized to reduce the inlet coolant temperature with the aim of further reduction of PVT. The dimensions and number of fuel rods and coolant holes, and the triangular pitch have been changed and optimized. Different packing fractions for the new core design have been used to conserve the number of fuel particles. Thermal properties for the fuel elements are calculated and incorporated into these analyses. The inlet temperature, mass flow and bypass flow are optimized to limit the peak fuel temperature (PFT) within an acceptable range.

Using both of these modifications together, the PVT is reduced to ~350 ^{0}C while keeping the outlet temperature at 950 ^{0}C and maintaining the PFT within acceptable limits. The vessel and fuel temperatures during low pressure conduction cooldown and

high pressure conduction cooldown transients are found to be well below the design limits.

The reliability and availability studies for coupled nuclear hydrogen production processes based on the sulfur iodine thermochemical process and high temperature electrolysis process have been accomplished. The fault tree models for both these processes are developed. Using information obtained on system configuration, component failure probability, component repair time and system operating modes and conditions, the system reliability and availability are assessed. Required redundancies are made to improve system reliability and to optimize the plant design for economic performance. The failure rates and outage factors of both processes are found to be well below the maximum acceptable range.

DEDICATION

My mother, for all her unconditional love, for her will to pursue all my dreams
The memory of my father
Tori, my wife for her love, sacrifices, understanding and supporting me in every situation
Nuha, my daughter for being the light and inspiration in my life

ACKNOWLEDGEMENTS

I express my appreciation to the almighty for the vigor, the enthusiasm and the knowledge with which I have been blessed. I convey my profound gratitude to my advisor, Kenneth Lee Peddicord, for his timely guidance, advice and encouragement through out my PhD program and my dissertation. I am very thankful to him for his continuous support, and appreciation of my work. I thank him for giving me the opportunity to work on this exciting project and for making the arrangements for me to work with the Idaho National Laboratory and General Atomics for my research. It was a great learning experience for me to work on this project with Dr. Peddicord and under the arrangements he made for me.

I would like to thank Marvin L. Adams, William H. Marlow, Karl T. Hartwig and Edwin A. Harvego for serving on my advisory committee, for their time and valuable advice during my dissertation. Special thanks to Ed Harvego for many insightful discussions and constructive advice during my research and dissertation writing.

I appreciate the cooperation from the Thermal Fluids and Heat Transfer Department, and Risk, Reliability and NRC Programs Department of Idaho National Laboratory for their support, especially Cliff Davis, for many helpful discussions and for answering my query on RELAP5-3D/ATHENA analysis and Mike Calley for introducing me to SAPHIRE code. I also would like to thank Matt Richard and Arkal Shenoy of General Atomics for their support, cooperation and time during my research work.

I thank the Nuclear Engineering Department at Texas A&M University for its commitment to excellence and for my financial assistance. Thanks to all faculty members and students for creating such a fabulous academic environment. Thanks to all others who helped me in different ways to enhance my education at Texas A&M University.

TABLE OF CONTENTS

Page

ABSTRACT…… iii

DEDICATION…… v

ACKNOWLEDGEMENTS…… vi

TABLE OF CONTENTS…… vii

LIST OF FIGURES…… x

LIST OF TABLES …… xii

NOMENCLATURE…… xiii

CHAPTER

I INTRODUCTION……... 1

A. Nuclear Hydrogen…..……... 2
1. Need for Nuclear Hydrogen……. 2
2. Nuclear Hydrogen Process…….……. 3
B. Modular Helium Reactor ……. 5
C. SI-Based H2-MHR…… 10
1. Main Coupled Chemical Reaction ……..……. 10
2. Bunsen Reaction Process…….. 11
3. Sulfuric Acid Concentration and Decomposition Section… 13
4. Hydrogen Iodide Decomposition Section…… 13
D. HTE-Based H2-MHR…… 16

II CURRENT STATUS AND PROPOSED RESEARCH……. 18

A. Current Status of the Problem……... 18
1. Design Modification for the MHR for Higher Temperature Operation …… 18
2. Reliability and Availability Studies…….……. 19
B. Proposed Research…….. ……. 20
1. Design Modification for the MHR for Higher Temperature Operation …… 20
2. Reliability and Availability Studies…….. 21

III RELAP5-3D/ATHENA PLANT MODEL…….…… 22

A. RELAP5-3D/ATHENA Code……... 22
B. Description of Plant Model…… 23
C. Validation of the Plant Model……... 27

CHAPTER Page

IV OPTIMIZATION OF NEW COOLANT CONFIGURATION FOR MHR…… 29
A. Effect of Increased Coolant Temperature…… 29
B. Design and Verification for New Coolant Path…… 32
C. Optimization of Amount of Graphite Removal and Coolant Velocity ……. 35
D. Radiation and Conduction Heat Transfer Calculation…….. 42
E. Optimized New Coolant Scheme and Steady State Calculation 46

V OPTIMIZATION OF NEW CORE DESIGN……..... 48

A. Block Design of MHR……..……..... 48
B. POKE and ATHENA Calculations for GT-MHR……. 49
C. Bypass Flow Optimization…… 55
D. New Core Design; Calculation and Optimization…… 56
1. Design Optimization……. 56
2. Thermal Properties for Fuel Rod…….……. 58
3. Radial Power Distribution…… 60
4. Inlet Temperature Optimization…… 60
E. Steady State Calculation for New Block Design…..……. 62
F. Back Calculation for a Vessel Temperature of 350 ^{0}C…….. 66

VI TRANSIENT ANALYSIS OF MHR……..……... 72

VII RELIABILITY AND AVAILABILITY STUDIES……... 78

A. SAPHIRE Code……..……..... 80
B. SAPHIRE Model Development…… 81
C. Failure Data……...…… 82
1. Failure Data Description……... 82
2. Selection of Calculation Type…..……. 83
D. Data Sources and Data Selection……..……. 85
E. Fault Tree Analysis…….……... 88
1. Quantifying Fault Tree…….. 89
2. Uncertainty Analysis……. 90

VIII SAPHIRE ANALYSIS OF SULFUR IODINE PLANT……. 91

A. The SAPHIRE Model Development for SI Plant..……..... 92
B. Data Collection and Selection for Component of SI Plant..…... 99
C. Calculation for SI Plant...……. 99

CHAPTER Page

IX SAPHIRE ANALYSIS OF HTE PLANT……... 105

A. The SAPHIRE Model Development for HTE Plant...…….. 106
B. Data Analysis for the Components of HTE Plant…….. 106
C. Calculation for HTE Plant....……. 108

X SUMMARY…… 114

REFERENCES…… 118

APPENDIX A……. 122

APPENDIX B……. 128

VITA……... 135

LIST OF FIGURES

Page

Fig. 1. MHR and the power conversion system. 5
Fig. 2. MHR pressure vessel and internal details. 6
Fig. 3. Annular core arrangement of MHR. 8
Fig. 4. Schematic of a TRISO coated fuel particle, compacts and fuel elements. 9
Fig. 5. Coupled chemical reactions of SI cycle. 10
Fig. 6. Process schematic of Bunsen reaction process. 12
Fig. 7. Schematic of sulfuric acid concentration and decomposition section. 14
Fig. 8. Hydrogen iodide decomposition section. 15
Fig. 9. Schematic diagram of HTE plant 17
Fig. 10. Original reactor vessel nodalization. 24
Fig. 11. Containment and RCCS nodalization in ATHENA model. 26
Fig. 12. The original and the new inlet coolant flow. 32
Fig. 13. ATHENA nodalization for reactor primary to optimize pressure drop, inlet flow area and inlet coolant velocity. 36
Fig. 14. HS model for PSR and core barrel and the location of new coolant holes. .. 43
Fig. 15. ATHENA nodalization for reactor primary with modified coolant flow 44
Fig. 16. GT-MHR core layout for POKE analysis. 50
Fig. 17. Thermal analysis model used in ATHENA and POKE models 52
Fig. 18. Variation of PFCT with the variation of bypass flow. 55
Fig. 19. Thermal conductivity of fuel 58
Fig. 20. Specific and volumetric heat capacity of fuel 59
Fig. 21. Radial temperature distribution at hot channel 60
Fig. 22. Variation of PFCT with inlet temperature 61
Fig. 23. Axial temperature distribution in the hot channel 62
Fig. 24. Column and axial power distributions used for sensitivity study 63
Fig. 25. Fuel temperature distribution as a function of fuel volume fraction 64

Page

Fig. 26. Fuel temperature distribution as a function of fuel volume fraction for different power distributions and different bypass flows 67
Fig. 27. Vessel temperature as a function of leak through annular path between reactor core barrel and reactor vessel wall 71
Fig. 28. PVT during LPCC and HPCC transients. 74
Fig. 29. PFT during LPCC and HPCC transients. 75
Fig. 30. RCCS power and decay power during transient 77
Fig. 31. Fault tree for common cause failure. 87
Fig. 32. Master fault tree model for SI thermochemical plant 95
Fig. 33. Fault tree for Bunsen reaction process. 96
Fig. 34. Uncertainty analysis: Probability distribution for SI plant model 104
Fig. 35. Main fault tree for the HTE process. 107
Fig. 36. Uncertainty analysis: Probability distribution for HTE plant model 113

LIST OF TABLES

Page

TABLE I MHR Design Value and Steady State Calculated Value 28
TABLE II Result of MHR Transient Validation 28
TABLE III Effect of Increased Inlet Temperature from 490 ^{0}C to 950 ^{0}C 30
TABLE IV Optimization of Flow Area, Inlet Velocity and Pressure Drop 38
TABLE V Final Selection for Coolant Flow Configuration 41
TABLE VI Final Optimized Coolant Flow Configuration 46
TABLE VII ATHENA and POKE Results with Original Block Design 54
TABLE VIII Block Design Parameters 57
TABLE IX ATHENA and POKE Results with Modified Block Design 65
TABLE X PFCT for a PVT of 350 ^{0}C 69
TABLE XI Transient Analyses for MHR 76
TABLE XII Cut Set for SI Based Hydrogen Production Plant 100
TABLE XIII Cut Set for SI Based Plant with Redundancies for Seven Number of Components 101
TABLE XIV Cut Set for SI Plant with Redundancies for Eleven Numbers of Components 103
TABLE XV Cut Set for HTE Plant Including BC-PCS and No Redundancy 109
TABLE XVI Cut Set for HTE Plant without Any Redundancy 110
TABLE XVII Cut Set for HTE Plant Only with Three Redundancies 112

NOMENCLATURE

ASME	American Society of Mechanical Engineers
ATWS	Anticipated Transient Without Scram
C_{pf}	Heat Capacity (J/kg. K)
D	Diameter, Characteristics Length (m)
DOE	Department of Energy
G	Gap conductance
GA	General Atomics
GT-MHR	Gas Turbine Modular Helium Reactor
HTE	High Temperature Electrolysis
H2-MHR	Hydrogen Production Modular Helium Reactor
HPCC	High Pressure Conduction Cooldown
INL	Idaho National Laboratory
LOCA	Loss of Coolant Accident
LPCC	Low Pressure Conduction Cooldown
LWR	Light Water Reactor
MHR	Modular Helium Reactor
NERI	Nuclear Engineering Research Initiative
NRC	Nuclear Regulatory Commission
RCCS	Reactor Cavity Cooling System
SI	Sulfur Iodine
SNL	Sandia National Laboratory

CHAPTER I

INTRODUCTION

A conceptual design to produce hydrogen using Modular Helium Reactor (MHR) is currently being developed under the Nuclear Energy Research Initiative (NERI) project sponsored by United States Department of Energy (DOE). This project is led by General Atomics (GA) and is supported by the Idaho National Laboratory (INL), Texas A&M University and Entergy Nuclear Inc.

The purposes and goals of these studies are to:

- Make the nuclear hydrogen production process more efficient and more economic by increasing process temperature and system reliability.
- Evaluate design options to increase the coolant outlet temperature of the Modular Helium Reactor (MHR) for higher overall efficiency of nuclear hydrogen production using both the Sulfur-Iodine (SI) thermochemical process and High Temperature Electrolysis (HTE) process.
- Keep the reactor vessel temperature as low as possible in spite of this higher coolant outlet temperature. This will allow the use of low cost materials for the reactor vessel.
- Develop Probabilistic Risk Analysis (PRA) models for both the SI and HTE plant and perform the reliability/availability studies for both these nuclear hydrogen production processes.
- Improve the overall system reliability/availability by using component redundancies where it is necessary for high efficiency hydrogen production.

This dissertation follows the style of *Nuclear Technology*.

A. Nuclear Hydrogen

1. Need for Nuclear Hydrogen

Hydrogen is considered a promising energy carrier for the 21st century. It holds the potential to provide a clean, reliable and affordable energy supply that can enhance the world's economy and environment. It also has the potential to replace or supplement the fossil fuels used in the transportation sector throughout the world. Combustion of fossil fuel is used for transportation, electricity generation, process heat, fuel for industries and other important applications. As the reserves of new resources are declining, the limited supply of fossil fuel is becoming a key concern for the energy sectors throughout the world. The pollutants and carbon dioxide emissions from fossil fuel are also an increasing concern. The carbon dioxide emissions from the fossil fuel are thought to be responsible for global warming, which is now a part of international treaties[1].

These drawbacks argue for the reduction of the consumption of fossil fuel as well as for the replacement with a less polluting, environmentally friendly and potentially more sustainable primary energy such as nuclear energy. Conventional nuclear power plants produce electrical energy. However, currently the transportation section is completely dependent on fossil fuel.

The world currently produces more than 50 million metric tons of hydrogen per year[2]. Most of this hydrogen is used in chemicals production, petroleum refining, metal treating, electrical applications, etc. But currently there is no large-scale cost-effective environmental friendly commercial hydrogen production plant. Most of the hydrogen production plants use natural gas as a raw material which produces CO_2 as a byproduct. Hydrogen can be produced in different ways including steam reforming, electrolysis, thermochemical cycles, high-temperature electrolysis, etc. More than 95% of current hydrogen production in the United States comes from steam methane reforming which releases large amounts of CO_2 to the atmosphere. In addition to overall system efficiency, the need to severely curtail of CO_2 emissions might be one of the most important criteria for selection of a hydrogen production process[3]. Nuclear driven

hydrogen production processes appear to be the best selection where water is cracked at high temperature using nuclear heat without any CO_2 emissions.

2. Nuclear Hydrogen Process

Nuclear hydrogen production focuses on water splitting technologies[4-5]. Nuclear driven water splitting can be accomplished by either high-temperature electrolysis or thermo-chemical processes. Both of these processes can produce hydrogen with a reasonable efficiency without the emissions of CO_2 or any other air pollutions. In order to get competitive efficiencies, both processes require very high process temperature (850 ^{0}C or above). As a result, both of these hydrogen production technologies can benefit from the development of advanced high-temperature GEN-IV nuclear reactors capable of delivering heat at temperature in the range of 850 ^{0}C -1000 ^{0}C.

Much works have been done and published regarding nuclear driven hydrogen production technologies. In one study, the University of Kentucky (UK) collected all chemical processes that have been published until then for hydrogen production. GA developed a data base with those chemical processes. With a number of screening criteria such as process efficiency, number of chemicals, temperature range, equipment requirements, etc, GA selected the SI cycle for further studies[1].

The reactor selection task was headed by Sandia National Laboratory (SNL). SNL took into consideration 9 different kinds of reactor starting from Light Water Reactor (LWR) which have been successfully commercialized, to helium and metal cooled reactors which have not been commercialized but have been demonstrated. Evaluating all of these reactors based on a set of design requirements and performance criteria which are required for hydrogen production, SNL rated the helium cooled reactor, liquid metal reactor and the molten salt reactor as the best. Since nuclear hydrogen production using the helium gas cooled reactor requires the least amount of further development, the MHR was selected as the most promising reactor concept for nuclear hydrogen production[6].

Although much of the initial focus by GA has been on the thermochemical process, recent evaluations recommend that the development of the HTE process should be pursued in addition to the thermo-chemical (SI) cycles[7-8]. HTE water splitting supported by nuclear heat and electricity has the potential to produce H_2 with overall system efficiencies of 45%~55%, which is comparable to the efficiencies achievable with the SI process. However, the HTE process does not have corrosion concerns like the thermo-chemical processes and the design appears to be much less complicated (with fewer components) than the design of many thermochemical processes.

An electrolysis process without heat source has an overall efficiency of about 25% which is the product of electricity production efficiency ~33% and hydrogen production efficiency ~75%. Both the electrolysis without heat and HTE process do not produce CO_2 as byproduct. Also by electrolysis process without heat, hydrogen can be produced at the site of use instead of a central location which eventually reduces the hydrogen transportation cost. In lieu of all these advances, HTE process is preferable for its higher efficiency.

As of the current direction of global hydrogen economy and roadmap of hydrogen energy, DOE expects to produce hydrogen using both the SI thermo-chemical process and the HTE process. Required heat for these hydrogen production plants will be provided by nuclear reactor which in our case is the MHR. In this first and demonstration nuclear driven hydrogen production plant, the total 600 MWt power of each reactor will be used for hydrogen production only. In addition to hydrogen, electricity will be produced for utilities in the near future with this kind of reactors.

The designs discussed in this dissertation consist of four individual and completely separate chemical/HTE plants. Each plant will be connected to a 600 MWt MHR. The complete nuclear plant will have 4 identical reactors each of 600 MWt. The reactor core is a helium-cooled, graphite-moderated, prismatic block design. These concepts are referred to as the SI-based H2-MHR and HTE-based H2-MHR respectively.

B. Modular Helium Reactor

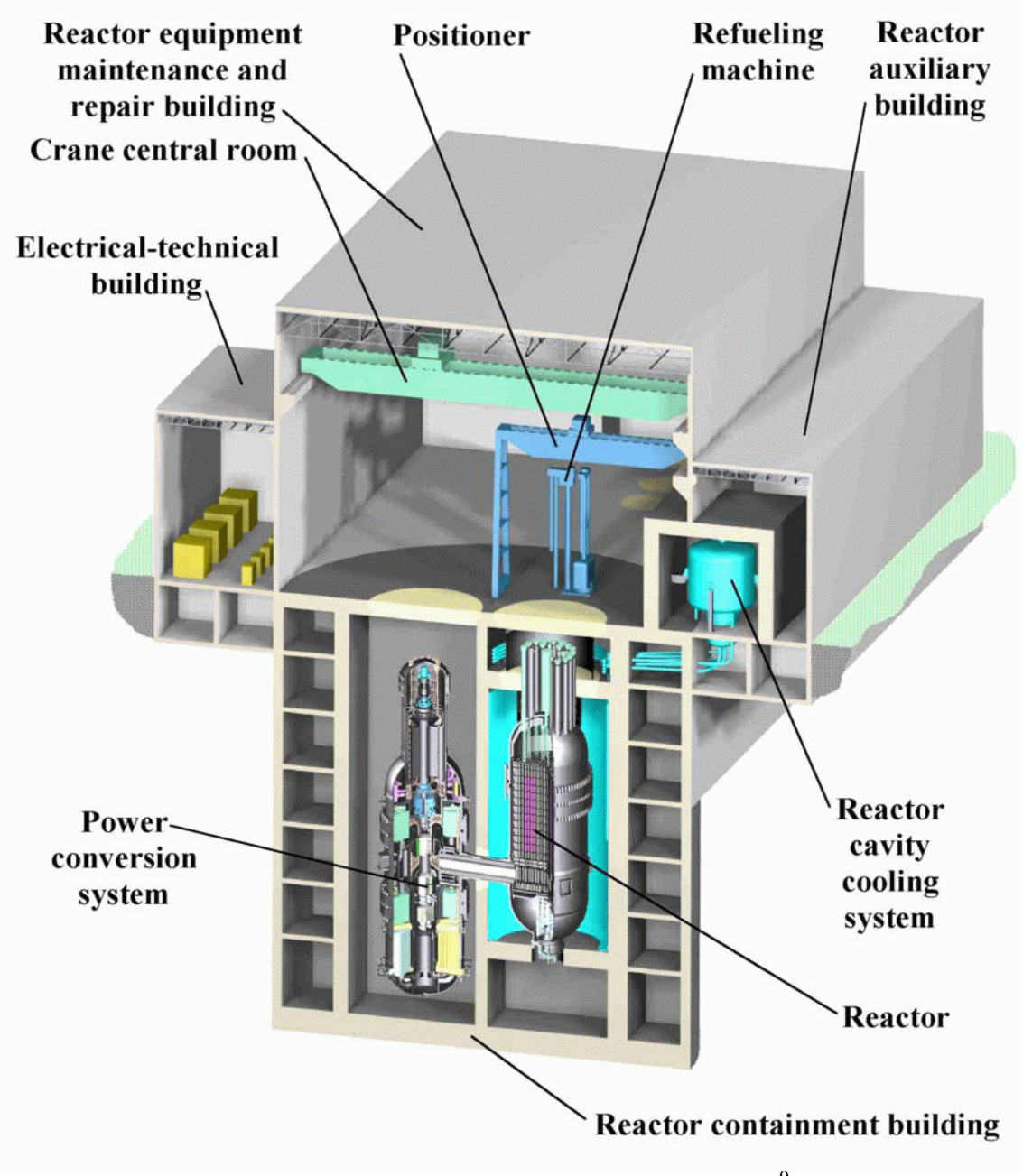

Fig. 1. MHR and the power conversion system.[9]

The reactor system design is based on the Gas Turbine-Modular Helium Reactor (GT-MHR) design. This concept is chosen by GA as the representative very high temperature gas cooled reactor for further development and demonstration. Figure 1 shows the reactor vessel and the Power Conversion System (PCS) within the reactor building.

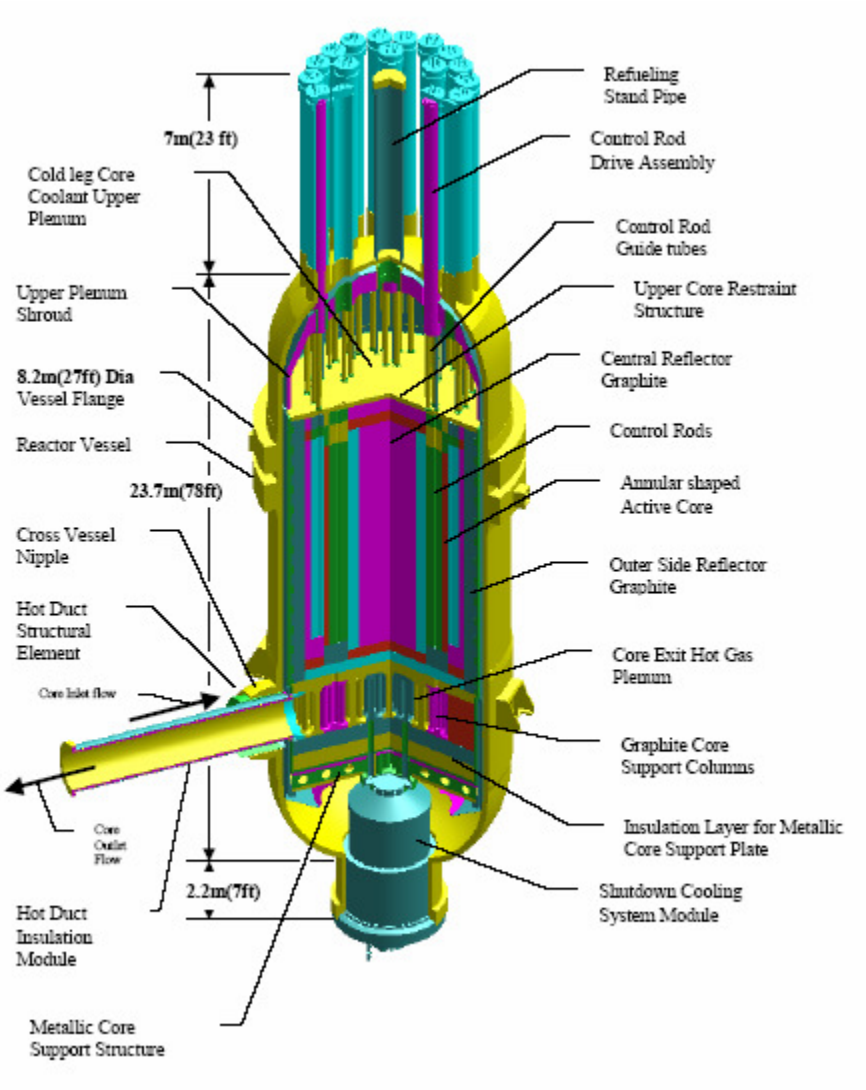

Fig. 2. MHR pressure vessel and internal details.[9]

The entire reactor confinement structure is located underground. The reactor vessel and PCS are located side by side and are connected directly with each other by a cross vessel. The reactor vessel is located somewhat higher than the PCS vessel to avoid any natural circulation from reactor vessel to the PCS vessel during loss of flow accident (station blackout).

Figure 2 shows the detailed arrangement of the reactor vessel internals of the MHR. The inlet helium at 490 ^{0}C and ~7 MPa pressure flows upwards through the rectangular box-shaped path located at the annulus between reactor core barrel and reactor vessel wall. The inlet helium temperature is the main determinant of vessel operating temperature. The helium then flows through the upper core plenum and flows downward through the core. The majority of the coolant flows through the reactor core i.e. through the coolant holes. A fraction of flow (~10%) bypasses these channels, passing through the gaps between the reactor core blocks, reflector blocks and through the gaps surrounding the control rod assemblies.

The plant is designed for a 60 years life with a capacity factor of at least 80%. The reactor is helium cooled and graphite moderated with a power density as low as 6.5 w/cm^3. The prismatic reactor core consists of hexagonal graphite blocks. The fueled region is annular as shown in Figure 3 and is surrounded by inner and outer reflectors. About one third of the graphite blocks are fueled blocks and the remaining two thirds are reflector blocks. During transients the large amount of graphite acts as a temporal heat sink to keep the Peak Fuel Temperature (PFT) well below the design limit. Also during transients, the high volumetric heat capacity of the graphite core material ensures a long delay before the fuels attain its peak temperature.

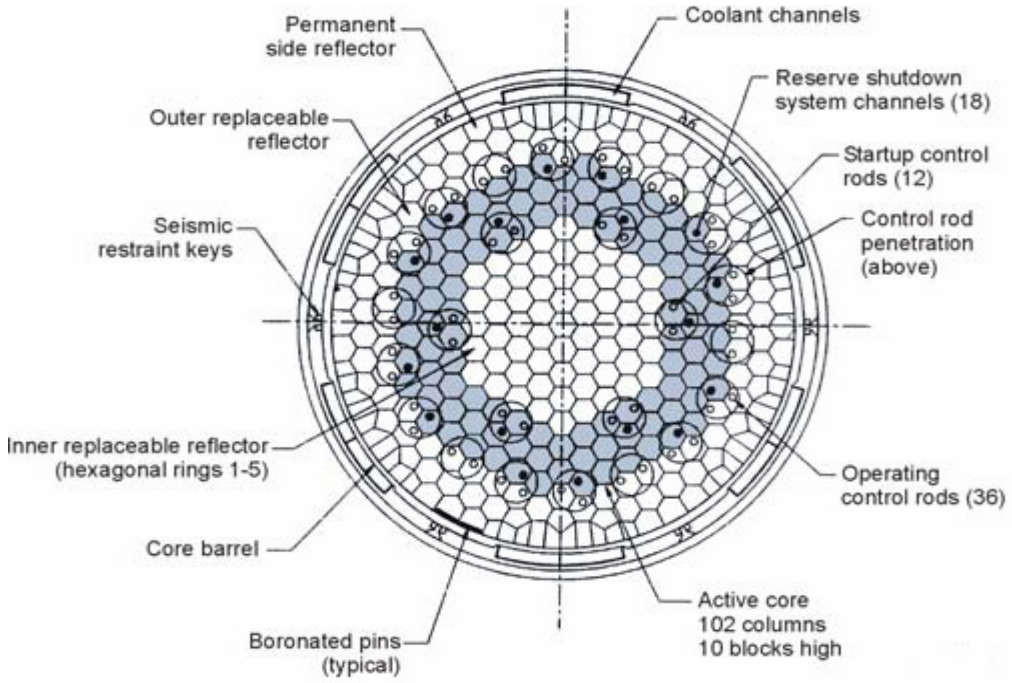

Fig. 3. Annular core arrangement of MHR.[9]

The MHR fuel element consists of coated particle fuel kernels formed into fuel rods and inserted into graphite fuel elements. The fuel consists of spherical TRISO coated fuel particles which are 1 mm in diameter having several composite layers as shown in Figure 4. Each particle consists of a kernel of uranium oxycarbide (UCO) surrounded by a porous carbon buffer, pyrolytic carbon layer, silicon carbide layer and finally the second pyrolytic carbon layer. The porous carbon buffer absorbs radiation damage, allows space required for fission gas produced during irradiation, and resists kernel migration at very high temperature. The silicon carbide layer is the primary pressure boundary for the micro-sphere. It is also the primary containment of fission products produced during irradiation and accident condition. The pyrolytic carbon layers shrink under irradiation, providing compressive forces that protect the silicon carbide layer. The inner pyrolytic carbon layer protects the kernel from corrosive gases that are present during the deposition of silicon carbide layer.

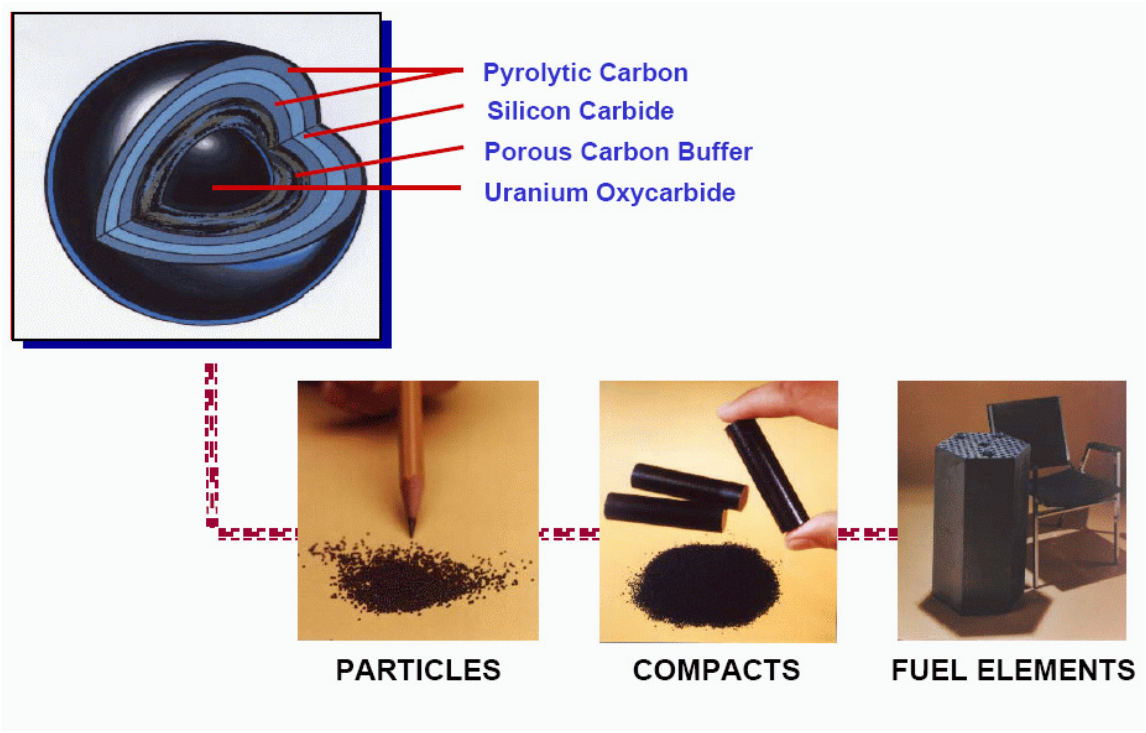

Fig. 4. Schematic of a TRISO coated fuel particle, compacts and fuel elements.[9]

The passive safety of this reactor system is achieved by designing a core cool-down system that limits the peak fuel temperature to below 1600 ^{0}C during any postulated loss-of-coolant accident. This is accomplished by conducting the decay heat rapidly through the core and pressure vessel and radiating it into passive air-cooled Reactor Cavity Cooling System (RCCS). The reactor also has Reserve Shutdown Control (RSC) that is redundant to the reactor scram by insertion of control rods. If both the control rod and reserve shutdown control fail, the temperature coefficient of reactivity will shutdown the reactor from any power level during loss of forced convection cooling. There is also a non-safety shutdown cooling system used only to remove decay heat during normal shutdowns. Several references can be referred to for more details of conceptual design of MHR.[3, 10]

C. SI-Based H2-MHR

1. Main Coupled Chemical Reaction

In the case of the SI-based H2-MHR, the total 600 MWt power is provided as process heat for the SI plant through an Intermediate Heat Exchanger (IHX). Figure 5 shows the coupled chemical reaction for this process. The complete SI plant has three interconnected sections. The sulfuric acid decomposition plant needs a higher temperature than the hydrogen iodide decomposition plant. The nuclear reactor will provide heat for these plants through heat exchangers. The sulfuric acid production plant (Bunsen reaction process) is exothermic and does not require heat addition for the reactions.

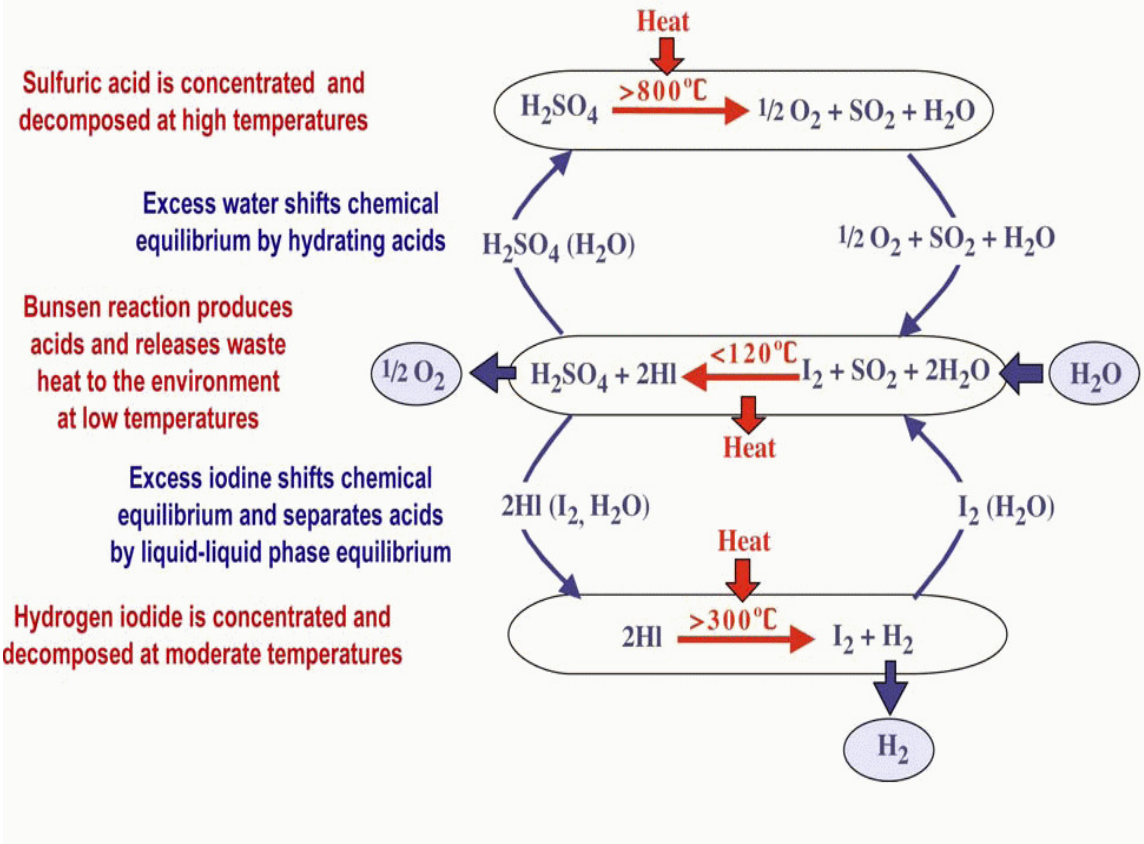

Fig. 5. Coupled chemical reactions of SI cycle.[9]

As the further development of these flow sheets is on going, recent modified flow sheets have been considered for this analysis. All three sections are described here briefly. Details of these flow sheets including pressure, mass flow, material balance, content of each stream, component size, numbers of each component, etc, are available in the GA report[1].

2. Bunsen Reaction Process

Figure 6 is a schematic for Bunsen reaction process where the HI and H_2SO_4 are formed. This reaction is central to the overall process as shown in the previous figure. The majority of the Bunsen reaction takes places at chemical reactor R101 at 7 bars. This reaction also takes place in the primary oxygen scrubber C101, the secondary oxygen scrubber C104 and the sulfuric acid boost reactor C103. The output of heat exchanger and chemical reactor R101 consists of three phases that are separated in separator S101. From the gas phase the SO_2 is separated at C101 and recycled. The residual H_2O is removed from O_2 at separator S104 and S105 and most of the O_2 is vented to atmosphere but a portion is recycled at stripper C102. SO_2 and O_2 are separated at C102 and are fed to the H_2SO_4 boost reactor C103 where the concentration of H_2SO_4 is increased from 15% mole to 20% mole. Further improvement of acid concentration takes place at S102 and a relatively high concentrated sulfuric acid with SO_2 and H_2O in it, is fed to the H_2SO_4 decomposition section through streamline 140. The HI from C102 having I_2 and H_2O in it, is sent to HI decomposition section through stream line 138.

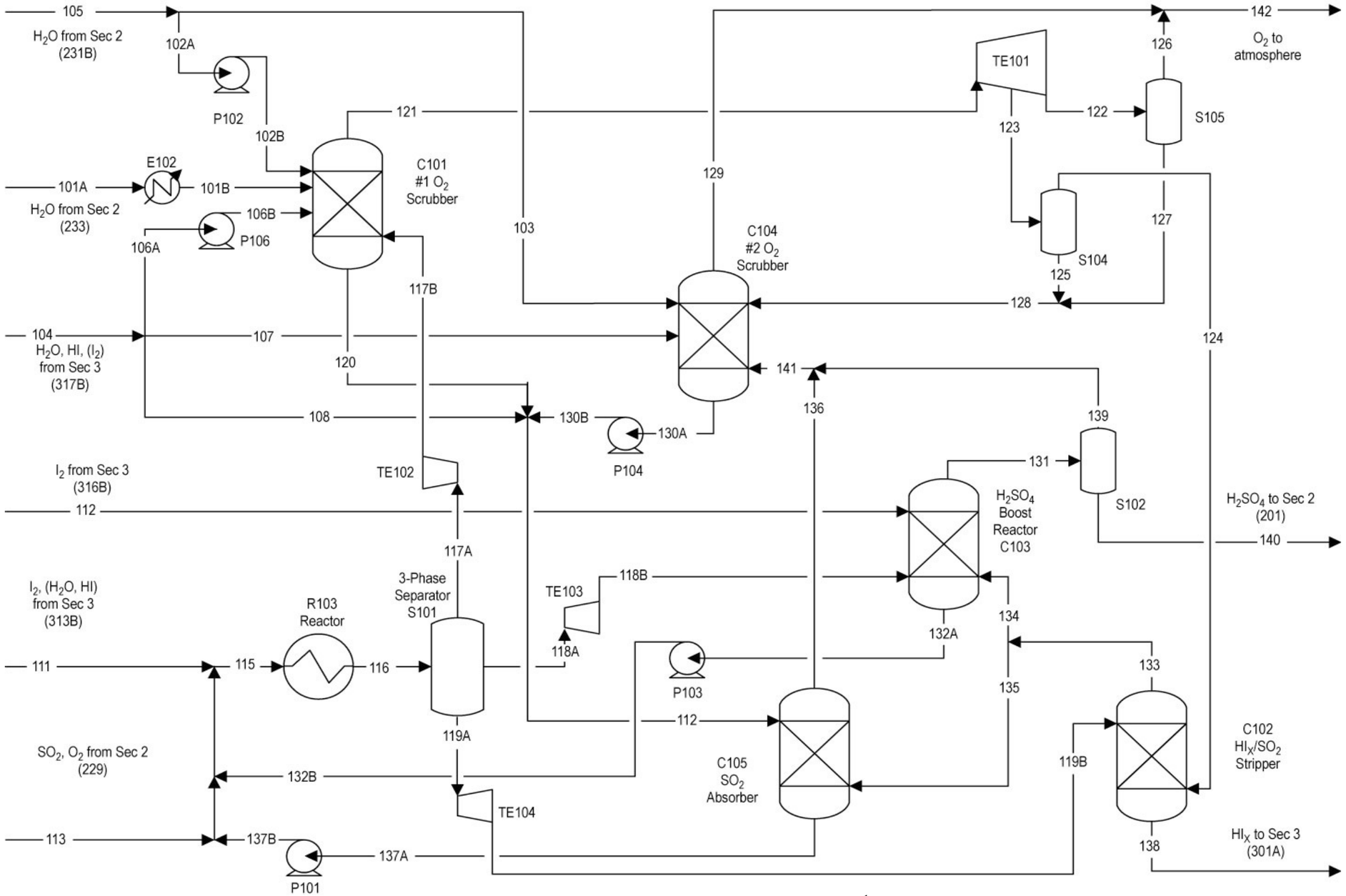

Fig. 6. Process schematic of Bunsen reaction process.[1]

3. Sulfuric Acid Concentration and Decomposition Section

This section has the highest process temperature. The schematic diagram for this section is shown in Figure 7. This flow sheet was developed independently at the University of Kentucky and Aspen Plus®. Aspen process simulator software was used for generating this flow sheet. The purposes of this section are to concentrate H_2SO_4 and decompose the concentrated H_2SO_4 into SO_2 and O_2. Dilute H_2SO_4 is fed from the Bunsen reaction section through pump P204. Then the H_2SO_4 is heated and water is removed by a series of flash drum and separator. Required heat for heating, vaporizing and decomposing H_2SO_4 is provided by the high temperature helium from the MHR. The main decomposer E207 is the heat exchanger where H_2SO_4 is decomposed. The product SO_2 is sent to the Bunsen reaction section. To reduce the amount of heat required in the decomposer to decompose the H_2SO_4, the concentration of H_2SO_4 is increased before it enters the decomposer. Due to this increased concentration the total volume of H_2SO_4 is reduced and as a result a smaller heat exchanger for the system can be used. This also helps to improve the thermodynamic efficiency of the heat exchanger.

A baseline flow sheet was designed at 827 ^{0}C peak process temperature. The flow sheet shows reasonable efficiency and reduced cost at the 827 ^{0}C level, with the potential for higher efficiency and further reduced costs at higher process operating temperatures. The H_2SO_4 absorber recovers essentially all of the un-reacted H_2SO_4 and uses the heat of condensation of H_2SO_4 to concentrate H_2SO_4 before it is fed to the high temperature H_2SO_4 decomposition system. The remaining thermal energy in the H_2SO_4 decomposition products is recovered and used to concentrate the acid.

4. Hydrogen Iodide Decomposition Section

The $HI/I_2/H_20$ product from the Bunsen reaction section is pumped to the hydrogen iodide decomposition section which is shown in Figure 8 and then it is heated and fed to the reactive distillation column (C301). After reaction, the portion containing most of the iodine and the portion containing most of the water are fed back to the Bunsen reaction section. The H_2 product is scrubbed and the final product is collected.

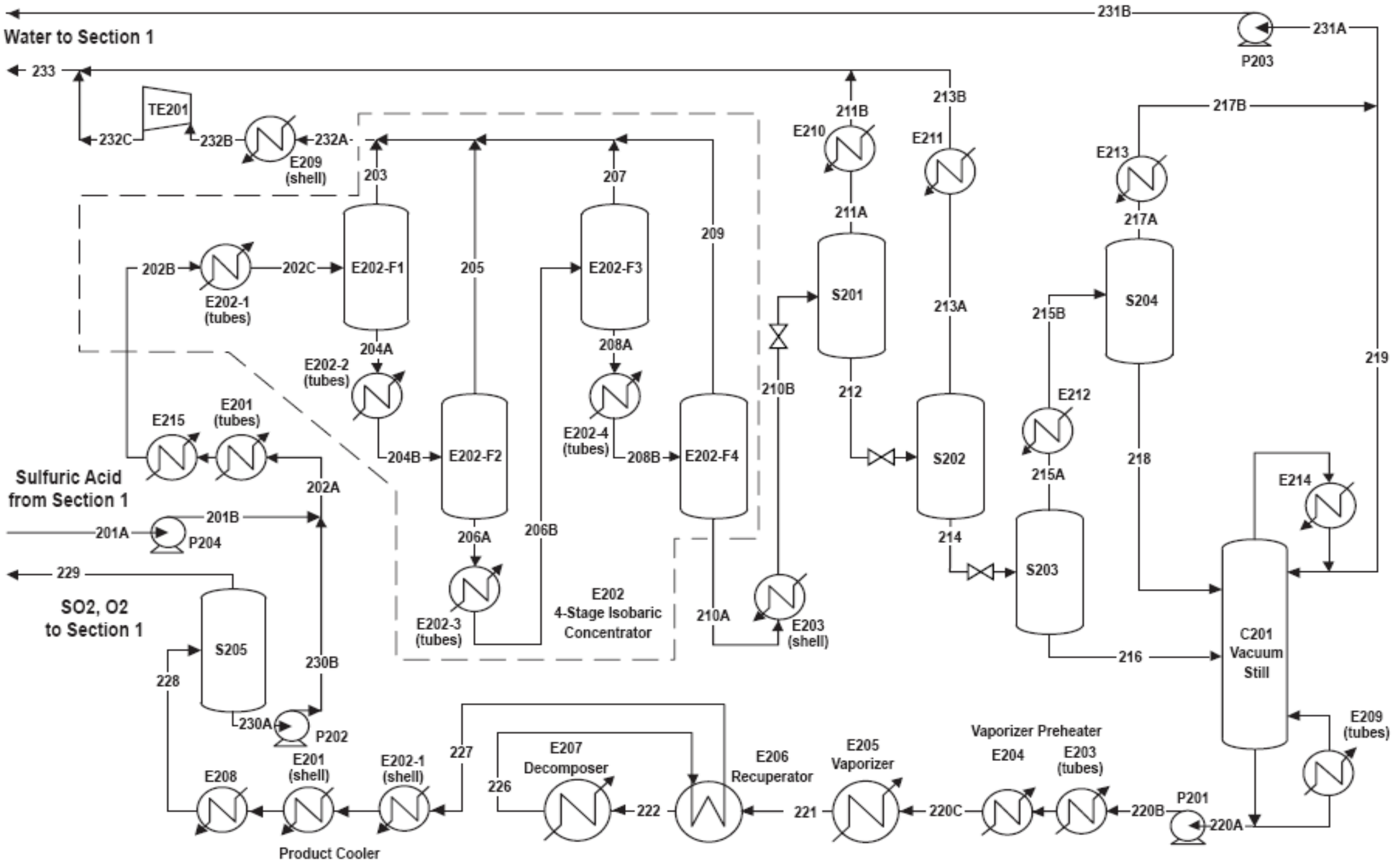

Fig. 7. Schematic of sulfuric acid concentration and decomposition section.[1]

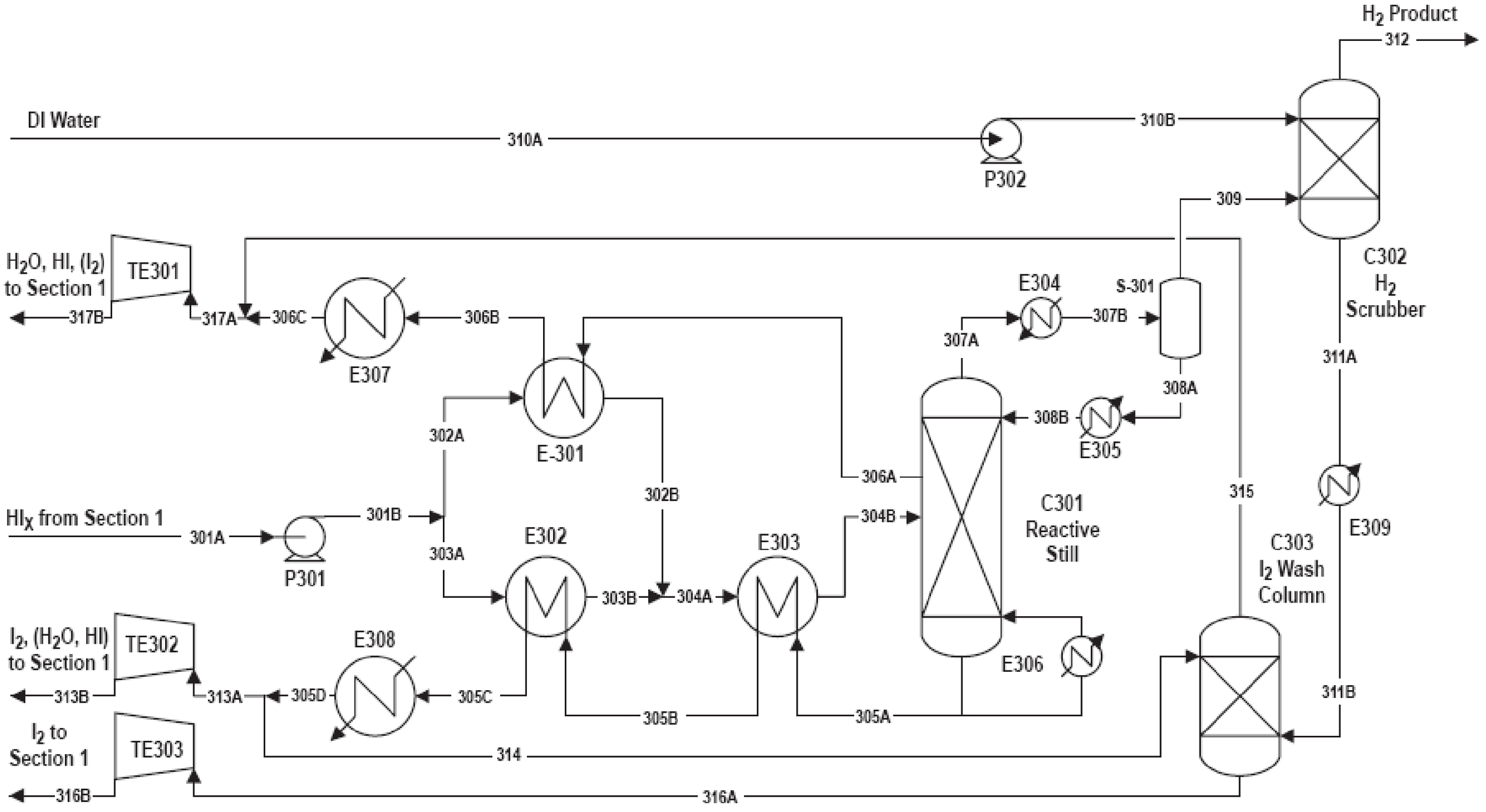

Fig. 8. Hydrogen iodide decomposition section.[1]

D. HTE-Based H2-MHR

High temperature electrolysis involves the splitting of water into hydrogen and oxygen at high temperatures. The primary advantages of HTE over the conventional electrolysis which is a well established technology is that considerably high hydrogen conversion efficiencies can be achieved. This is because the conversion efficiency of heat to electricity is low compared to using heat directly in the hydrogen production process. Therefore, in the HTE process, a portion of total energy needed to split the water is added as heat instead of electricity, so the required energy is reduced and as a result the overall process efficiency is improved.

In the case of HTE-based MHR, the total 600 MWt power is split into two major parts. About 10% of the thermal power (~68 MWt) is used to heat the feed water delivered to the electrolysis stack[8]. The remaining thermal power is provided to a Brayton Cycle Power Conversion System (BC-PCS) to produce the electricity required to drive the electrolysis process (about 290 MWe). The BC-PCS consist of compressor, turbine, recuperator, intercooler, generator, etc. The conceptual design of HTE based hydrogen production plant developed at INL[11] using HYSYS code and is shown in Figure 9.

The HTE plant consists of several interconnected sections such as heat transfer section, hydrogen production and collection section, sweep water section etc. The heated steam (~90%) and hydrogen (~10%) mixture is fed to high temperature electrolysis stack. The portion of hydrogen is re-circulated from the final product and it helps to prevent oxidation of the nickel at the electrolysis stack. The residual heat is recovered from the final product to increase the thermal efficiency of the process.

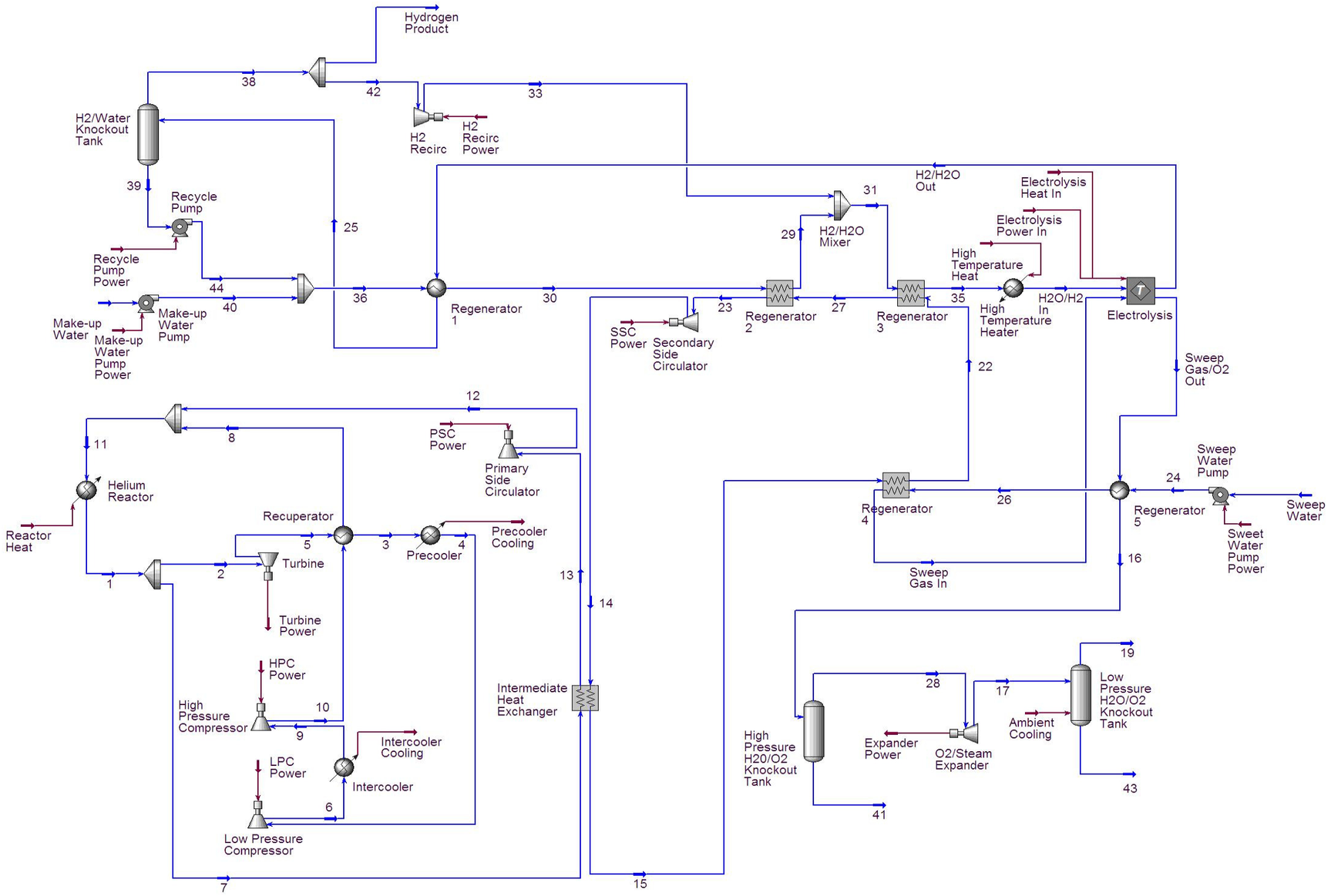

Fig. 9. Schematic diagram of HTE plant.[9]

CHAPTER II

CURRENT STATUS AND PROPOSED RESEARCH

A. Current Status of the Problem

1. Design Modification for the MHR for Higher Temperature Operation

The design of the reactor for hydrogen production applications based on the Gas Turbine-Modular Helium Reactor (GT-MHR) was developed at GA. The reactor itself is referred to as the MHR and the reactor connected to a hydrogen production process is referred to as the H2-MHR. A thermal hydraulic analysis model which includes the MHR vessel system, RCCS and the containment system has been developed at the INL for steady-state and transient analyses.

A number of studies have been performed to evaluate design options for optimizing the MHR to achieve higher reactor outlet operating temperature. A number of thermal hydraulic computer codes have been used for analyses. The results of these analyses showed that although increasing the coolant outlet temperatures of the MHR resulted in higher hydrogen production efficiencies, the resulting steady-state reactor vessel temperatures were found to be higher than the desired vessel temperatures.

In one study GA evaluated the possible minimum inlet temperature for a certain coolant outlet temperature[3]. It may be noted here that, the inlet coolant temperature is one of the main determinants of the steady state vessel temperature. So a reduction of coolant inlet temperature would cause a reduced vessel temperature for MHR. Reactor having different core heights (10, 12 and 14 blocks high of core) with different power densities and coolant flow rates had been considered for those analyses. The results demonstrate that, there is a limit beyond which the ΔT across the core may not be increased for current graphite block core design. The inlet temperature may not be reduced below a certain limit for a particular core length and for a particular coolant outlet temperature.

Several studies[12-13], were under taken in an effort to reduce the steady-state reactor vessel temperature. In those analyses the inlet coolant flow path was shifted from the annular path between reactor core barrel and vessel wall into the center of the inner reflector. For that modification a numbers of graphite columns (7 to 19) were removed from the center reflector to create the flow path for the inlet helium coolant. Calculations were performed for core inlet temperatures of 490 ^{0}C to 600 ^{0}C and a core outlet temperature of 1000 ^{0}C. The results of this initial assessment were found to be promising. The steady-state reactor vessel temperatures were reduced to values that were within the design limit of the reactor vessel material, and the peak vessel temperature and peak fuel temperature during transient conditions were found to be within the acceptable limit. However, since the central graphite reflector in a MHR serves as both a heat sink and moderator, the removal of graphite blocks from the center of the reactor is not a desired option from some other thermal hydraulic and neutronic points of view.

2. Reliability and Availability Studies

Reliability, availability and maintainability assessments of the MHR had been performed by 'Strategic Power System Incorporation' using the 'Operational Reliability Analysis Program' and the results of these studies had been reported[10]. However, no effort had been taken for the reliability studies of the entire nuclear hydrogen production process with the MHR coupled to the hydrogen production processes.

To perform the reliability studies for the entire nuclear hydrogen production processes, the PRA models for both the HTE and SI based nuclear hydrogen production plants will need to be developed. The reliability code which is capable and commonly used to analyze nuclear system needs to be used for the reliability studies of these hydrogen production plants and the Brayton cycle power conversion system with the aim of having a complete PRA model for this couple nuclear hydrogen production process.

B. Proposed Research

1. Design Modification for the MHR for Higher Temperature Operation

Two design modifications for the MHR will be performed and evaluated to allow the reactor a higher outlet temperature than the current outlet temperature of 850 ^{0}C. The conventional coolant inlet path and the current reactor core design will be modified to achieve the desired goal. The objective of this proposed study is to reduce the steady-state reactor vessel temperature, while allowing the coolant outlet temperature to increase to achieve higher hydrogen production efficiencies and maintaining the fuel centerline temperature within acceptable limit.

First, the design of an alternative configuration for the reactor coolant inlet flow path of MHR will be performed. In the existing reactor design, the rectangular boxed channels located at the annular channel between the reactor vessel wall and the reactor core barrel, are used for the coolant inlet flow. In this proposed configuration the inlet coolant flow path will be through the permanent outer reflector or permanent side reflector (PSR).

This alternative configuration for the coolant inlet flow is a completely new concept. With this new configuration the PVT during steady state and transient operation is expected to be well below the ASME code limit for the current vessel material. This reduced steady state vessel temperature will result in a significant reduction of cost for the reactor vessel material. A thermal hydraulic code will be used for these analyses and for the optimization of the reactor coolant flow passage design. During this modification, the total pressure drop, amount of graphite removal from the core to create the coolant path and the inlet coolant velocity will be optimized and maintained within the acceptable limits.

In addition to modified coolant scheme through PSR another way the vessel temperature can be reduced is by reducing the inlet coolant temperature. The modification and optimization of the new core design in a MHR which will allow an

increase in the ΔT across the reactor core while maintaining the Peak Fuel Centerline Temperature (PFCT) within limit will be performed and evaluated.

With the current block core design, the ΔT across the core would be ~360 ^{0}C. Therefore, the inlet temperature of MHR for a higher outlet temperature of 950 ^{0}C can not be reduced below 590 ^{0}C. The new block core design will allow an increased ΔT across the reactor core. This increased ΔT across the reactor core will result in a reduced coolant inlet temperature for the same coolant outlet temperature of 950 ^{0}C. This reduced inlet temperature will lead to a reduced vessel peak temperature during normal operation.

2. Reliability and Availability Studies

For this part of study, the object is to develop a PRA model for both SI based and HTE based hydrogen production plants. Using the developed models the reliability and the availability of the plant design will be calculated. Where appropriate, component redundancies will be incorporated into the designs to improve system reliability for better economic performance. Using a PRA code to analyze a process plant with lots of recycling of fluids is a unique effort. The fault tree model for the SI plant and the HTE plant will be developed. From the available reliability data source for the components, the mean failure probability for each component, its mean repair time and uncertainty of these data will be evaluated. Reliability data for a particular component from different data sources will be compared and the most relevant data will be incorporated for this reliability study. The fault tree analysis will provide the system reliability and availability for a particular mission time.

CHAPTER III

RELAP5-3D/ATHENA PLANT MODEL

A. RELAP5-3D/ATHENA Code

The RELAP5-3D© (Reactor Excursion and Leak Analysis Program-3 Dimensional) code[14] is an outgrowth of the one-dimensional RELAP5/MOD3 computer code developed at Idaho National Laboratory (INL). It was developed under the sponsorship of the U.S. Nuclear Regulatory Commission (NRC), the U.S. Department of Energy (DOE), and a consortium of several countries and domestic organizations that were members of the International Code Assessment and Application Program (ICAP), and its successor, the Code Application and Maintenance Program (CAMP). The code has been regularly updated since the time of its inception in 1979. Following the accident at Chernobyl, DOE decided to reassess the safety of all existing reactors throughout the United States. The RELAP5 code was chosen at that time as the thermal-hydraulic analysis tool because of its widespread acceptance. It is a best estimate code that can be used for transient simulation during postulated accidents such as Loss of Coolant Accident (LOCA), anticipated transient without scram, loss of offsite power, loss of feed water, turbine trip, etc.

The RELAP5-3D version of the code contains several important enhancements over the previous single dimensional RELAP5 code. The most prominent attribute that distinguishes the RELAP-3D code from the previous single dimensional RELAP5 code is it is fully integrated, and capable for multidimensional thermal-hydraulic and kinetic modeling. These capabilities remove any restrictions on the applicability of the code to the full range of postulated reactor accidents. The other enhancements of RELAP5-3D are the inclusion of a new matrix solver for 3-D problems, new water properties and improved time advancement for greater robustness of the code.

The code has two options for the computation of reactor power. They are: point reactor kinetic model and multidimensional neutron kinetic model. The point reactor kinetic model developed at the INL is the simplest model which is used to compute the transient behavior of neutron fission power. The power in this model is computed using point reactor kinetic approximation. This approximation is adequate for cases where the space distribution remains nearly constant. The multidimensional neutron kinetic model was developed at North Carolina State University under an INL initiative. It solves the two or four group neutron diffusion equations in either Cartesian or hexagonal geometry using the Nodal Expansion Method (NEM) and the non-linear iteration technique. Several different core symmetry options and several boundary options are available in this model.

The foundation of the Advanced Thermal Energy Network Analysis (ATHENA) computer code[15] is RELAP5-3D. The ATHENA code was also developed at the INL under the sponsorship of U.S. Department of Energy. To expand the capability of RELAP code, new working fluids, new heat transfer models, and a new hydrodynamic model was added to the ATHENA code. In addition to LWRs, ATHENA can be used to analyze reactors with a variety of working fluids including helium, hydrogen, nitrogen, ammonia lithium, sodium, lead-bismuth etc. ATHENA can also be used for space reactor applications since a user defined gravitational constant can be used.

B. Description of Plant Model

A RLAP5-3D/ATHENA model of MHR was developed at the INL in support of the GEN IV program. A detail description of the original ATHENA plant model and results of the initial thermal hydraulic analyses has been reported[3]. The current ATHENA model of MHR is a simplified model that is designed to examine the core behavior. This ATHENA model is basis for further development and further calculation for reactor primary system. Components outside the primary system and some of the vessel internals are ignored.

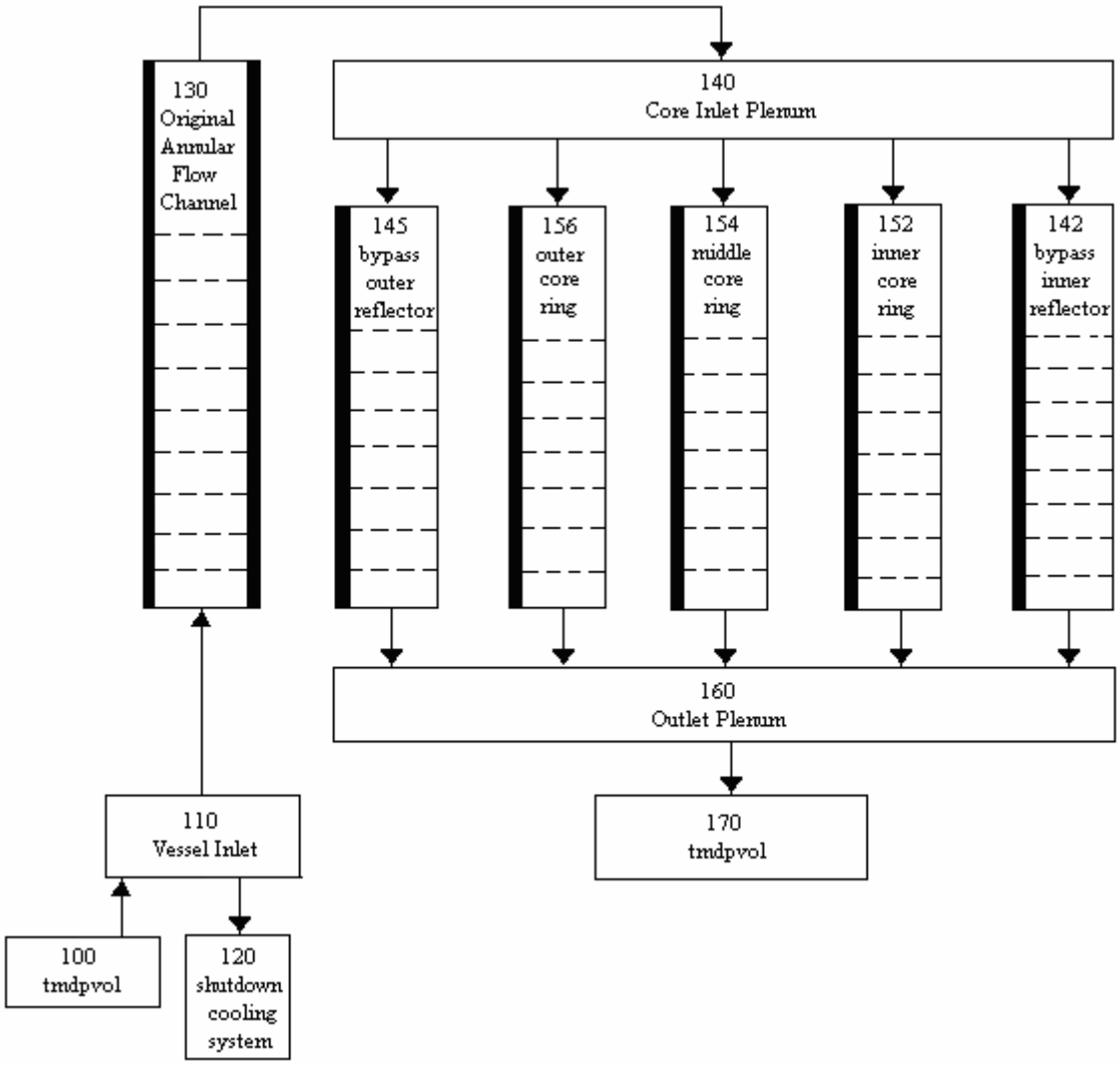

Fig. 10. Original reactor vessel nodalization.

Figure 10 shows the original reactor vessel nodalization developed by the INL. As shown in the nodalization, the coolant enters the vessel through the vessel inlet (component 110), flows upward through the annular channel boxes located between reactor vessel and reactor core barrel (component 130), and up to the inlet plenum (component 140). The inlet flow is assumed to occupy the entire region between the core

barrel and the reactor vessel since the dead helium volume is not modeled. Two time dependent volume (components 100 and 170) provide the system boundaries.

From the inlet plenum, the coolant flows down through the core. The core is modeled with three parallel channels (components 152, 154 and 156), each representing one of the three rings in the annular fueled region. Two core bypass channels are modeled, one in the inner reflector (component 142) and the other in the outer reflector (component 145). After exiting the core the coolant flows through the core outlet plenum (component 160) and finally flows out of the vessel. The inlet flow is controlled to achieve the desired helium outlet temperature.

The heat structures are used to model most of the structural component in the vessel. The active core has ten axial nodes each representing one of the fuel blocks. Each axial node of the active core has 102 fuel blocks. The inner ring, middle ring and the outer ring of the annular shaped active core contain 30, 36 and 36 assemblies, respectively, in each level. The upper and the lower reflectors are also modeled as two additional axial blocks. The outer permanent and replaceable reflectors along with the core barrel are modeled as a single integrated component in the ATHENA model.

The RCCS and containment nodalization are shown in Figure 11. The containment (component 900) and the reactor cavity cooling system (RCCS) which is located on the interior of the containment are also modeled. The surrounding wall of the containment is modeled as a very thick wall consists of a ~1 m thick of concrete and 5 m thick of surrounding soil.

Air from atmosphere enters the RCCS inlet plenum (component 955) and flows downward through the down comer to the RCCS lower header distributor which is located at the bottom of the containment. Then the hot air flows through the riser and passes through outlet plenum and eventually flows to the atmosphere.

Radial and axial conduction are modeled in the core and reflectors. Radiation heat transfer is modeled from the core barrel to the reactor vessel, from the vessel to the RCCS, and from the RCCS to the containment. The RCCS is modeled as a dry air-filled system. The risers are modeled as three separate structures, connected by conduction.

The loss coefficients in the plena are adjusted to provide the desired heat removal rate for the MHR. The reactor vessel structure outside the core region is modeled. The vessel below the core extends as a cylinder to half the depth of the hemispherical lower head. The entire upper head hemisphere is modeled, as is a hemisphere in the inlet plenum separating the upper plenum from the up flow annulus.

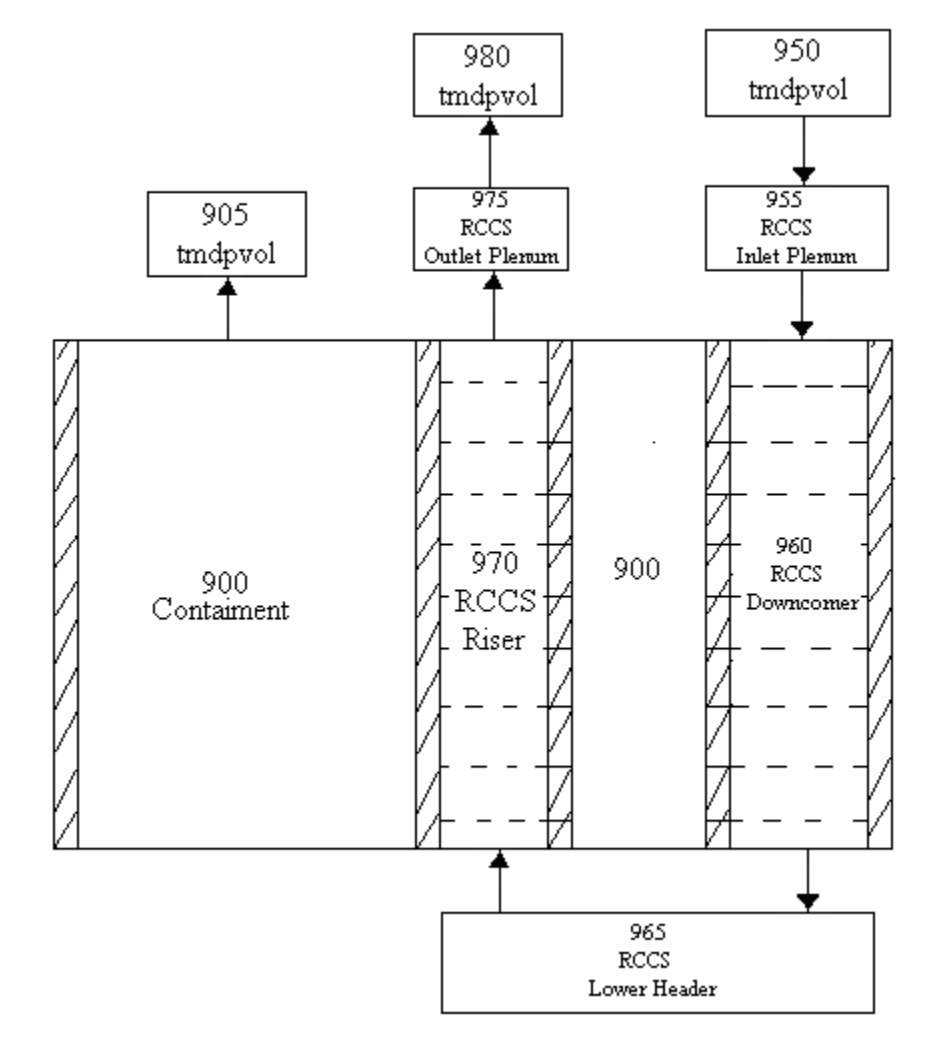

Fig. 11. Containment and RCCS nodalization in ATHENA model.

C. Validation of the Plant Model

It is always advisable to validate the accuracy of any model before proceeding with additional calculations. If there is any mistake in the original model, that will negate the whole calculation process. The original model may not have come directly from the developer. Sometime it comes through other person or agency, and in some cases may have been changed or modified by others. These modeling changes could lead to inaccurate or unrealistic results unless the model is adequately validated.

For our case, it is necessary to obtain satisfactory steady-state conditions from the ATHENA model before initiating any transient calculations. A limited validation of this original ATHENA model was performed using available design data for the MHR[16]. The validation process assessed the accuracy of the original and any modification made to the model. Usually a plant model is considered validated[17] if:

- It is in geometrical agreement with the described system
- It reproduces the supposed condition of the system and
- It shows a satisfactory behavior under transient or time dependent conditions

The ATHENA model has been validated for a number of thermal hydraulic transients including Low Pressure Conduction Cooldown (LPCC) and High Pressure Conduction Cooldown (HPCC) at INL. The basis for this present validation process has been the design data of MHR.

The steady-state validation consists of the acquisition of structural and operational data from the MHR. When the nominal measured steady-state is reproduced, this validation process is considered complete. For validation of transient result, the results of transient calculation such as LPCC and HPCC from GA calculated values and the ATHENA calculated values are compared. The steady-state validation consisted of a comparison of several nominal steady-state values (GA calculated values) and the ATHENA calculated values are shown in Table I. The transient validation results are shown in Table II.

TABLE I MHR Design Value and Steady State Calculated Value

Parameters	Expected	ATHENA
Coolant flow rate (kg/sec)	320	324.18
Core pressure drop (MPa)	0.051	0.0508
RCCS power (MW)	3.3	3.2926
RCCS flow rate (kg/sec)	14.3	14.1481
RCCS air outlet temperature (C)	274	270.757
Reactor vessel temperature (C)	446	453

TABLE II Result of MHR Transient Validation

Parameters	LPCC Transient pressure 1 atm		HPCC Transient pressure 5.03 MPa.	
	Expected	ATHENA	Expected	ATHENA
Peak fuel temperature (C)/time (h)	1447/63	1437/58.7	1223/45	1276/58
Peak vessel temperature (C) /time (h)	502/81	500/77.5	457/70	467/73.8

.

CHAPTER IV

OPTIMIZATION OF NEW COOLANT CONFIGURATION FOR MHR

A. Effect of Increased Coolant Temperature

As was mentioned before, the coolant inlet and outlet temperatures in the original GA MHR design were 490 ^{0}C and 850 ^{0}C, respectively. The thermal efficiency of the SI based hydrogen production process with a peak process temperature which corresponds to coolant outlet temperature of 850 ^{0}C from a MHR is found to be ~42%. With a higher peak process temperature which corresponds to coolant outlet temperature of 950 ^{0}C, the estimated thermal efficiency is ~52%[1]. The thermal efficiency of HTE process is also a strong function of its process temperature and increases with the increase of MHR coolant outlet temperature at the similar range.[7]

To achieve higher hydrogen production efficiencies from both SI and HTE processes, the coolant outlet temperature of the H2-MHR has been increased from 850 ^{0}C to 950 ^{0}C. A coolant outlet temperature beyond this will increase the hydrogen production efficiency even further, but the coolant outlet temperature is limited to 950 ^{0}C to avoid any potential adverse impacts on fuel performance during steady state normal operation of the MHR[18]. The temperature limit of structural and vessel materials are also need to be considered. In addition, a higher coolant outlet temperature beyond 950 ^{0}C for MHR may require significant advances in technology to develop a viable design of intermediate heat exchanger (IHX) which is used to transfer process heat from MHR to hydrogen production plants. In order to maintain the same coolant flow rate through the core and to maintain the same convective heat transfer rate within the core, the inlet coolant temperature is also increased from 490 ^{0}C to 590 ^{0}C.

Table III shows the effect of the changes in inlet and outlet temperatures on some of the plant parameters. Case 1 shows nominal steady-states ATHENA calculated

parameters with core inlet and outlet temperatures of 490 ^{0}C and 850 ^{0}C respectively, which corresponds to the GT-MHR baseline design conditions. A hypothetical case where the inlet coolant temperature is kept same as the original case but the coolant outlet temperature is increased to 950 ^{0}C is shown in case 2. Case 3 shows the expected inlet temperature for an outlet temperature of 950 ^{0}C for the MHR with current block core design, where this higher coolant outlet temperature is assigned to get higher efficiency for the MHR driven hydrogen production process. The reason why the inlet temperature can not be reduced below 590 ^{0}C for a coolant outlet temperature of 950 ^{0}C is discussed in more details in Chapter V where this inlet temperature is reduced by modifying the reactor core design.

TABLE III Effect of Increased Inlet Temperature from 490 ^{0}C to 950 ^{0}C

Case	Coolant Inlet Temp (C)	Coolant Outlet Temp (C)	Coolant Flow Rate (Kg/Sec)	Inlet Pressure (MPa)	Total Core Pressure Drop (KPa)	ΔP_{Total}- ΔP_{Core} (KPa)	Maximum Vessel Temp (C)	Heat Loss to RCCS	Core max velocity
1	490	850	324	7.0	50.8	0.86	453	3.29	53.0
2	490	950	253	7.0	33.86	0.82	452	3.25	41.9
3	590	950	324	7.0	56.0	0.86	541	4.49	53.02

Case 1 is considered as the base case for this analysis which is same as the original reactor design. Coolant flow rate for case 1 is 324 kg/sec and will remain same during this modification since ΔT across the reactor core is expected to be same. Total pressure drop for this case is about 50 KPa.

In the current design of the coolant inlet flow the inlet coolant flow cross sectional area is huge, and the hydraulic diameter of the coolant inlet flow path is much higher than the hydraulic diameter of the core. So almost all the pressure drop occurs in the core, a negligible pressure drop occurs in the coolant inlet flow path. The maximum steady-state vessel temperature in this case is 453.3 ^{0}C which is within acceptable range for the current vessel material. During this analysis the vessel is discritized into several volumes and the 'maximum vessel temperature' is determined in each time step from the volume wherever it is the maximum at that time step. The core maximum velocity is also calculated in the same way. The coolant flow path through the core is discritized into several control volumes. First the velocity for each of the volume at each time step is calculated and then the maximum core velocity is determined from a volume wherever it is the maximum at that time step.

As mentioned before, there is a limit beyond which the coolant inlet temperature can not be reduced for a constant outlet temperature and for a particular core height with current block core design. Based on this, case 2 is an unrealistic case. But it might be helpful to observe the different parameters with this inlet and outlet temperatures. There is a huge reduction of mass flow rate, core maximum velocity and pressure drop in this case compared to case 1, but the steady state peak vessel temperature and the heat rejected through RCCS remain within the same range.

With the increased inlet temperature from 490 ^{0}C to 590 ^{0}C and coolant outlet temperature of 950 ^{0}C (case 3), the coolant flow rate, the coolant velocity and the pressure drop are increased from case 2. In addition, the steady-state maximum vessel temperature and the heat loss to RCCS increase with this higher inlet temperature. This investigation shows that with the inlet and outlet helium temperatures of 590 ^{0}C and 950 ^{0}C respectively the steady state reactor vessel temperature is about 541 ^{0}C which is well above the ASME code for current reactor vessel material.

B. Design and Verification for New Coolant Path

In an attempt to reduce the steady-state reactor vessel temperature, an alternative configuration of the coolant inlet flow path is developed and verified. The coolant inlet flow path is shifted from the annular region between reactor vessel and the core barrel to inside the permanent outer reflector (i.e., permanent side reflector). Figure 12 shows the schematic of the flow path for both the old and the new coolant flow. The original coolant inlet flow which flows between reactor core barrel and vessel wall is shown with cross (X) sign.

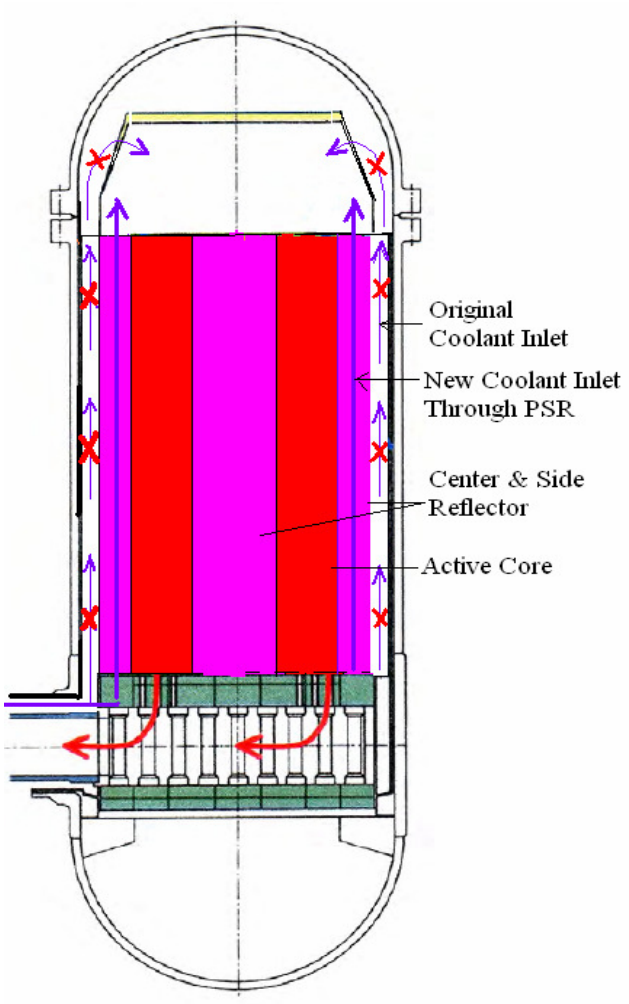

Fig. 12. The original and the new inlet coolant flow.

In the original flow path the helium enters the vessel inlet plenum and flows upward through the channel boxes in the annular region between the core barrel and the inner vessel wall. This configuration allows direct heat transfer from the hot inlet helium flow to the vessel wall. The figure shows the helium in the new flow configuration enters the core inlet plenum through the outlet side. In the new configuration, the helium flow path is moved away from the vessel inner wall, and into the outer reflector region. This configuration provides greater separation between the coolant flow path and the vessel, thereby eliminating direct heat transfer between the hot inlet helium and the vessel wall.

A horizontal cross vessel connects the PCS vessel and MHR vessel. Any heat transferred from hot inlet helium direct to the cross vessel wall will result in a higher steady state reactor vessel temperature. Therefore, reactor vessel wall also needs to be insulated from vessel inlet plenum to prevent any direct heat transfer to the vessel wall from the hot helium at the vessel inlet plenum. The cross vessel wall also needs to be insulated from hot inlet coolant to prevent direct heat transfer from hot inlet coolant to the cross vessel wall. In order to prevent direct heat transfer from the hot inlet helium to the vessel wall or to the cross vessel, the necessary insulation has been incorporated in the ATHENA model to insulate both the vessel wall and the cross vessel wall from the hot inlet coolant.

The limiting criteria for the design of this new coolant flow configuration can be summarized as follows:

- Percentage of graphite removed ≤20% of outer reflector
- The reactor vessel pressure drop ≤90 KPa
- The coolant/helium velocity in the revised inlet flow passage will be consistent with the coolant velocity in the core
- Steady-state peak vessel temperature will be reduced significantly
- The modification will not affect the total core bypass assumed for the base case model

The amount of graphite in the outer reflector is about one half of the total graphite in the MHR core. Therefore, a 20% reduction in the graphite in the outer permanent reflector represents about 10% of total graphite in the core. If too much graphite is removed from the outer reflector then increased neutron leakage from the reactor core through the PSR will occur. To overcome the increased leakage, we have to add more fuel or we have to remove some burnable poison from the reactor. In addition, it would be difficult to limit the neutron dose to the reactor vessel if an excessive amount of graphite removal from the PSR is required for this modification.

The total reactor vessel pressure drop is another important consideration in the design of the new coolant inlet flow configuration. The total reactor pressure drop is caused by wall roughness, entrance loss coefficient, exit loss coefficient, internal loss coefficient etc. The pumping power is proportional to volumetric flow rate and total pressure drop of the system. For the original design the pressure drop within the core was 50.8 KPa (from Table III) and the pumping power was ~2%[3]. This pumping power corresponds to the total pressure drop of the primary loop. In addition to the reactor vessel, the primary system has pressure drop of about ~20 KPa, which occurs out side of the reactor vessel. Therefore, the total pressure drop that corresponds to the pumping power is ~70.8 KPa. If the pumping power of the system is allowed to increase by up to 3%, which is still below the pumping power of a PWR (~4%-5%), then the total allowable pressure drop for the entire primary loop becomes (70.8 X 1.5 =) 106.2 KPa. If the modified system has the same velocity, mass flow rate, loss coefficient etc as of the original design, then with an increased pumping power of 3%, the pressure drop within vessel would be allowed to increase to (106.2 – 20 =) 86.2 Kpa.

The difference between the coolant flow velocity through the reflector coolant passage and the coolant velocity through the reactor core is also an important design consideration for the new inlet flow configuration. If there is too much difference between these velocities, there may be increased lateral pressure gradients between the core and reflector which increases the potential for flow-induced vibrations and cross flow. Also, at this point no study has been done to assess the maximum allowable

coolant velocity through the nuclear grade graphite. Therefore, limiting the coolant inlet velocity in the reflector region to something close to that of the core velocity should be a conservative approach.

The development and evaluation of this new coolant flow path has been done in several steps. In the first step the coolant inlet velocity and amount of graphite removed to create the inlet flow path are optimized. Based on the optimization results and the available thickness of permanent outer reflector, the number of coolant inlet holes and their dimensions are selected in the second step; also pressure drops are calculated more accurately. In the third step, the relevant changes for the radiation and conduction heat transfer calculation in the ATHENA model are made. Due to this final step of calculation, the ATHENA model would take in consideration the removal of graphite from reactor core during the calculation of radiation and conduction heat transfer in the core. The model also would consider the new coolant path exactly at its physical location. As a result, the new ATHENA model should compute accurate temperature profiles within the core and reflector region, and accurately predict the heat transfer from the core and vessel region to the RCCS during normal operation and during transient.

C. Optimization of Amount of Graphite Removal and Coolant Velocity

Figure 13 shows the nodalization of reactor vessel used for optimization of coolant velocity and the amount of graphite removal. Volume 132 is the new coolant flow path through the outer permanent reflector. In this modified coolant flow path, the outlet of the flow is fed to the outlet side of the core inlet plenum instead of inlet side as of the original model. This is because if the outlet is fed to the inlet side of core inlet plenum (component 140), the hot inlet helium will transfer heat to the upper head region of reactor vessel directly. The reactor vessel wall also needs to be insulated from the coolant in the inlet plenum (component 110). These modifications are incorporated in the ATHENA model accordingly. Volume 130 is modeled as a stagnant volume with the inlet connected to the outlet of the vessel inlet plenum but the outlet is no more connected to the core inlet plenum.

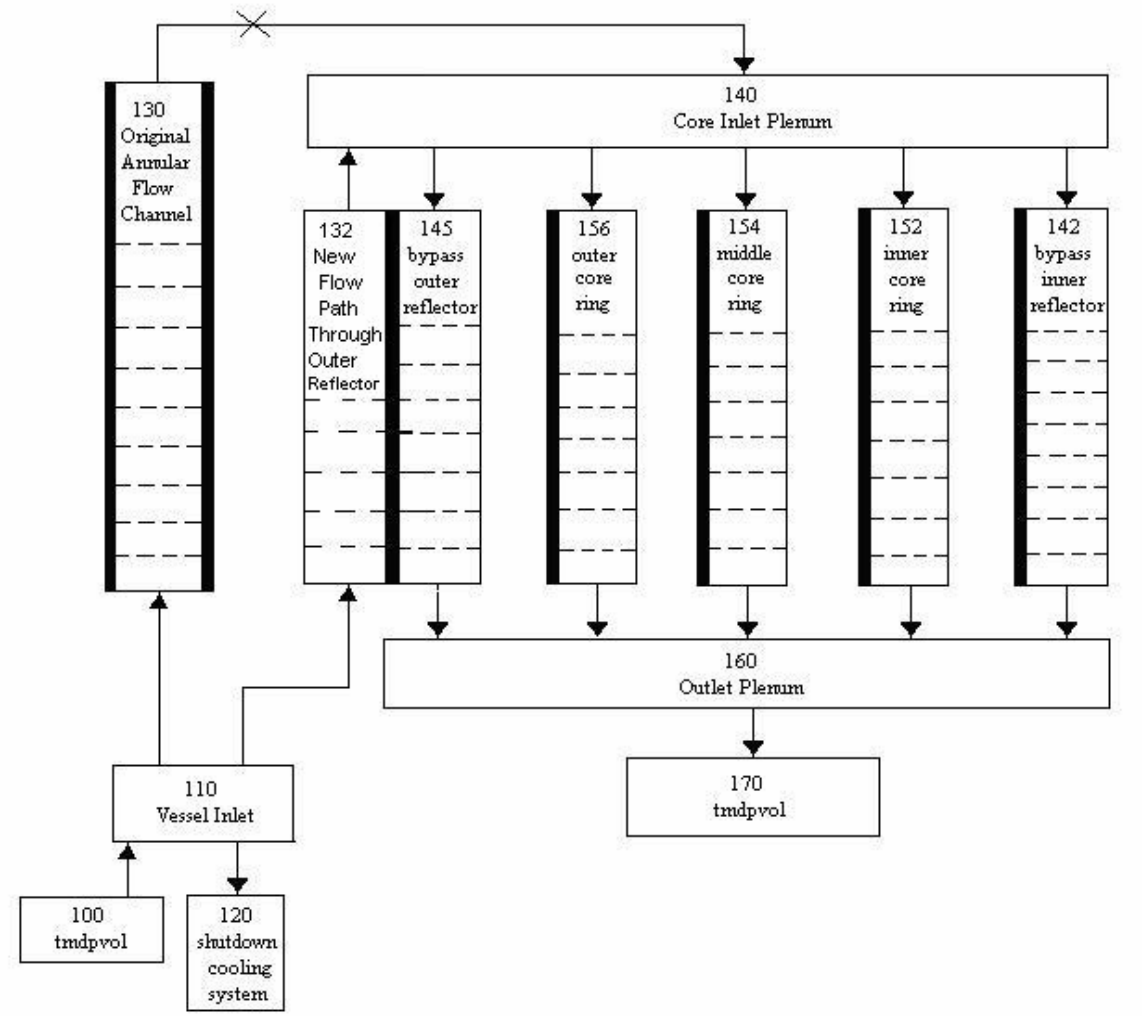

Fig. 13. ATHENA nodalization for reactor primary to optimize pressure drop, inlet flow area and inlet coolant velocity.

The heat structures are closely associated with the hydrodynamic volumes in the RELAP5-3d/ATHENA model. Any heat structure is solid and there is no flow. The hydrodynamic volume can be connected to either the left side (inner surface) or right side (outer surface) of a heat structure. The total system response depends on heat

transfer between the structures and the fluid. The temperature distributions in the structures are often important requirements of the simulation.

During the optimization step, the outer replaceable reflector, permanent side reflector and the reactor core barrel are modeled as a single heat structure as in the original model. In this case this heat structure is associated with three hydrodynamic volumes. Volume 145 represents the bypass flow through outer reflector which is downward, volume 132 is the new coolant upward flow, and volume 130 is the stagnant helium. The bypass through the outer reflector and the new coolant flow through permanent side reflector are modeled as the left and right volumes respectively. The stagnant volume is considered as an adiabatic. This approximation is made only for the first step of the analysis, i.e. during the optimization of pressure drop, amount of graphite removal and the inlet velocity. This approximation will give us a conservative vessel temperature which is higher than the actual vessel temperature. To calculate the vessel temperature precisely in the subsequent calculation,, this heat structure is divided into two heat structures which is discussed later.

During optimization, a higher flow area for the inlet flow (volume 132) through the permanent outer reflector will result in a higher percentage of graphite withdrawn from the permanent side reflector. A reduced cross section area for the inlet flow on the other hand will result in a larger pressure drop and the higher inlet velocity. Sensitivity studies are performed to determine the effect of changes in total cross sectional area for coolant inlet flow, number of holes and dimensions of each hole on the steady-state vessel temperature. Table IV shows the results of this study.

In the original ATHENA model of the MHR, the inlet flow was assumed to occupy the entire region between the core barrel and the reactor vessel. The dead helium volume was eliminated and was included with the inlet flow path. The total cross sectional area in the original ATHENA model for the inlet flow was 4.6193 sq meter.

TABLE IV Optimization of Flow Area, Inlet Velocity and Pressure Drop

Case Number	Total Flow Area for Inlet Coolant (m^2)	Graphite from Outer Reflector Reduced by (%)	Number of Holes	Hydraulic Diameter (m)	Total Pressure Drop (KPa)	Steady State Fuel Temp (C)	Steady State Vessel Temp (C)	Heat Loss to RCCS (MW)	Max Core Velocity (m/sec)	Inlet velocity (m/sec)
1	2.30965	14.13	36	0.2858	57.9	1106	454	2.5	53.2	34.83
2	2.285085	13.98	30	0.31142	57.8	1106	454	2.5	53.2	35.2
3			24	0.3482	57.7	1106	453.6	2.5	53.2	35.2
4			18	0.40204	57.5	1106	453	2.5	53.2	35.2
5	1.52339	9.32	24	0.3482	60.5	1106	453.8	2.5	53.2	52.81
6			18	0.3283	60.1	1106	453.5	2.5	53.2	52.81
7			12	0.40204	59.7	1106	453	2.5	53.2	52.81
8	1.14254	6.99	24	0.2462	64.9	1106	453.7	2.5	53.2	70.43
9			18	0.2843	64.1	1106	453.4	2.5	53.2	70.42
10			12	0.3482	63.1	1106	453	2.5	53.2	70.42
11	0.57127	3.495	24	0.1741	102.0	1106	453.5	2.5	53.5	141.1
12			18	0.201	97.0	1106	453.2	2.5	53.4	141.1
13			12	0.2462	91.4	1106	452.8	2.5	53.4	141.0

For Case1, the total coolant inlet flow area is taken as $2.30965m^2$ which is half of the inlet flow area in the original ATHENA model. For cases 2 to 4, the total flow areas are taken equal to the total flow area through the reactor core including the bypasses. As seen in Table IV, the flow areas in cases 1 to 4 are close to each other. For cases 2 to 4, the total flow area and the amount of graphite removed are constant, but the number of

holes and their dimension are different. For cases 5 to 7, 8 to 10 and 11 to 13, the total flow areas are taken as 66.67%, 50% and 25% of total flow area through the reactor core.

Column 3 of the above table shows the percentage of graphite removed from the outer reflector in the different cases. Column 6 shows the total vessel pressure drop for each case which is the sum of the pressure drop at the inlet flow path and pressure drop in the reactor core. Pressure drop out of the vessel is not included here. Out of these total pressure drops shown in column 6, about 55 KPa pressure drop occurs in the core and the rest of the pressure drop occurs within the inlet flow path region.

By observing the total pressure drop in the above table (column 6) it can be concluded that, total core pressure drop is changed with the change of total inlet flow area. It can also be noted here that, the maximum velocity through core (column 10) as calculated by ATHENA is not substantially changed by these modification of coolant inlet path (except for small changes in core velocity, due to changes in the coolant density in the core). Therefore, for each case, the velocity through the core is almost the same, but the inlet velocities (column 11) are different for different inlet flow areas.

The inlet pressure drops (not shown separately in the table) are also different due to different hydraulic diameters (column 5). For cases 1 to 10, the inlet pressure drop (column 6 minus ~55 KPa) is a small fraction of core pressure drop. As a result, with the change of number of holes for a constant inlet flow area, the changes in total pressure drop are insignificant. But for cases 11 to 13, pressure drops within the inlet section are high compared to the pressure drop in the core. In these cases (case 11 to 13) the change in the number of holes for a constant inlet flow area results a change in the calculated hydraulic diameter, which in turn produces a significant change in the inlet pressure drop and the total core pressure drop.

The pumping power is the product of coolant volumetric flow rate and pressure difference. Table IV shows the pressure drop within the vessel only. The pressure drops within primary system but out of vessel, i.e. the pressure drop in the intermediate heat exchanger and in the primary system piping are not included here. We intend to keep the

pressure drop in the vessel within ~90 KPa to limit the pumping power to within about 3% of the total core power, which is reasonable for the MHR. Column 7 shows the pressure drop within the vessel for each case. We also want to limit the coolant inlet velocity (column 11) and coolant velocity through the reactor core (column 10) to approximately the same range.

Considering all limiting criteria it can be concluded from Table IV that, with the removal of about 10% of graphite from outer reflector which gives a flow area of ~1.53 m^2, the inlet velocity would be consistent with the velocity in the core. The steady-state vessel temperatures shown in column 8 are not accurate; it is higher than the actual vessel temperature. The details modifications of the ATHENA model to predict the accurate vessel temperatures have not been implemented at this point and will be performed in the subsequent sections.

At this point in this analysis process, the pressure drop is reasonable (~60 KPa) but the hydraulic diameters and the pressure drops are based on some simplifying assumptions regarding the number of holes and their dimensions (column 4 and 5), We may end up with a small different pressure drops if the number of holes in the details calculation (which is performed in the following sections) for the coolant inlet scheme is different than those in the above table. A reduced hydraulic diameter will also result in a higher pressure drop and vice versa. To make the inlet flow area and dimension of holes more specific, a closer-look to the geometry of outer permanent reflector is necessary.

The radial thickness of outer permanent reflector is not constant throughout the periphery of the reactor core. It varies from about 11 inches to 6.5 inches. Out of this available thickness, we have to leave 1 inch at outer edge next to the core barrel for boronated pins. Leaving an additional inch at the inner side of the reflector for structural integrity, the holes for coolant flow can be made with a diameter of ~4 inches to ~9 inches. Finally a total of 72 holes with diameters of 4 inches (10.16 cm), 6 inches (15.24 cm) and 8 inches (20.32 cm) are selected as shown in Table V.

TABLE V Final Selection for Coolant Flow Configuration

Total Flow Area for Inlet Coolant (m^2)	Graphite from Outer Reflector Reduced by (%)	Number of Holes for each sizes		
		10.16 cm	15.24 cm	20.32 cm
1.6417	10.04	18	18	36

The average area of each hole is:

$$\bar{a}=\frac{1.6417}{72}=0.0228\ m^2$$

where

1.6417 is the total cross sectional area of coolant flow path

72 is the total number of holes

From this we have the average or equivalent hydraulic diameter of 0.170386 m

The average radial distance from the inner face of reactor core barrel to the center of these coolant holes is:

$$\frac{4''\times 18+6''\times 18+8\times 36}{72}+1''=7.5''=0.1905\ m$$

where

18 and 36 are number of holes of corresponding sizes

4", 6" and 8" are diameter of holes

72 is the total number of holes

1" is thickness of permanent side graphite that is left for the boronated pins

D. Radiation and Conduction Heat Transfer Calculation

Up to now the outer replaceable reflector, PSR and core barrel were modeled as a single heat structure in the ATHENA model. The inlet flow is modeled at the right boundary (outer face) of this heat structure. Since in the physical reactor, the stagnant helium (the original annular passage) is on the right boundary of the core barrel and the inlet helium has a much higher temperature than that of the stagnant helium, this assumption artificially increases steady-state vessel temperature. To overcome this situation and calculate the vessel temperature correctly, the replaceable outer reflector, the PSR and the core barrel are modeled as two different heat structures. The separation point is 0.1905m from the inner face of the core barrel as calculated and shown above. This separation point is likely to be through the center of the new coolant holes and through the outer permanent reflector.

Therefore, the heat structure for 'outer reflector-inner region' includes the replaceable outer reflector and a portion of the permanent side reflector. This heat structure uses the new coolant path as its right boundary and the bypass flow as the left boundary. The heat structure for the 'outer reflector-outer region' includes the rest of the permanent side reflector and the core barrel. This heat structure uses the new coolant path as its left boundary and the stagnant helium as the right boundary. With this splitting of heat structure for the outer reflector of the original ATHENA model, the new coolant path is modeled at its physical location in the modified ATHENA model.

To calculate the volumetric heat capacity, the coolant holes are considered as homogenized throughout an annular portion of the permanent side reflector. The density of graphite in that portion of the permanent side reflector is reduced to account for the reduction of graphite and for the reduction of heat capacity of the permanent side reflector. These reductions were made with the percentage at which the graphite from permanent side reflector is reduced or removed due to the addition of these new coolant holes. Figure 14 shows a view of the portion of the reactor core with the location of new coolant holes and the new heat structure model for the outer reflector and the reactor core barrel to calculate the heat conduction.

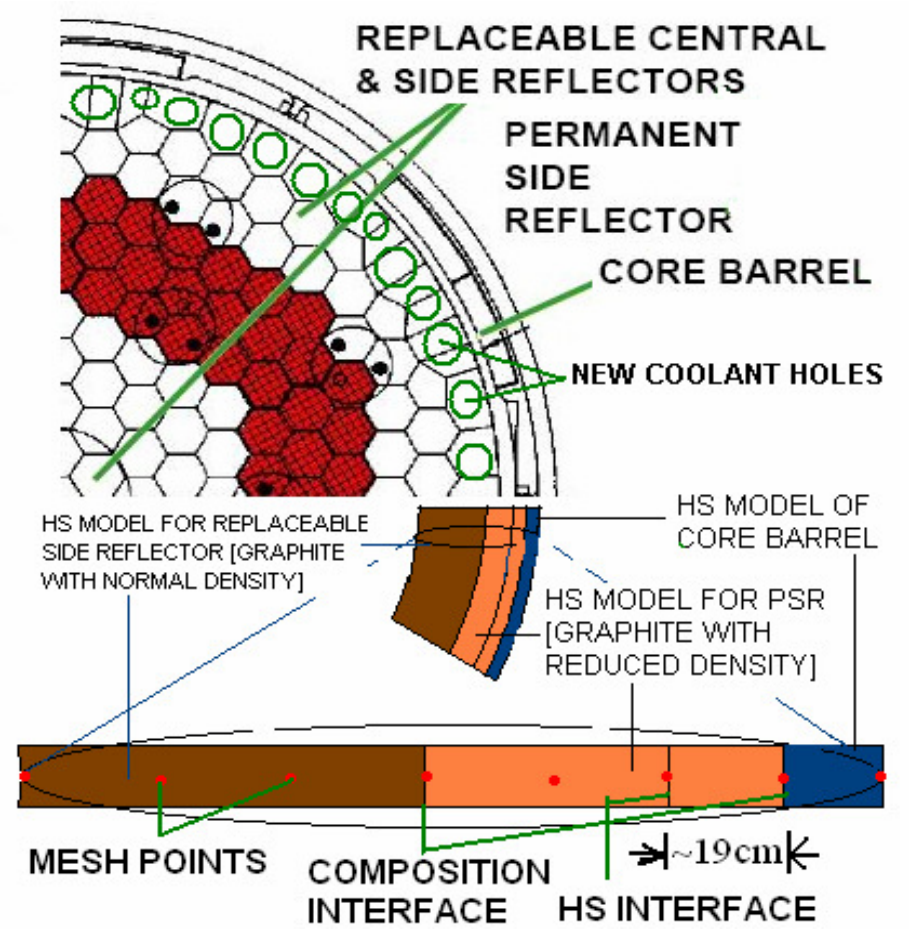

Fig. 14. HS model for PSR and core barrel and the location of new coolant holes.

Radiation heat transfer is calculated as in the original ATHENA model except for the radiation from the core barrel. In the original ATHENA model, the core barrel was an integral part of the heat structure for the outer reflector but it is included in outer reflector outer region in this modified model. The final modified nodalization for the reactor vessel system as used in this calculation which includes the new coolant path through outer permanent reflector is shown in Figure 15.

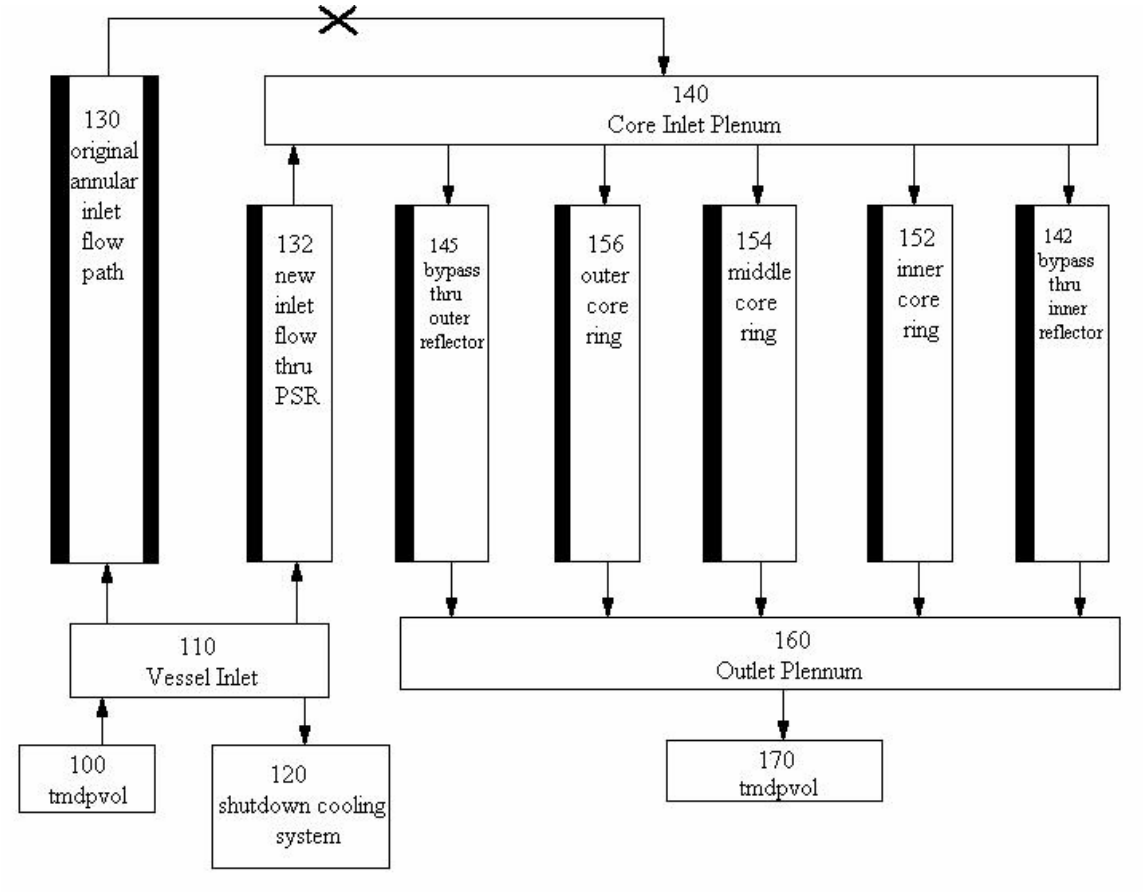

Fig. 15. ATHENA nodalization for reactor primary with modified coolant flow.

The tedious part of performing the radiation heat transfer calculation is finding the view factors. Two restrictions are imposed for the calculation of radiation heat transfer.

- The view factors from each surface to all other surfaces must sum to 1. i.e.

$$\sum_{1}^{n} F_{im} = 1.0$$

- To conserve energy, the area times the view factor for each surface i to any other surface m must be equal to the area of m times the view factor from m to i. This restriction is known as the reciprocity rule and is expressed as:

$$A_i F_{im} = A_m F_{m1}$$

The conduction enclosure model calculates heat transfer from one heat structure to another. Gap conductance (G) is used to characterize the thermal connection between heat structures in the conduction enclosure model. If the surface node i of a heat structure thermally coupled to the surfaces node of m of another heat structure, then the conduction enclosure surface heat flux is calculated by using equation:

$$Q = G A_i \Delta T F_{im}$$

where

Q = heat transfer rate (W)

G = gap conductance (W/m^2-K)

A_i = surface area of face i

F_{im} = view factor between the heat structure i and the heat structure m, or the fraction of the surface area of heat structure i in contact with the heat structure m.

The model can be used to simulate multidimensional heat conduction in a lumped parameter fashion. The gap conductance is provided for conduction enclosures. The gap conductance is computed as the thermal conductivity divided by the appropriate length. For axial conduction, the length is the distance between the heat structure centers. For a gap between structures, it is the spacing between the adjacent structures. An energy balance is performed on conduction enclosures to ensure that the model is working as desired. View factors to calculate heat transfer using the gap conduction

model are calculated and conservation of energy is evaluated using the reciprocity rule. All those view factors are introduced into the ATHENA model.

E. Optimized New Coolant Scheme and Steady-State Calculation

With the optimized new coolant configuration the steady state calculation is performed first. Table VI shows the ATHENA calculated results, which include the steady-state vessel temperature, pressure drop, coolant inlet velocity, steady-state fuel peak temperature, etc for the modified coolant configuration. As expected the pressure drop is increased from 56 KPa to 61.7 KPa. Since the core design is the same, the pressure drop across the reactor core remains the same and the additional pressure drop occurs in the new coolant inlet path.

TABLE VI Final Optimized Coolant Flow Configuration

Total Flow Area for Inlet Coolant (m^2)	Graphite from Outer Reflector Reduced by (%)	Number of Holes for each diameter			Hydraulic Diameter (m)	Total Pressure Drop (KPa)	Steady State Fuel Temp (C)	Steady State Vessel Temp (C)	Heat Loss to RCCS (MW)	Max Core Velocity (m/s)	Inlet velocity (m/sec)
		10.16 cm	15.24 cm	20.32 cm							
1.6417	10.04	18	18	36	0.170386	61.7	1106	421	2.13	53.2	49.1

The steady-state vessel temperature is reduced from ~541 ^{0}C (as shown to Table III) to ~421 ^{0}C. Due to this reduced vessel temperature the heat loss through the reactor vessel wall to the RCCS is also reduced from ~4.5 MW (as shown in Table III) to 2.13

MW. Up to this point, all calculated parameters from the ATHENA analysis are found to be within acceptable range.

A further reduction of vessel peak temperature below 421 ^{0}C while keeping the coolant inlet temperature as high as 590 ^{0}C, is not likely. Therefore, a reduction of vessel temperature during normal operation by reducing the coolant inlet temperature will be evaluated in the following chapter. The transient calculation for this modified coolant scheme discussed in this chapter will be followed by that task.

CHAPTER V

OPTIMIZATION OF NEW CORE DESIGN

A. Block Design of MHR

The MHR consists of a number of hexagonal graphite blocks. Each block has a side length of 0.207827 m. Each block has a total of 216 holes for control rods, where 6 holes are filled with burnable poison rods. In the current graphite block design 10 fuel rods are accommodated in a row between two opposite sides of a hexagonal block. This design is referred as 10 row block design. For the case with 12 fuel rods in a row between two opposites side of the graphite block, the design is referred as 12 row block design.

With the current graphite block core design, the maximum ΔT across the reactor core would be ~360 ^0C[3]. Due to this limiting criterion, for MHR calculations in Chapter IV, the core inlet temperature was set to 590 ^0C for a core outlet temperature of 950 ^0C. The inlet coolant temperature is one of the main determinants of the steady-state vessel temperature. For a constant core outlet temperature, with the reduction of core inlet temperature, the total mass flow rate is decreased to conserve the reactor power. Due to this reduced mass flow rate, the overall Reynolds number is reduced which results in reduced forces convection heat transfer from the fuel rod surfaces to the primary coolant. Since the coolant temperature is the convective boundary for a sub-channel in the core, the reduced heat transfer results in higher fuel centerline temperatures for the same coolant temperatures.

For a constant coolant hole centerline temperature the fuel surface temperature decreases with the decrease of both coolant hole diameter and thickness of graphite between fuel rod and coolant hole. Also, for a constant fuel surface temperature the fuel centerline temperature decreases with the decrease in fuel rod radius.

The reactor inlet and outlet temperatures of 590 ^0C and 950 ^0C respectively correspond to a vessel temperature of 541 ^0C which is reduced to 421 ^0C by the

alternative coolant scheme through the PSR as discussed in Chapter IV. The peak vessel temperature needs to be reduced to ~350 - 360 ^{0}C to use standard LWR vessel material for the MHR vessel material.

The purpose of this part of the study is to verify different block designs and optimize the design modification to allow an increased ΔT across the reactor core and reduce the coolant inlet temperature while keeping the coolant outlet temperature as high as 950 ^{0}C, and maintaining the PFCT during normal operation within ~1250 ^{0}C. The reduced inlet temperature will result in a reduced PVT during normal operation.

The modifications and optimizations of block fuel-element and the fuel rods design have been performed. The dimensions of fuel rods, coolant holes and triangular pitch have been changed. The thermal properties for new fuel rods have been calculated and new inlet boundary conditions have been introduced using thermal hydraulic codes. The peak vessel temperature and the peak fuel centerline temperature have been calculated with all these modifications. The transient response for the MHR with this new block core design has been calculated and compared to that of the original design.

B. POKE and ATHENA Calculations for GT-MHR

In addition to RELAP5-3D/ATHENA code, the POKE[19] thermal hydraulic code which was developed at General Atomics is used for this modification. POKE is used to optimize the peak fuel centerline temperature and RELAP5-3D/ATHENA is used to calculate the steady-state peak vessel temperature and to evaluate the transient behavior of the MHR with the modified reactor core and the graphite blocks design.

POKE computer code was developed at GA for simplified and steady state thermal hydraulic analysis of MHR. In the POKE analysis, the reactor is assumed to consist of a number of regions, each containing parallel coolant channels connected to a common inlet and outlet plenum. Figure 16 shows the layout of the core used in the POKE model.

The core is designed with 120-degree symmetry and the control rods are also operated symmetrically. Due to this symmetry one third (34 columns) of the core is

modeled. Each column consists of an upper reflector, active or fueled section and a lower reflector. POKE can calculate the steady-state coolant mass flow, pressure drop, coolant and moderator temperature, fuel temperature distribution, etc, for this MHR. A precise temperature distribution from fuel centerline to the bulk coolant temperature is possible to calculate using the POKE model.

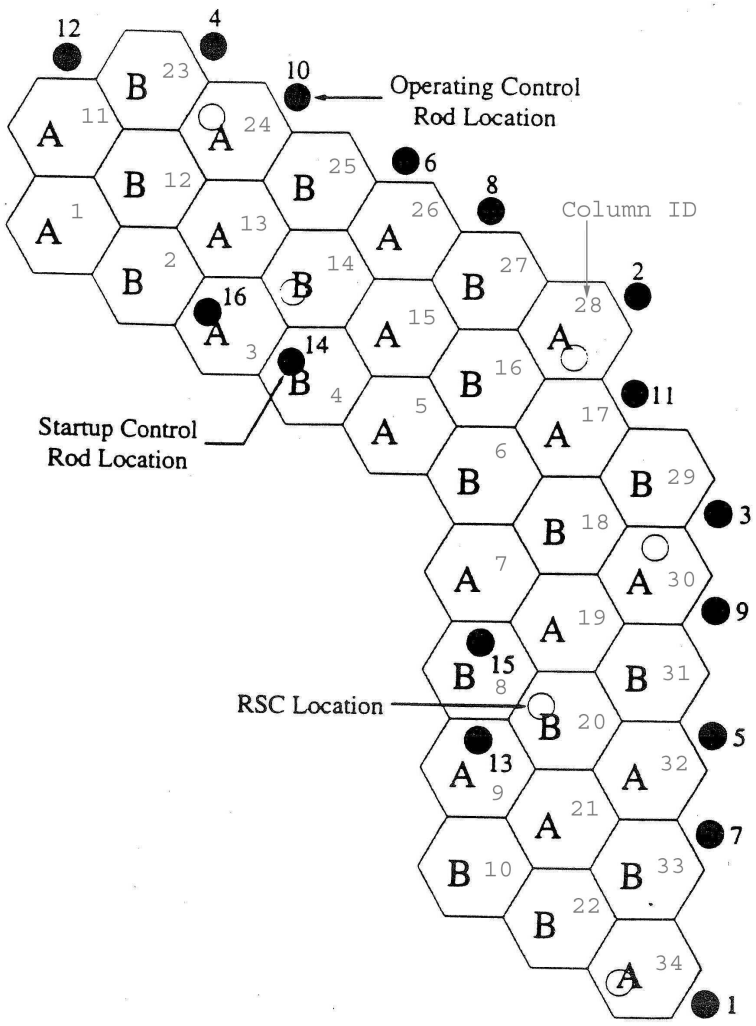

Fig. 16. GT-MHR core layout for POKE analysis.[9]

As discussed in Chapter IV, the RELAP5-3D/ATHENA model includes inner reflector, active core, upper and lower reflector, outer reflector, core barrel, vessel wall, RCCS, etc. On the other hand, the POKE model includes the active core and upper and lower reflector only. Before the RELAP5-3D/ATHENA and POKE models are used for this modification, some other significant differences in modeling and calculation between these two models are discussed.

The equivalent thermal analysis models for the reactor core used in the POKE and ATHENA analyses are not the same. Figure 17 shows the equivalent annular model used in RELAP5-3D/ATHENA to represent the hexagonal sub-channel and a triangular element of a unit cell used for the thermal analysis in POKE. For each region, the thermal analysis model of POKE uses an average coolant channel that is coupled to an adiabatic unit cell. For the prismatic fuel block, the unit cell is a right triangular element containing one third of the area of a fuel compact and one sixth the area of the coolant hole.

In ATHENA, a coolant channel is coupled with a hexagonal sub-channel as shown in Figure 17. In both calculations, the coolant channel temperature is used as a boundary condition for convective heat transfer. Fuel and moderator temperatures are calculated based on that. For the same bulk coolant temperature both models will predict exactly the same temperature difference between bulk coolant temperature and fuel rod centerline temperature.

The results of the calculations from these two codes for identical input boundary conditions are compared with each other and are verified. Due to different analysis models and different output parameters, direct comparison of some of the parameters is beyond our scope. The inlet temperature, pressure, bypass flow, etc, are set the same, and the power distributions are set identical into both models. The calculated results from one code such as mass flow rate, flow distribution, temperature, pressure drop, etc, are compared with the corresponding results from the other code.

POKE can be run in several modes depending on the user's interest or boundary conditions specified. In this study, the coolant flow rate, inlet pressure and temperature

are specified. The POKE model is used to calculate the flow distribution, and the temperature of the coolant, fuel and moderator at each axial location for each column. In addition, POKE calculates the maximum fuel centerline temperature, maximum moderator temperature, maximum fuel surface temperature, and core average temperature for the fuel and moderator.

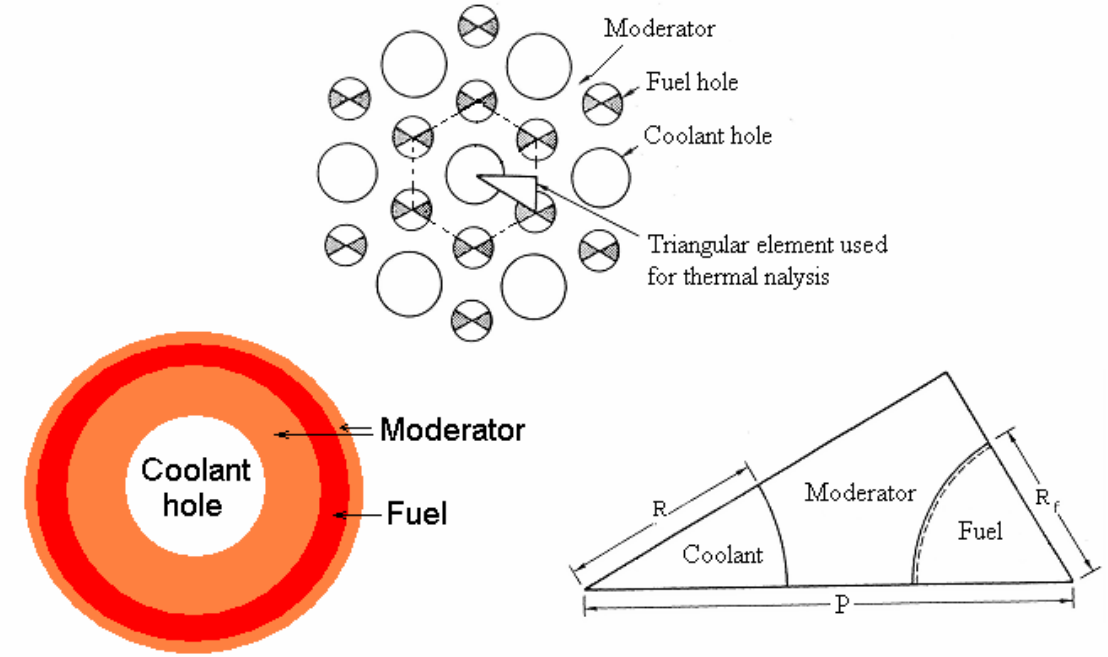

a) Equivalent annular model of hexagonal sub-channel in ATHENA

b) Triangular element of a hexagonal sub-channel used for thermal analysis in POKE

Fig. 17. Thermal analysis model used in ATHENA and POKE models.

The power distribution is the key input for reactor analysis using both the POKE and the ATHENA codes. The POKE model uses a comparatively more detailed power distribution. The ATHENA model which is capable of transient analysis is not capable of calculating fuel centerline temperature precisely since the power distribution used for the ATHENA calculation is averaged for all columns in the same ring. ATHENA also calculates the volume average temperature of fuel. The user can specify whether moderator will be included or excluded to calculate the volume average temperature.

In this study, the ATHENA model is run with both options to calculate the volume average temperature of fuel including and excluding the graphite moderator in the core. Using the number of fuel rod in a standard, control and reserve shutdown assembly, the volume fractions of fuel and moderator in each graphite block in the inner ring, middle ring and outer ring are calculated. Using those volume fractions and the volume average temperature calculated by ATHENA, the volume average temperatures of fuel and moderator are calculated and compared with the corresponding temperatures calculated by POKE.

Table VII shows the comparison of some of the parameters in the POKE and ATHENA analyses for the original block (10-row block element) reactor core design. Using the ATHENA model the thermal power loss to the RCCS is calculated and the reactor power in the POKE calculation is reduced to account for heat losses to the RCCS.

The core average temperatures of fuel and moderator calculated by POKE are shown in Table VII. The volume average temperature for fuel calculated in ATHENA and the volume average temperature of moderator calculated from ATHENA results are also shown. The core average temperatures of fuel and moderator in ATHENA and in POKE are close. The difference in peak fuel centerline temperature is mainly due to the different power distributions used in the two models. In addition, the equivalent thermal analysis model, thermal conductivity and bypass flow model used for POKE and ATHENA analyses are different.

TABLE VII ATHENA and POKE Results with Original Block Design

Code used	Temperature ^{0}C		Bypass Flow	ΔP KPa	Core Average Temperature, ^{0}C		PFCT ^{0}C
	Intel	Outlet			Fuel	Mod	
ATHENA	590	950	0.1	56	914.2	896.8	1108
POKE	590	950	0.1	59.7	926	875.9	1207

POKE assumes the thermal conductivity of the fuel and moderator are temperature independent but ATHENA uses temperature dependent correlations for the thermal conductivity of materials, including fuel and moderator. There are also significance differences in the way bypass is modeled in ATHENA and POKE model. In ATHENA bypass flow is only calculated through inner and outer reflectors. The hydraulic diameters of the flow paths through the reflectors are tuned to get a certain fraction of flow as bypass flow. In the POKE model, the inner and outer reflectors are not modeled. Therefore, all bypass flow is considered through the active core in POKE model, and the user can specify (1) the fraction of bypass flow to the total mass flow and (2) the ratio of bypass temperature rise to average core temperature rise in the core.

The POKE model uses a friction factor that corresponds to smooth pipe. The ATHENA model uses wall roughness of 1.51E-5 m, which also corresponds to the roughness of a smooth pipe. The small difference in pressure drop across the reactor core as calculated by the POKE and ATHENA models are due to the differences in modeling assumptions as discussed. In addition, both models include entrance and exit loss coefficients, and orifice loss coefficients, but ATHENA model does not include offset or internal loss coefficients which are included in the POKE analysis.

C. Bypass Flow Optimization

The original ATHENA model assumed 10% of bypass flow, while previous POKE calculations used 20% bypass flow. In this study the same bypass flow is used for both POKE and ATHENA analyses. A sensitivity study is performed to calculate the influence of the bypass flow on the fuel and moderator temperatures.

A similar study was done in the past considering a constant ratio (0.3) of temperature rise of the bypass flow to the average temperature rise of the core flow[3]. In the present study the bypass is varied from 8% to 22% and the ratio of temperature rise of the bypass flow to the average core temperature rise is calculated. The calculation shows that with 10%, 15% and 20% bypass flow, the fraction of power removed by the bypass flow would be 3.45%, 4.78% and 6%, respectively, and the ratios of bypass temperature rise to the average core temperature rise would be 34.5%, 31.8% and 30%, respectively. Figure 18 shows the variation of fuel centerline temperature with bypass flow. For an inlet temperature of 590 ^{0}C, the peak fuel centerline temperatures (PFCT) with 10%, 15% and 20% bypass flows are found to be 1206 ^{0}C, 1231 ^{0}C and 1260 ^{0}C, respectively.

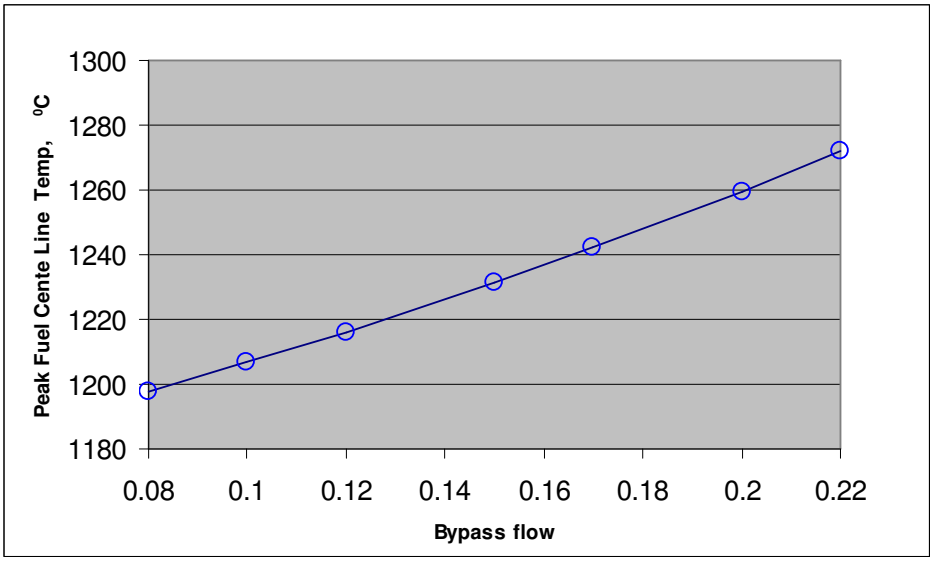

Fig. 18. Variation of PFCT with the variation of bypass flow.

The axial and regional power peaking factors provided by GA are used for this study. A 15% of bypass flow (instead of 10% in previous ATHENA analyses and 20% in previous POKE analyses) is used for the rest of the analyses using both POKE and ATHENA codes. The calculations also show that the core average fuel and core average moderator temperatures increase with the increase in bypass flow.

D. New Core Design; Calculation and Optimization

1. Design Optimization

The calculation for the new graphite block core design for the MHR is performed and the design is optimized. The graphite block dimension is remained unchanged. The numbers of fertile and fissile particles in a single graphite block as well as in the entire core in the 10 row fuel block element design are considered as a reference and are conserved in the new design. From the manufacturing point of view, the fuel rod radius can not be less than 1 cm. For structural integrity, the minimum web thickness (i.e. the thickness of graphite between fuel rod and coolant hole) would be 0.45085 cm. The pressures drop needs to be maintained within acceptable limits during this optimization. In addition, PFCT and PVT both need to be within allowable ranges during normal operation and under transient conditions.

The original 10-row element core design is compared with a new 12-row element core design in Table VIII. The numbers of fuel rods, coolant holes, and their dimensions, etc., are presented for a standard assembly, control assembly and for a reserve shutdown assembly. The ratio of total graphite to total fuel volume in the core is increased from 3.147 to 3.72. Since the fuel rod radius is reduced from 0.00635 m in the 10-row block core design to 0.005 m in the 12-row block design, the volume of fuel compact is reduced from 0.00126 m^3 to 0.0011 m^3. The number of fuel compacts and the number of fuel particles per fuel compact are assigned in such a way that the total number of fuel particles in the core of the new design is conserved.

TABLE VIII Block Design Parameters

Parameters	10 Row Block			12 Row Block		
	Standard	Control	RSC	Standard	Control	RSC
Number of fuel rods	210	186	186	300	266	266
Number of large coolant holes	102	88	88	147	128	128
Number of small coolant holes	6	7	7	6	7	7
Fuel rod radius (m)	0.00635			0.005		
Large coolant hole radius (m)	0.0079375			0.0063115		
Small coolant hole radius (m)	0.00635			0.005		
Block side length (m)	0.207827					
Minimum web thickness (m)	0.0045085					
Triangular pitch (m)	0.018796			0.01582		
Number of assembly/layer	72	12	18	72	12	18
Graphite/fuel area	2.9973	3.4576	3.4508	3.5639	4.053	4.1468
Graphite/coolant hole area	3.8061	4.4501	4.5577	4.4506	5.0015	5.229
Fuel/Coolant area	1.2698	1.2872	1.2872	1.2488	1.261	1.261
Flow area (m2)	0.02095	0.01830	0.01830	0.01887	0.01657	0.01657
Graphite/fuel area; entire core	3.1473			3.724		
Fuel max temp	1231.3			1199.9		
Coolant maximum temp	1126			1123.8		
Fuel compact volume (m^3)	0.00126			0.0011		
Number of fuel compact	3126			4460		
Fissile particle/compact	4310			3021		
Fertile particle/compact	520			364		
Fissile volume fraction	0.17166			0.19619		
Fertile volume fraction	0.02786			0.03184		
Matrix volume fraction	0.39			0.39		
Shim volume fraction	0.41048			0.38197		

2. Thermal Properties for Fuel Rod

The thermal properties for the fuel rod in the new core design have been calculated and are used in both the POKE and ATHENA analyses. Using the available correlation[20] the temperature dependent thermal conductivity for the fuel rod is calculated. The correlation is developed from curve fit of experimental data where in addition to fuel temperature, the shim and matrix volume fractions are considered of the thermal conductivity for the fuel rods.

In ATHENA, as mentioned before, the fuel rods are modeled as an equivalent annular ring, where the thickness of fuel rod in the equivalent model is less than the actual radius of the fuel rod. Therefore, the thermal conductivity of fuel is reduced by an appropriate factor to achieve the same temperature rise across the fuel rod. Like other thermal hydraulic analyses[21] for the high temperature reactor, a comparison of the exact solution for the temperature rise across a cylinder to the exact solution for the temperature rise across an annular ring with an outer adiabatic surface is considered to calculate this factor. For this calculation this factor is found to be 0.37.

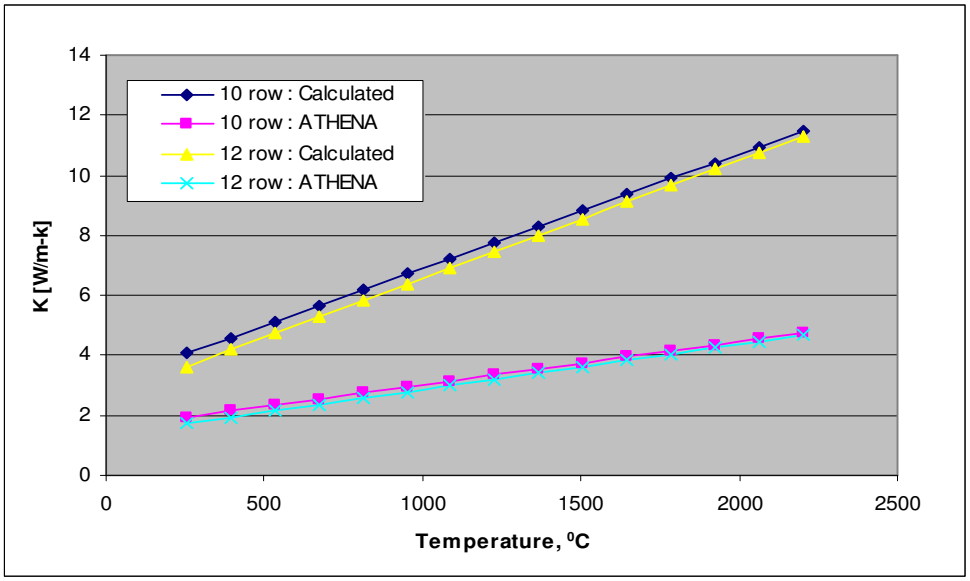

Fig. 19. Thermal conductivity of fuel.

Figure 19 shows the calculated thermal conductivity and the thermal conductivity used in the ATHENA model for the fuel rod in the new core design having 12-row fuel element. The thermal conductivities of the fuel rods in the original 10-row block core design are also shown in the figure. Since POKE uses a constant (i.e. temperature independent) thermal conductivity, a thermal conductivity which corresponds to a temperature of 1250 ^{0}C (close to the maximum fuel temperature) is used for the POKE calculation as it had been used in the previous calculations.

The specific heat capacity (C_p) of the fuel rods in the new block design is also calculated using the available correlation[20]. According to the correlation, the temperature dependent C_p is calculated as a function of shim volume fraction. Using the density for the each of the fraction of the fuel compact (fuel particles, shim and matrix etc.), the overall density for fuel rod and then the volumetric heat capacity (ρC_p) are calculated for use in the ATHENA analysis. Figure 20 shows the specific and volumetric heat capacities for fuel rods in both designs as a function of temperature. As shown in the figure the specific heat capacity of the new fuel is reduced by about 2.2%, but due to a small increase of density, the volumetric heat capacity remains about the same as the old design.

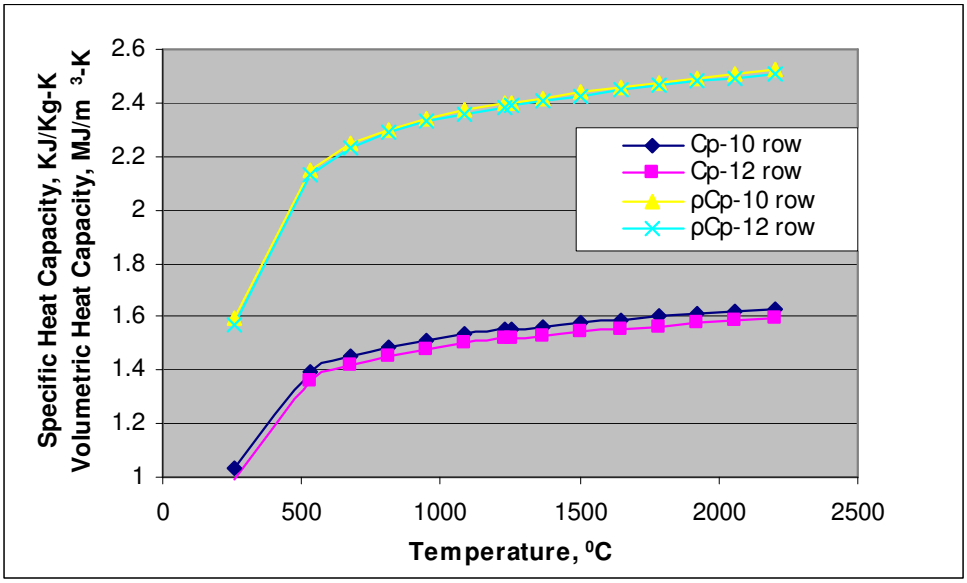

Fig. 20. Specific and volumetric heat capacity of fuel.

3. Radial Temperature Distribution

The radial temperature distribution at the hottest channels for a 10 row and 12 row block design with same inlet boundary conditions are shown in Figure 21. For the same power and the same inlet/outlet temperatures, the peak fuel centerline temperature is reduced by ~32 ^{0}C for the new design. The temperature drop from the fuel centerline to the fuel surface in the 12 row block fuel is reduced due to smaller rod diameter, even though the thermal conductivity of the new fuel rod is reduced by about 2.5%. The total temperature drop from the fuel centerline to the bulk coolant temperature is also reduced due to smaller fuel rod and smaller coolant hole diameter.

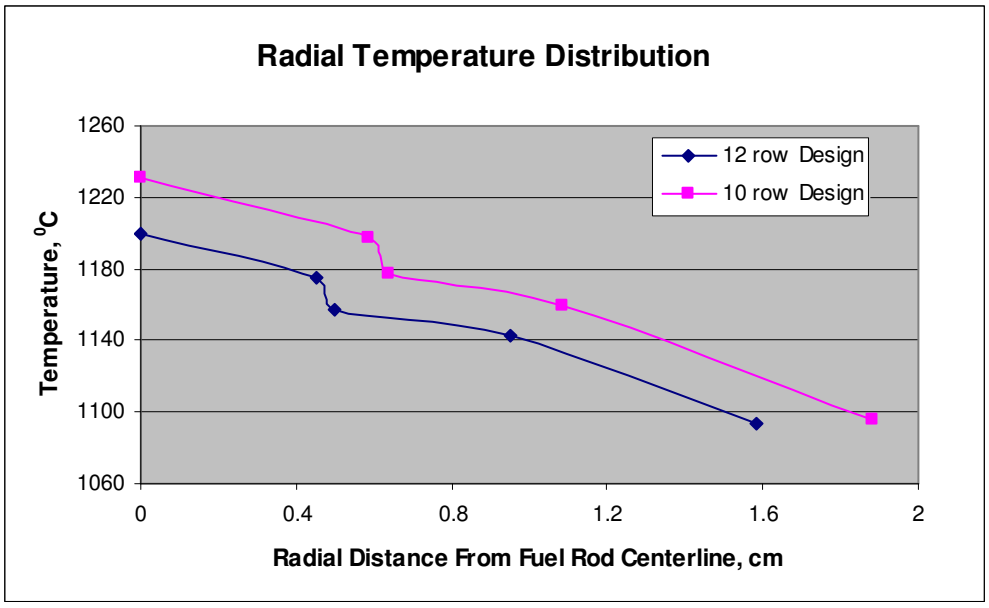

Fig. 21. Radial temperature distribution at hot channel.

4. Inlet Temperature Optimization

The parameters corresponding to the new block design such as fuel rod heated perimeter, coolant hole hydraulic diameter, number of equivalent channel in standard assembly, control assembly and in reserve shutdown assembly have been calculated and incorporated into the POKE calculation. With this new block core design, the fuel

centerline temperature is reduced from ~1231.3 ^{0}C to ~1200.0 ^{0}C for the same inlet temperature of 590 ^{0}C. Therefore, the inlet temperature can be reduced to reduce the steady-state vessel temperature while keeping the PFCT within acceptable limit.

There is a one-to-one relationship between the core inlet temperature and the coolant mass flow rate for a constant reactor power. Using several combinations of inlet temperatures and mass flow rates, the POKE calculations are performed to optimize the PFCT. Figure 22 shows the PFCT for different inlet conditions. This calculation shows that the core inlet temperature can be reduced from 590 ^{0}C to 510 ^{0}C while maintaining the PFCT below 1250 ^{0}C (for a 510 ^{0}C core inlet temperature the peak fuel centerline temperature is 1247.5 ^{0}C). The corresponding mass flow rate is reduced to 265.24 kg/sec. It should be noted here that the reactor power used in this POKE analysis is obtained by subtracting the RCCS loss from the total actual reactor power.

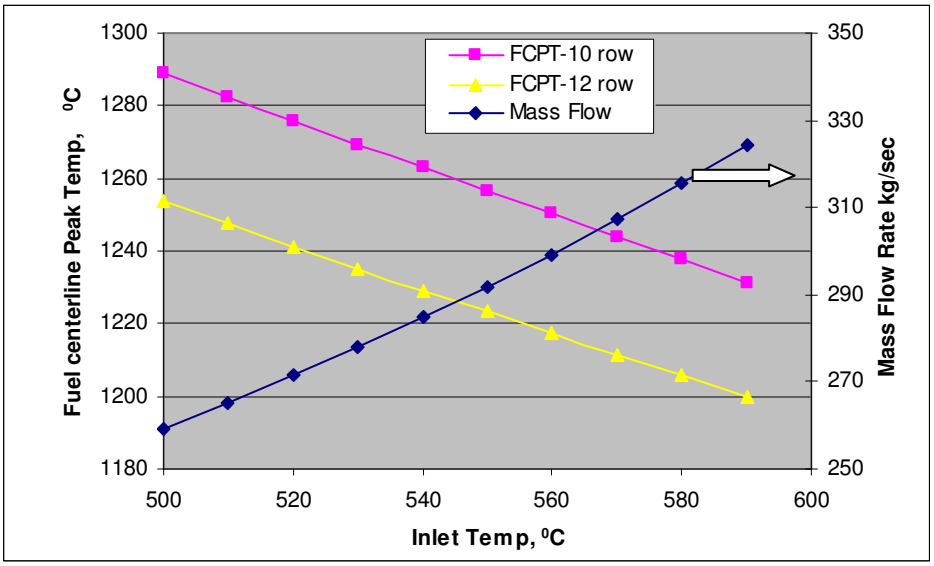

Fig. 22. Variation of PFCT with inlet temperature.

E. Steady State Calculation for New Block Design

Using the new inlet coolant temperature the steady-state calculations for the new design reactor have been performed using both POKE and ATHENA codes. The axial temperature distributions in the hottest channel are shown in Figure 23. The axial distribution of fuel centerline, fuel surface, fuel gap, graphite surface and bulk coolant temperatures are shown for a 12 row block design.

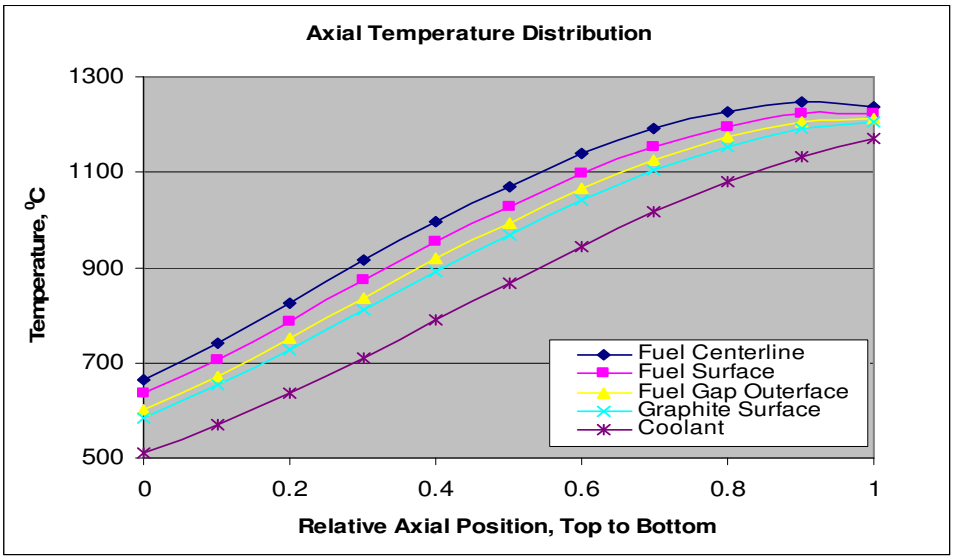

Fig. 23. Axial temperature distribution in the hot channel.

Several combinations of axial and column power distributions have been used to optimize the new block design. The baseline refueling scheme assumes that at the beginning of an equilibrium cycle one half of the core consists of fresh fuel and other half of the core consists of old fuel. The power distribution is flattened by using an appropriate fuel placement scheme. In this case each column consists of both fresh and old fuel at the beginning of an equilibrium cycle.

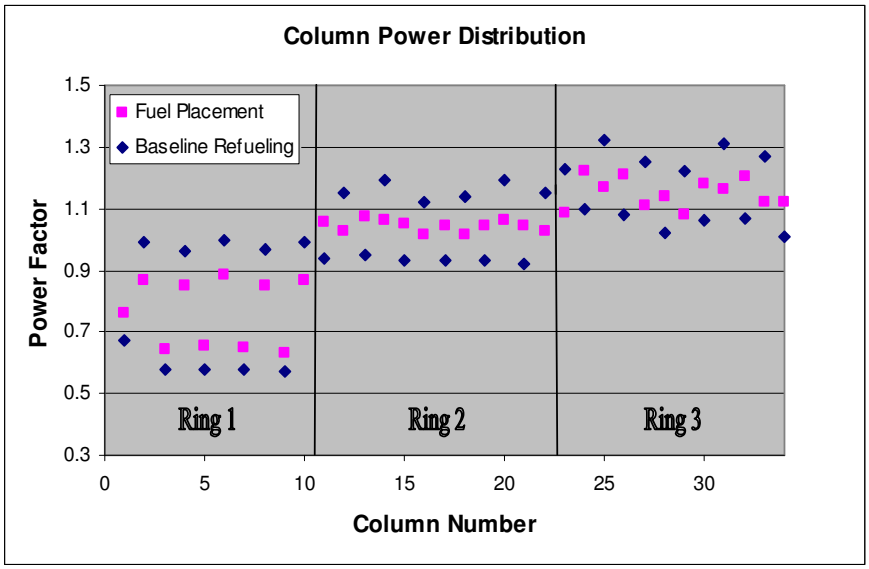

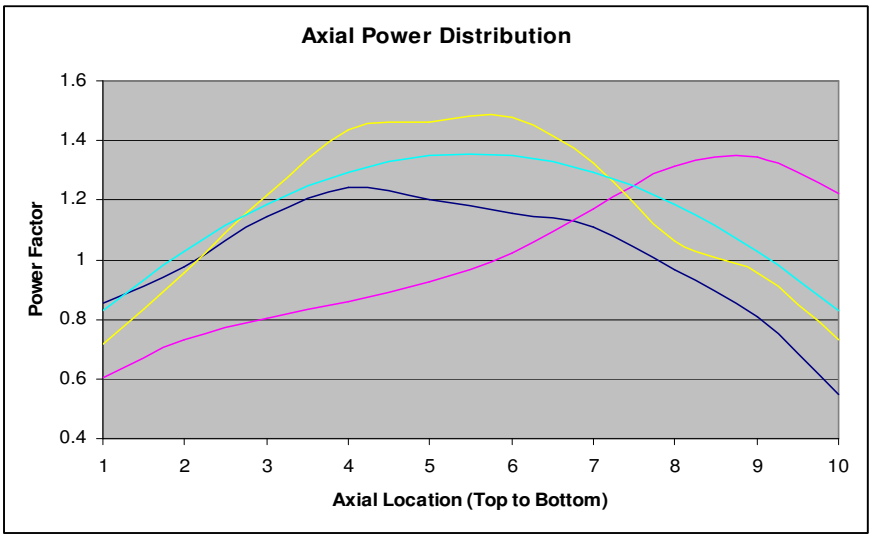

Fig. 24. Column and axial power distributions used for sensitivity study.

The axial power distribution used in this sensitivity study includes a distribution derived from the detailed core power distribution provided by GA. For other axial power distributions, an axial shape, cosine axial shape and bottom peak axial power distribution provided by GA have been used. Figure 24 shows the axial and column power distributions used for these sensitivity studies.

As shown in the figure, both the baseline refueling and fuel placement column power distributions result in the shifting of the peak power from the inner ring to the middle and outer rings. All axial power distributions shown in the figure are close to a cosine distributions except the bottom peak distribution which provides the maximum fuel centerline temperature of ~1349.5 ^{0}C.

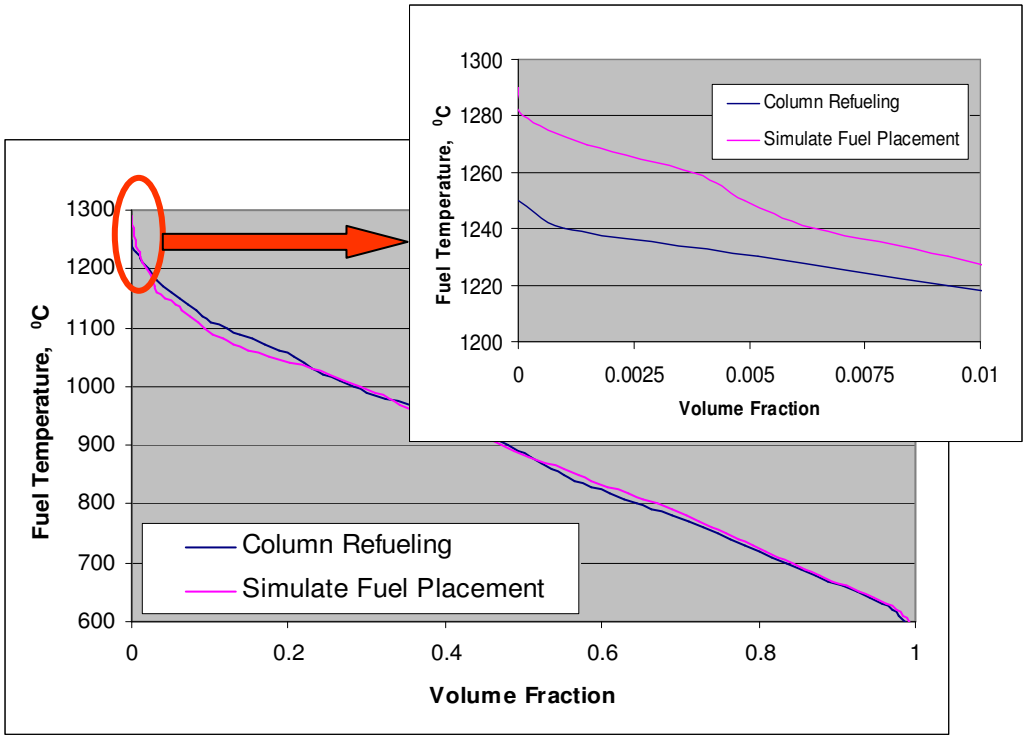

Fig. 25. Fuel temperature distribution as a function of fuel volume fraction.

Figure 25 shows the fuel temperature distribution as a function of fuel volume fraction for both types of column power distributions. A zoom for the small fuel volume fraction having the highest temperature has been included in the picture. For column refueling distribution, the maximum fuel centerline temperature is below 1250 ^{0}C, but for simulate fuel placement distribution the peak fuel temperature is 1282 ^{0}C and about 0.5% of total fuel volume operates at higher than 1250 ^{0}C.

The ATHENA model has been modified to represent the new graphite block core design. The new input boundary is set as already mentioned. The hydrodynamic model representing the active core, bypass flow, flow through upper and lower reflector, etc, has been modified. The heat structure model for the active core, upper and lower reflector, and the gap conduction enclosures model for axial and radial heat transfer during the transient have been modified in the ATHENA model to account the new graphite block core design in the ATHENA analysis.

Table IX below compares the POKE and ATHENA calculated results for the new block core design with all the above mentioned changes incorporated. Form this table, it can be seen that, with the new block design for an inlet temperature of 510 ^{0}C the steady-state vessel temperature is reduced to ~369 ^{0}C while the fuel peak centerline temperature is at or below 1247.5 ^{0}C.

TABLE IX ATHENA and POKE Results with Modified Block Design

Code	Temperature ^{0}C		Bypass Flow	Mass Flow kg/sec	ΔP KPa	Core Average Temp, ^{0}C		PFCT ^{0}C	Vessel Temp, ^{0}C
	Intel	Outlet				Fuel	Mod		
POKE	510	950	0.15	265.24	59.5	888.5	846.6	1247.5	----
ATHENA	510	950	0.15	265.24	56.0	878.8	859.5	1138.5	~369

The pressure drop for this inlet boundary condition and for the new core design as calculated by ATHENA is same as that for the previous design. The hydraulic diameter of the coolant hole is reduced from 0.79375 cm in a 10 row block design to 0.63115 cm in a 12 row block design. The expected additional pressure drop in the ATHENA calculation for this reduced hydraulic diameter is offset by the decreased mass flow rate and increased bypass flow.

F. Back Calculation for a Vessel Temperature of 350 ^{0}C

Up to this point, the peak vessel temperature calculated during steady-state is reduced to 369 ^{0}C. However, our goal is to reduce the vessel temperature to ~350 ^{0}C - 360 ^{0}C as mentioned before. To evaluate the possibility of achieving this ultimate goal, a backward calculation is done by fixing the peak vessel temperature at 350 ^{0}C for steady-state operation. The ATHENA calculation shows that with the alternative coolant flow path and the new core design, the inlet coolant temperature needs to be reduced to 482 ^{0}C (ΔT across the core is 468 ^{0}C) to achieve this reduced peak vessel temperature. This inlet temperature corresponds to a mass flow of 249.4 kg/sec. Since the peak fuel centerline temperature is influenced by the amount of bypass flow, different bypass flows are used for this analysis. Our goal is to maintain the fuel centerline temperature within acceptable limits while maintaining the vessel temperature at 350 ^{0}C.

Figure 26 shows the fuel temperature as a function of fuel volume fraction for different power distributions and for different bypass flows with a vessel temperature of 350 ^{0}C at steady-state operation. A zoom of this figure shows that for a 10% of bypass flow, only about 0.2% of fuel volume is above 1250 ^{0}C and the peak fuel centerline temperature is 1265 ^{0}C. With 15% bypass flow and the simulated fuel placement distribution, the peak fuel centerline temperature is 1303.3 ^{0}C and only about 0.85% of fuel volume operates at higher than the expected operating temperature of 1250 ^{0}C.

Form this figure, one can conclude that if it is possible to limit the core bypass flow to 10% of the total core flow, then with the alternative coolant flow configuration

through outer reflector and the modified 12 row block design, the vessel temperature can be reduced to 350 ^{0}C while maintaining the peak fuel centerline temperature below 1250 ^{0}C.

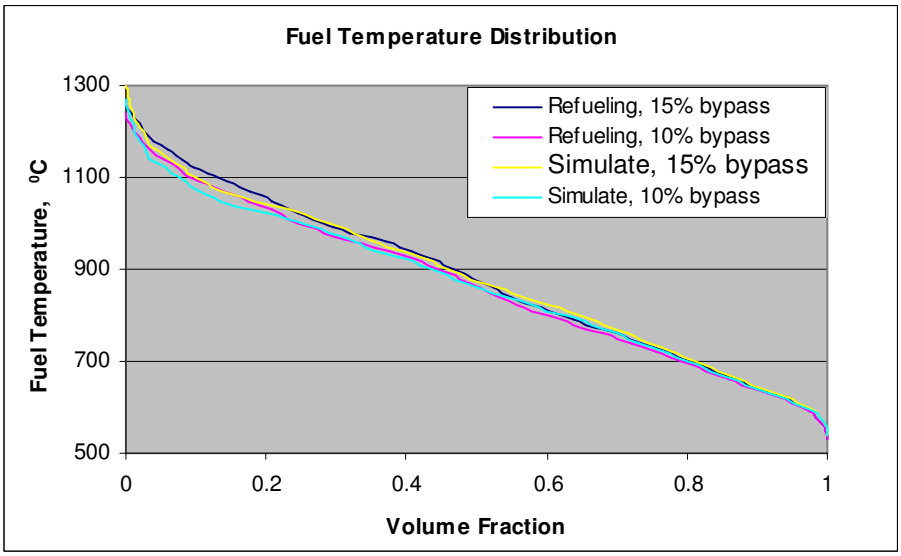

Fig. 26. Fuel temperature distribution as a function of fuel volume fraction for different power distributions and different bypass flows.

Until this point, all of the PFCTs for the new core design occur at the control assemblies or at the reserve shutdown assemblies (instead of the standard assemblies) where the number of sub channels has been reduced to accommodate the control rods. It should be noted here that, in the original POKE model, only four columns (column number 2, 3, 7 and 8) out of a total of 34 columns were modeled as control assembly, and no reserve shutdown assemblies were considered. The power distribution was provided accordingly.

In this analysis, a total of ten columns (column number 3, 4, 8, 9, 14, 20, 24, 28, 30 and 34) out of a total of 34 columns are modeled as either control or reserve shutdown assemblies. This change in the POKE model is made to provide consistency between the POKE model and the actual core layout as discussed at the beginning of this chapter and is shown in Figure 16. It also provides consistency between the ATHENA and POKE models. The ATHENA model assumed that the number of control assemblies and reserve shutdown assemblies are 12 and 18 respectively for the entire reactor core. In terms of sub channels per assembly, the reserve shutdown assembly and control assembly are identical. In both RELAP3-D/ATHENA and POKE models, the numbers of equivalent sub-channels in a standard and control (or reserve shutdown) assemblies are 105.84 and 92.48 respectively for a 10 row design, and 150.77 and 132.39 respectively for a 12 row design.

The column power distribution used for this analysis is based on four control or reserve shutdown assemblies for a one third of the reactor core. Therefore, the additional six control or reserve shutdown assemblies has power factor that correspond to standard assembly, even though the number of sub channels is reduced for all control and reserve shutdown assemblies. As a result, the power factors per sub channel for those six control and reserve shutdown assemblies are higher than it is supposed to be. Due to this inconsistent power distribution, these additional six control assemblies predict higher PFCT than actual PFCT.

During PFCT calculation, one of these control assemblies is hitting the maximum allowable fuel temperature limit prior to the standard assembly, even though the corresponding power factor for that particular control assembly is not the highest one. As a result, due to these inconsistent power distributions, both the PFCT and peak vessel temperature as calculated so far are over predicted. Both the PFCT and PVT are likely to be possible to reduce further.

Table X shows the PFCT for different bypass flows and for different power distributions. The PFCTs are shown separately for standard assembly and for control assembly. It shows that for a bypass flow of up to 15%, the PFCT remains at or below

1240 ^{0}C for all standard assemblies with a vessel temperature of 350 ^{0}C which corresponds to coolant inlet temperature of 482 ^{0}C, and a mass flow rate of 249.3 kg/sec. Even for 20% bypass flow, during the simulate fuel replacement distribution, the PFCT is within the limit for standard assemblies, but during baseline refueling distribution, it is ~1276 ^{0}C.

Table X also shows that, for a same bypass flow, the PFCT for standard assembly is reduced from 'Baseline Refueling' to 'Simulate Refueling' as expected. Considering the PFCT of control assemblies (column 3 of Table X) for which we don't have appropriate power distribution, the results are different.

For cases 1, 3 and 5, with baseline refueling power distribution, all PFCTs in the standard assembly occur at assembly number 25 for which the power factor is 1.32. However, all PFCTs in the control or reserve shutdown assemblies (which is higher than the PFCT of standard assembly) simultaneously occur at assemblies number 14 and 20 where the power factors are 1.19 for both assemblies.

TABLE X PFCT for a PVT of 350 ^{0}C

Case No.	Bypass flow	Power Distribution	PFCT for Control Assembly, ^{0}C	PFCT for Standard Assembly, ^{0}C	SC + RSC assemblies
1	10%	Baseline Refueling	1233	1209	10
2	10%	Simulate Replacing	1269.4	1147	10
3	15%	Baseline Refueling	1265	1240	10
4	15%	Simulate Replacing	1303.3	1175	10
5	20%	Baseline Refueling	1301.5	1275.9	10
6	20%	Simulate Replacing	1342	1207	10

An additional investigation was undertaken to determine whether a further reduction of coolant inlet temperature is possible by modifying the block design. The fuel rod dimension can not be reduced anymore from the manufacturing point of view. Keeping the fuel rod dimension same while reducing the coolant hole diameter may allow us to reduce the peak fuel centerline temperature. The results of the investigation showed that the reduction of coolant hole diameter to reduce the peak fuel centerline temperature is not feasible.

Since the diameter of the fuel rod and the number of fuel rods are not changed, with the reduction in coolant hole diameter the pitch is not decreased significantly. However the web thickness is increased with the reduction of coolant hole diameter since the graphite block dimension is not changed. Calculations for this revised design show that, a reduction in coolant hole radius from the current radius of 0.63115 cm to 0.5 cm will result a reduction of the peak fuel centerline temperature by only 5 ^{0}C, but the pressure drop across the reactor core is increased by about a factor of three.

With the revised coolant flow path through the PSR, it may be challenging to prevent any unexpected flow through the annular region between the reactor core barrel and reactor vessel wall or through the boxed channel in this region. Therefore, an investigation was undertaken to calculate the influence of leakage of hot inlet helium through the annular path and the boxed channel regions.

Figure 27 shows the vessel temperature rises during normal operation caused by the unexpected helium flow through the annular path between reactor vessel wall and the reactor core barrel. An inlet coolant temperature of 510 ^{0}C which corresponds to a vessel temperature of 369 ^{0}C is considered for this investigation. The figure shows that a flow of 2% of the inlet helium flow rate through the annular path or through the boxed channels which corresponds to mass flow of ~5 kg/sec of the inlet helium flow rate, results in a vessel temperature rise of ~40 ^{0}C. Therefore, even a small leak of inlet helium through the annular region needs to be carefully addressed to prevent an excessive vessel temperature rise.

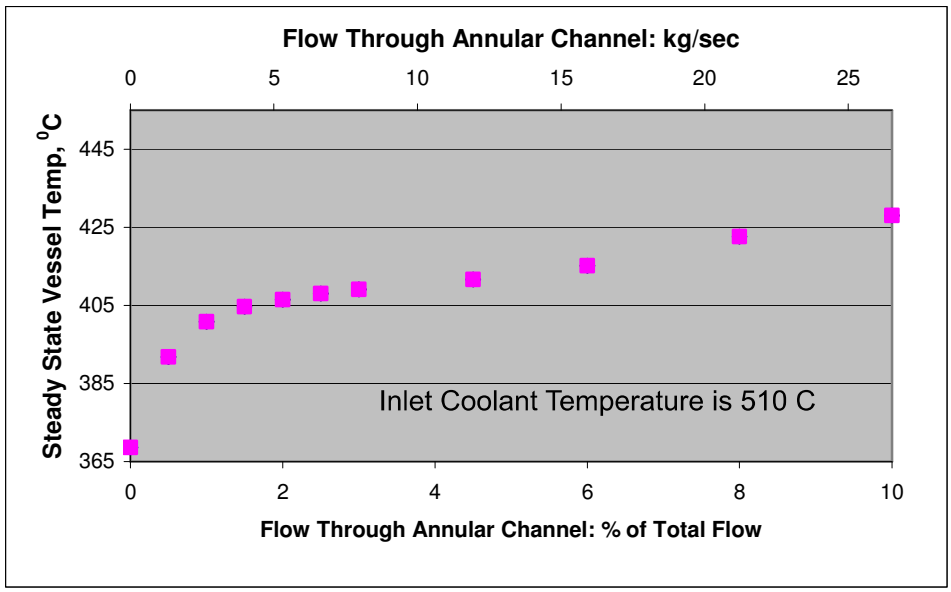

Fig. 27. Vessel temperature as a function of leak through annular path between reactor core barrel and reactor vessel wall.

CHAPTER VI

TRANSIENT ANALYSIS OF MHR

During normal operation of a MHR the helium coolant takes heat from the reactor core. The hot helium then transfers heat to the power conversion system (PCS) and/or the intermediate heat exchanger (IHX). When the reactor is in a shutdown condition, the Shutdown Cooling System (SCS) removes residual heat from reactor core. This heat is removed by the shutdown heat exchanger which is located below the core. Eventually the heat is rejected to atmosphere through the shutdown cooling water system.

If the reactor is scrammed and SCS fails to remove heat from reactor core, conduction cooldown events occur and decay heat then is removed from the core passively by RCCS. Two important types of accidents for the MHR are a High Pressure Conduction Cooldown (HPCC), which may also be referred to as the loss of coolant flow accident, and a Low Pressure Conduction Cooldown (LPCC), which may also be referred as loss-of-coolant accident (LOCA). The transient response of the MHR for the original design configuration, the alternative coolant flow path configuration and the final modified design with both the alternative coolant scheme and the new graphite block core design are analyzed for these two conduction cooldown events and discussed below.

The reactor vessel peak temperature response and the fuel peak temperature response were evaluated for both the HPCC and LPCC transients. For both cases the reactor is scrammed at the beginning of the transient. The initial conditions for these transient cases were taken from the steady-state operating condition. During an LPCC the loss of helium coolant and the resultant coolant pressure decrease occurs at a rate that depends on the size of the break. For this LPCC calculation, a rapid depressurization of the reactor primary system from steady-state primary pressure to atmosphere conditions in about 50 seconds is assumed. This rapid depressurization corresponds to large break

in the primary system. In reality, if the break is smaller and the depressurization occurs slowly, then additional convective cooling of the core will occur due to the continued presence of helium in the primary system. Therefore, the fuel and vessel peak temperatures for a smaller break will be less than those predicted in these calculations.

During this transient the reactor is scrammed and the core power quickly drops to decay heat levels. The helium is also rapidly exhausted from the primary system, so the only way for the decay heat to be removed from the reactor core is by conduction and radiation through the reactor vessel wall to the RCCS. During the transient, the graphite absorbs a large amount of heat due to its very high volumetric heat capacity. By removing graphite from the reactor for the new coolant configuration, we essentially remove a portion of the total volumetric heat capacity. Therefore, in the modified design, the reactor will result higher vessel peak temperature during transient due to reduced amount of graphite.

For a HPCC, the reactor is scrammed and the forced (pumped) flow to the reactor core is lost, but the helium remains in the primary system and only a small drop in primary system pressure is experienced. In this case, a gradual depressurization of primary system pressure to about 5 MPa over a period of about 50 hours is assumed. PVTs during a LPCC and HPCC events for the original reactor design configuration, the reactor design configuration with the alternative coolant scheme (ACS) and the reactor design configuration with both the ACS and the new 12 row block core design are shown in Figure 28. For the original reactor configuration (Base Case) the outlet temperature is 850 ^{0}C and for the rest of the cases the outlet temperature is 950 ^{0}C.

Since the pressurized helium promotes heat transfer by natural circulation in the HPCC transient, the PVT is lower for the HPCC when compared to that for the LPCC as shown in Figure 28. The calculated PVT for the original 'Base Case' is ~500 ^{0}C for LPCC transient and it occurs at about 82.8 hours from the beginning of the transient. With the modified coolant configuration the PVT is found to be 510 ^{0}C for LPCC transient and it occurs at approximately 74 hours after transient initiation. This increased PVT occurs because of the reduction of graphite in the core to accommodate the

alternative coolant scheme. The PVT during the LPCC for the new block core design is reduced from that for the ACS but it is approximately the same that for the original base case because the graphite-to-fuel volume ratio in the new block core design is increased.

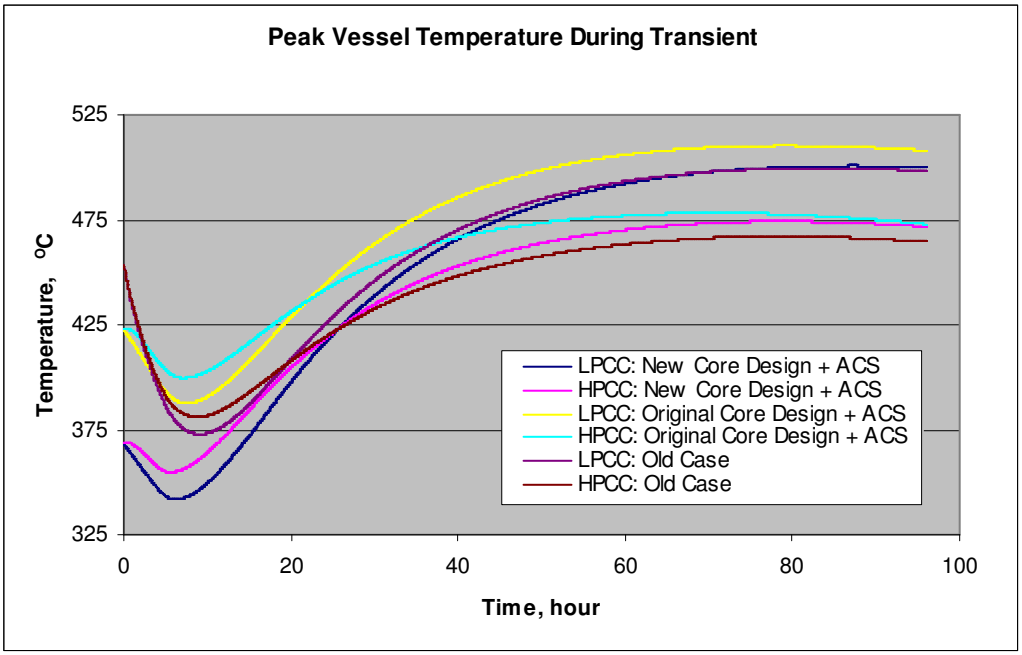

Fig. 28. PVT during LPCC and HPCC transients.

For the HPCC transient, the PVT is increased from ~467 ^{0}C to ~478 ^{0}C from the original design to the new coolant scheme due to the reduction of graphite, but the PVT is reduced in the third case where we use the alternative coolant scheme and the new block core design simultaneously, since the graphite-to-fuel volume ratio is increased as described above. During normal steady-state operation and at the beginning of the transients, the PVT occurs in the bottom part of the reactor vessel. But during transient this PVT occurs at about the middle of vessel. All calculated PVTs are found to be within acceptable limits during the transients.

Peak fuel temperatures during the LPCC and HPCC transients are shown in Figure 29 for original design case for the modified coolant scheme and for the new block core design. For the original design, the calculated peak fuel temperature is 1438 ^{0}C and it occurs about 62 hour after the transient is initiated. The calculated PFT for the reactor having ACS is 1471 ^{0}C which is higher than that for the original design case. This increased PFT is again the result of the removal of graphite moderator from PSR. The calculated PFT during a LPCC for the MHR having both the ACS and new block core design is 1438 ^{0}C and occurs about 62 hour after the transient is initiated.

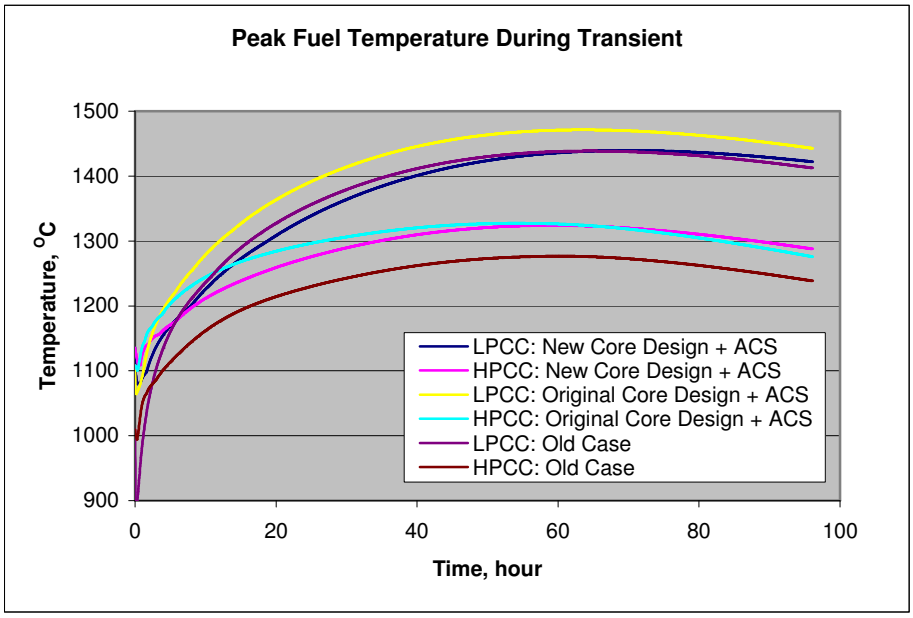

Fig. 29. PFT during LPCC and HPCC transients.

During the HPCC transient the calculated PFT for original base case, the MHR design with the ACS and MHR with both the ACS and the new graphite block core design are 1277 ^{0}C, 1327 ^{0}C and 1324 ^{0}C, respectively. All of these vessel and fuel peak

temperatures are consistent with other thermal analyses for MHR, and are well below the specified design limits.

The results of these transient analyses are also summarized in Table XI. For the MHR having both the ACS and the new graphite block core design not only the graphite fuel volume ratio is increased from the previous cases but also the amount of helium in the reactor system is reduced due to the reduced mass flow rate. This reduced volume of helium has significant role in case of HPCC transients.

During normal operation the PFT occurs at the bottom of the reactor core for each of the power distributions. The mass flow rate and the hydraulic diameter are constant throughout the channel length but the viscosity is increased with the increase in temperature as the fluid flows from top to the bottom of the core. As a result, the Reynolds number in a particular channel is reduced from the top to the bottom of the core, and the convective heat transfer rate is also decreased. Therefore, even with the higher heat fluxes in the middle portion of the core for an axial cosine power distribution, the bottom end of the fuel rods will have higher temperatures.

TABLE XI Transient Analyses for MHR

Case	LPCC				HPCC			
	PFT		PVT		PFT		PVT	
	Temp ^{0}C	Time hr	Temp ^{0}C	Time hr	Temp ^{0}C	Time hr	Temp ^{0}C	Time hr
Original Design	1438	62.1	499.6	82.8	1277	60.6	466.8	73.0
New Coolant Scheme	1471	65.1	510	74	1327	54.7	478.1	67.5
New Coolant Scheme + New Block Core Design	1438	70.6	500.0	82.8	1324	58.7	474.2	76.8

During transients, the location of PFT is determined by the axial and radial power distributions, especially for the LPCC since there is no helium flow. For an axial cosine power distribution, the PFT will be at the middle (axially) of the inner ring for the LPCC. For the HPCC transient, the location of the PFT will shift upward and will be located approximately 6 volumes from the bottom of the core due to upward natural circulation of helium through reactor core during the transient.

The decay power distribution and the heat loss through the reactor vessel to the RCCS during these transient are shown in Figure 30 for the MHR having both the ACS and the new graphite block core design. The steady-state heat loss to the RCCS for the original base case design was above 3 MW and is reduced to below 2 MW due to the reduced vessel temperature. The maximum RCCS losses during the calculated transients are 2.1 MW for the LPCC and 2.21 MW for the HPCC, which occur approximately 81 and 75 hours, respectively, after transient initiation.

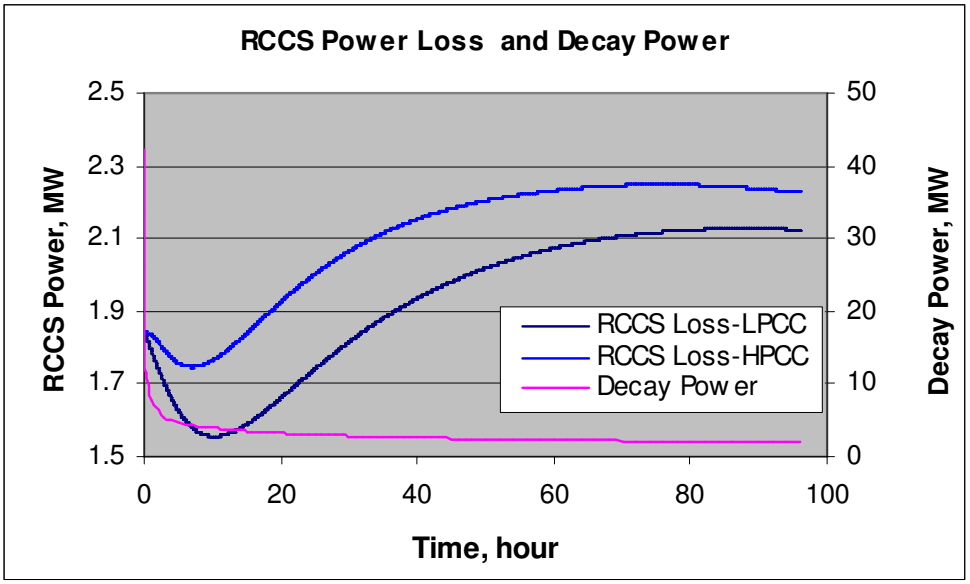

Fig. 30. RCCS power and decay power during transient.

CHAPTER VII

RELIABILITY AND AVAILABILITY STUDIES

Various quantitative and qualitative techniques may be used to assess the reliability and availability of process systems, system equipment and system manufacturing operations. The interactions of equipments, systems and personnel that have potentially undesirable consequences may be identified by these techniques.

For reliability and availability analyses of the coupled nuclear hydrogen production plant, these undesirable consequences include plant shutdown, excessive downtime, production of hydrogen with some undesired mixture in the final product, etc. These incidents reduce the system reliability and availability as well as the system profitability by decreasing the production and increasing the maintenance cost. The fault tree analysis technique is used to define the particular process or equipment failures that will result in these incidents of concern.

The probabilistic risk analysis consists of five steps[22]; these are accident frequency analysis, accident progression analysis, source-term analysis, offsite consequence analysis and risk calculation. Also there are three levels of PRA. A Level 1 PRA consists of accident frequency analysis and risk calculations. A Level 2 analysis consists of a Level 1 PRA, accident progression analyses and source term analyses. A Level 3 analysis consists of all five steps of analyses i.e. it includes Level 2 PRA and offside consequence analyses. Since the Level 1 PRA includes risk analysis, each subsequent level of PRA analysis includes the risk calculation in its results.

The Level 1 PRA mainly deals with accident frequency. For example, in case of nuclear power plant, the Level 1 PRA calculates the core damage frequency. Accident sequences and their groups are identified in the Level 1 PRA and these accident sequence groups are used as an input for the Level 2 PRA. The scope of the present study encompasses a portion of the Level 1 analysis, where the failure probability of the system is calculated. A PRA analysis of the complete nuclear hydrogen production

process would include the hydrogen production plant, Brayton cycle power conversion system and the modular helium reactor, along with all the support subsystems and piping. These developed models of hydrogen production plants are considered as the part of a complete PRA model for coupled nuclear hydrogen production process. Risk analysis for this portion of PRA model is not desirable instead the focus will be concentrated on evaluating the reliability and availability of the hydrogen production plants.

Since the reactor provides heat for the hydrogen production plants, the failure of the hydrogen production plants will result in complete or partial loss of heat removal capability (loss of load) for the nuclear reactor. In this circumstance, some action might be needed for the nuclear reactor to avoid any undesired consequences or upset condition. From an availability standpoint, it is desired that as long as the reactor is in operation, both hydrogen production plants will also be operating. If for some reason the reactor is in the shutdown condition, say for component replacement or routine maintenance, required and routine maintenance would be done simultaneously for the hydrogen production plants. For this coupling between nuclear reactor and the hydrogen production plants, an increased concern is sustained about how reliable the hydrogen production plants compared to the reactor. To address this concern, a reliability and availability assessment of the hydrogen production plants has been performed.

This study includes the calculation of the reliability and availability of both hydrogen production plants. The results of this study will help to determine whether design improvements are required to improve system reliability, and what improvements (system/component redundancies, etc.) will be most beneficial. The models developed for this study can also be used to analyze the risk increase and risk reduction ratios as well as other factors influencing individual component and entire system reliability .

Since reliability and maintainability studies for the MHR have already been performed and reported[10], maintainability analyses for the SI and HTE-based hydrogen production plants will not be performed. Instead, it is assumed both plants will follow the same maintenance schedule as the reactor.

A. SAPHIRE Code

SAPHIRE[23] stands for 'System Analysis Programs for Hands-on Integrated Reliability Evaluation. The previous version of this PRA code is IRRAS (The Integrated Reliability and Risk Analysis System). The IRRAS code was developed at the INL under the sponsorship of the U.S. Nuclear Regulatory Commission (NRC) and the U.S. Department of Energy (DOE). The development of IRRAS was started because of a recognized need for microcomputer based software to aid the task of probabilistic risk assessment. The initial scope of this code development was to provide software that could show the feasibility of using microcomputers for performing probabilistic risk analysis.

The IRRAS code was developed with the capabilities of providing certain essential functions such as fault tree construction, failure data input for basic events, cut sets generation, cut sets quantification, etc. The very first version of the SAPHIRE code was developed at the INL with the same capabilities as IRRAS, but included improvements in the Graphical User Interface (GUI) and the option to run the code in Windows 95 and Windows NT. Further improvement and development of the SAPHIRE code has continued to make this code more powerful and more user-friendly.

SAPHIRE refers to a set of several microcomputer programs with the capability of creating and analyzing probabilistic risk assessments for both nuclear and non-nuclear systems but was developed primarily to analyze the nuclear power plants. The SAPHIRE code can be used for fault-tree analysis, event tree analysis, cost-benefit analysis, balancing risks and benefits in situations involving human safety, environmental risks, and financial uncertainties. It can also be used for the evaluation of the effectiveness of emergency systems, accident prevention, accident mitigation, and for the assessment of radioactive releases to the environment.

B. SAPHIRE Model Development

Both the SI thermochemical and HTE based nuclear hydrogen production processes use the MHR as the heat source. To complete the reliability study of the entire nuclear hydrogen production process, PRA models for both the SI thermochemical and the HTE-based nuclear hydrogen production plant need to be developed. The reliability code which is capable and commonly used to analyze nuclear system need to be used for the reliability studies for these plants. The code selected for this development effort is the SAPHIRE code, which was described in the previous section.

The SAPHIRE code is not commonly used for the analysis or assessment of chemical plants since it was primarily developed for nuclear power plant analyses. However, since both the hydrogen production plants are coupled to the MHR system, the SAPHIRE code has been used to perform these reliability and availability studies with the aim of having a complete model in future for the entire nuclear hydrogen production process.

The capabilities of the code were more than adequate to meet most of the needs for our analysis of the nuclear hydrogen production processes. The one area that presented a unique challenge was the closed loop component dependencies inherent in the hydrogen production processes. These closed loop component dependencies are the result of a lot of recycling of materials in the hydrogen production process flow sheets. SAPHIRE has been used by nuclear industries to analyze systems which are open loop or once through in nature. This code can not be used to analyze a system having closed loop component dependency unless the system is modeled as an equivalent open loop system for fault tree analysis in the SAPHIRE model. In case of closed loop component dependency in the fault tree model, the code will run for ever without generating and displaying the output. Therefore, the fault tree model developed in this study used equivalent open loop system for model development and analysis.

For this study, fault tree models are first developed for both the HTE and SI-based hydrogen production processes. Using information obtained on system configuration, component failure probability, component repair time and system

operating modes and conditions, the system reliability and availability are assessed in the next step. Required redundancies are made to improve system reliability and to optimize the plant design for economic performance. Due to these redundancies, the failure rates and outage factor of both nuclear hydrogen production processes are reduced to an acceptable range which is essential for high efficiency nuclear hydrogen production using Modular Helium Reactor.

C. Failure Data

1. Failure Data Description

Component failure is defined as the incapability for a component to perform its required functions[24]. A critical failure causes immediate and complete loss of a system's capability of providing its output. A failure which is not critical but which prevents the system from performing its function within specifications is a degraded failure. This type of failure may develop into a critical failure in time. Therefore, degradation of the ability of an item to perform its required work may also be considered as failure. Another class of failure is incipient failure. A failure, which does not immediately cause loss of a system's capability of providing its output, but which, if not attended to, could result in a critical or degraded failure in the near future is referred to as an incipient failure.

The failure data considered here includes complete failure of the item, partial failure of the item and failure of the part of the item that causes unavailability of the system or a part of the system. Incipient failure is not included in these analyses. Since there will be an option for an emergency maintenance during plant operation and the entire nuclear hydrogen production process will have a routine maintenance schedule, incipient failure may not result in a complete failure of the system if the incipient failure conditions are recognized and addressed during normal scheduled maintenance.

The total failure data for any equipment may be a combination of both time dependent and demand related failures. However, all equipment considered for these analyses are operating equipment and their demand is continuous. Therefore, all failure data used for these analyses are time dependent. The failure rate for each basic event (i.e.

each component) is the combination of ‘failure during operation’ and ‘failure due to maintenance’. The fractional contribution for each of these two failure modes to the total failure rate is not provided separately to the code.

For all equipment, the mode of operation was chosen as running mode, or continuous mode or operation mode provided that the data was available. Data for standby equipment were not considered since all our equipment are in continuous operation and not standby. For pumps, all data were selected for centrifugal pumps and was classified according to the pump size and type of fluid. For heat exchangers, all data were taken for Tube-Shell heat exchangers and the data was classified according to the type of fluid in the primary side and secondary side. Data for the power recovery equipments were classified by size and type of fluid. The data for vessels were classified based on the function and size of the vessels.

2. Selection of Calculation Type

There are 17 different calculation types in SAPHIRE numbered 1 through 9, T, F, I, S, G, L, M and H. The calculation type is a numerical reference to the calculation that represents the way the failure data of the component will be treated. For some of the calculation types the failure rate of the basic events is directly used by the code as the basic event failure probability. Different calculation types are used for non-repairable component, repairable component and for standby components. Based on our mission, available component types in the SAPHIRE and the developed model, the following three calculation types were used for these calculations:

- Calculation type 3
- Calculation type 5
- Calculation type T & F

Calculation type 3 is the full equation for the failure probability of an operating component without repair in a non-demand failure mode. All components in the hydrogen production flow sheets are operating component and this calculation type was

used for the initial calculation or during the intermediate step of the analysis to determine the failure probability or failure frequency of the component and the plant. Results of this initial calculation were used to optimize the plant flow sheet and component specification. Even though this calculation type is appropriate for non repairable components only, it was used for the preliminary analysis to determine the comparative failure contribution of different components. Once the component sizing and plant optimization was completed, this type was no longer used for the final step of the analysis. The equation used for this calculation is:

$$P=1-e^{-\lambda t}$$

where

P = failure probability

λ = failure rate (per hour or per specific number of hours)

t = mission time expressed in hours, the default 24 hour mission time is used.

Calculation type 5 is the full equation for the failure probability of an operating component with consideration given to the ability to repair the component in a non-demand failure mode. For components in the hydrogen production flow sheets this calculation type is used for the final calculation to evaluate the unavailability of the plant for the given mission time. For this calculation one year is used as a mission time. The equation used for this calculation is:

$$P=\frac{\lambda\tau}{1+\lambda\tau}.\left[1-e^{-\left(\lambda+\frac{1}{\tau}\right)t}\right]$$

where

P = failure probability

λ = failure rate (per hour or per specific number of hours)

τ = average time to repair expressed in hour

t = mission time expressed in hours, one year (8760 hours) mission time is used.

Calculation types T and F are used for the components that are not physically included in the hydrogen production plants but are used in the SAPHIRE model as the complement component for the model development. These components are used to provide more modeling flexibility for the users. Both the T and F type of calculation are house events where T is used to represents the component as a 'failed component' and F is used to represent the component as a 'successful component'. Events that are defined as either T or F calculation type do not appear in the cut sets. The failure probability of T and F type components are 1.0 (100% failed) and 0.0 (100% success), respectively.

D. Data Sources and Data Selection

There are no large-scale existing commercial plants for hydrogen production. So data for equipment based on historical site experience in a commercial hydrogen production plant is not possible. All data used for this study were from the databases from industries other than nuclear hydrogen production. From a number of available reliability data sources, the mean failure probability for each component, its mean repair time and uncertainty of these data are studied. Reliability data for a particular component from different data sources are compared and the most relevant ones are incorporated into the SAPHIRE analysis. Some data may have been misinterpreted, since the system configuration from with the data was obtained may not be same as the system configurations in our analyses.

The Offshore Reliability Data (OREDA[24]) covers reliability data from a wide range of equipment used in oil and natural gas exploration and production industries. Offshore topside and sub sea equipment as well as some onshore exploration equipment are also included. The major data source for the European Industry Reliability Data Bank (EIReDA[25]) is the reliability database of the probabilistic safety assessment of the

nuclear power plants in France. It includes failure rates of electric motors recorded by seven European utilities. In addition, it includes reliability data for electric transmission grids, distribution grids, electric stations, components etc.

The Process Equipment Reliability Data[26] by the Center for Chemical Process Safety (CCPS) of the American Institute of Chemical Engineers accumulated and aggregated data from a variety of plants and industries, such as nuclear power plants, chemical process industries, offshore petroleum platforms, etc. 'Reliability Data of Components in Nordic Nuclear Power Plants (T-book[27])' provides reliability data for components used in Swedish nuclear power plants. This data book includes only critical failures (i.e., failures that stop component functions and require immediate repair). Another data source that has been used for these analyses is 'The Reliability Data Handbook[28]'.

These five data banks were used to develop reliability data for individual components in each of the nuclear hydrogen production process flow sheets. From the above-mentioned five databases, failure data for each component have been studied and compared. The data that best matched the individual component specifications and description were selected for these analyses.

In those cases with high system or component failure rates, possible redundancies were examined to improve the system reliability. In addition, to address common cause failures several references were consulted to obtain data on common cause failure[29-30] probabilities. In those cases where common cause failure data could not be found, 10% of the total failures were considered to be common cause failures as a thump rule which is consistent with other similar studies.

An example of a fault tree (or sub tree) which includes common cause failure probability, and was used to calculate component redundancies is shown in Figure 31. The similar sub tree is used for any redundancy that is used in the fault tree model for both SI thermochemical and HTE based plant. Component TE104 which is a 'Turbine and Liquid Expander' is taken as an example.

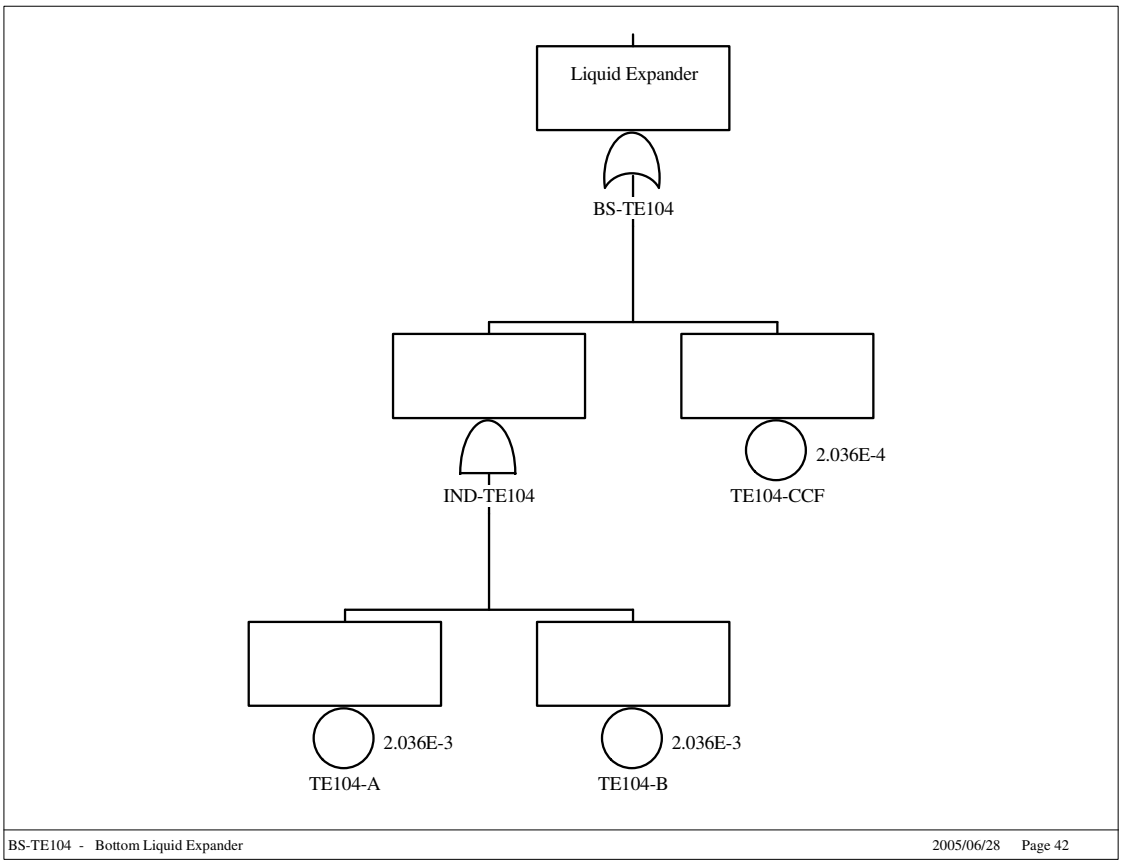

Fig. 31. Fault tree for common cause failure.

The failure probability of this component is 2.03E-3 which is considered high and a redundancy is recommended. Therefore, another TE104 component is added with an AND gate IND-TE104. The AND gate calculates the simultaneous failure probability of both liquid expanders (i.e. TE104). Therefore, the AND gate IND-TE104 fails if both components (i.e., both liquid expanders) fail simultaneously for independent reasons. If there is a common cause that results in the simultaneous failure of both turbines, that failure mode is included through component TE104-CCF which is connected to IND-TE104 with an OR gate BS-TE104. So the top gate of this sub tree BS-TE104 will fail if either both the expander fails for independent reason (IND-TE104 fails) or both of them fails simultaneously for a common cause (TE104-CCF fails). For a pump this common

cause may be low frequency power from same source. In the following example the common cause failure probability (2.03E-4) is considered as 10% of component's independent failure probability (2.03E-3). In absence of common cause component TE104-CCF, the calculated failure probability will be less than the actual one.

E. Fault Tree Analysis

A fault tree is a model of a system which is suitable for reliability analysis. The model is usually tailored for the study of system failures. A system can be represented graphically or logically. The fault tree is the graphical representation of the system, but a developed fault tree for the system can be easily converted to a logical representation. Both the fault tree graphic and logic can be thought of as a group or set of equations which describe the possible failure combinations in the system.

Solving the fault tree includes generating cut sets for the selected fault tree based on cut sets generation cut off values. The SAPHIRE fault tree model is capable of generating cut sets for a selected fault tree or group of fault tree or all fault trees within the current project. The cut sets is the combination of events leading to system failure. Three cut set generation cut off values can be specified such as:

- Cut off by cut sets probability
- Cut off by event probability and
- Cut off by size or zone.

For a cut off by cut set probability, two options can be selected. For the 'global' option, only those cut sets whose product for all its events probabilities is greater than or equal to the magnitude in the 'global cut off value' field are considered. The numerical value in the field of the 'global cut off value' is a user defined value; if no value is defined the SAPHIRE code will continue calculation with a default value.

For the 'cut off by event probability' option the minimum cut off value for events is provided and all events having failure probability less than that minimum cut off value are removed from the calculation. If the cut off by size is selected, then all cut sets

whose number of events is equal to or less than the provided cut off value are kept and all other cut sets are removed from the result.

1. Quantifying the Fault Tree

The fault tree quantifying process includes:

- Re-quantifying the cut sets using current data values
- Re-quantifying the cut sets using minimum cut sets upper bound approximation
- Re-quantifying by adding together the probabilities for the cut sets of the top event
- Re-quantifying using the exact calculation for the union of cut sets via the inclusion and exclusion rule

The widely used minimum cut sets upper bound approximation method of calculation approximates the probability of the union of the minimum cut sets of the fault trees. The mathematical equation for the minimum cut sets upper bound approximation is:

$$S=1-(1-C_i)^m$$

where

S = minimum cut sets upper bound for the fault tree unavailability

C_i = probability of the i^{th} cut sets

m = number of cut sets

The Min Max method of quantification quantifies the current case cut sets using the exact probability quantification algorithm. To determine the minimum and maximum quantification, the 'number of pass' is provided by the user at the beginning. The number of passes is the number of the intermediate terms SAPHIRE will calculate when determining the maximum and minimum values.

2. Uncertainty Analysis

Failure data for basic events are statistical data and are incomplete without the information on the uncertainty of each data set. Due to this uncertainty in the basic events probability, the variability of SAPHIRE results such as cut sets generation need to be calculated. SAPHIRE uses two sampling techniques to do this uncertainty analysis: Monte Carlo simulation and Latin Hypercube simulation. SAPHIRE samples the user specified distribution for each of the basic events in a group of cut sets then quantifies these cut sets using the sample values.

The Monte Carlo simulation is a fundamental and widely used uncertainty sampling approach. To perform the sampling following this simulation process, the SAPHIRE code makes repeated quantifications of the fault tree (or sequence or end state) cut sets using samples from the basic events uncertainty distributions. This type of simulation requires more samples than Latin Hypercube simulation. The Latin Hypercube simulation is a stratified sampling technique where the random variable distributions are divided into equal probability interval. Generally the Latin Hypercube simulation requires fewer samples than the Monte Carlo simulation for similar accuracy, but due to the stratification method, it takes a longer time to complete the calculation.

Both the probability distribution and the cumulative distribution plots can be generated by the SAPHIRE code. The uncertainty of failure data for each of the components in the two hydrogen production plants is collected and is added to the developed SAPHIRE model. A probability distribution based on the Monte Carlo simulation is presented for each plant in the corresponding chapter.

CHAPTER VIII
SAPHIRE ANALYSIS OF SULFUR IODINE PLANT*

The development of the Probabilistic Risk Analysis (PRA) model for the Sulfur-Iodine thermochemical based nuclear hydrogen production process is the initial step in performing the reliability, availability and maintainability studies, and for economic analysis of the plant. This chapter will discuss the development of the SAPHIRE model for the SI plant, the performance of the reliability and availability studies, the use of component redundancies for the improvement of system reliability, and optimization of the plant design.

The system was modeled based on three-coupled chemical reactions for hydrogen production using the Sulfur Iodine (SI) process as shown and discussed in Chapter I. To develop a SAPHIRE model of this hydrogen production chemical plant, a master fault tree is first developed which represents these coupled chemical reactions. The system configuration and component information for this model was obtained from General Atomics Report GA-A24285, Revision 1, dated December 2003.

The model was developed to the level of detail at which sufficient information and data existed to reflect the performance of the hydrogen production chemical plant. The analysis included only those components that correspond to specific functions in the chemical hydrogen production process. Therefore, the model assumes no failure of the hydrogen production process happens due to failures of heat supply from the reactor, power supply for the process plant and distilled water supply to the system. All these additional sub-systems can be added to the model in the future. The development of the PRA model includes:

- Familiarization with the hydrogen production chemical plant
- Identification of the fault tree top events for this plant

---

*Part of the study reported in this chapter is reprinted with permission from "An Evaluation of Reactor Cooling and Coupled Hydrogen Production Processes Using Modular Helium Reactor," by E. A. HARVEGO, S. M. M. REZA, M. B. RICHARDS, A. S. SHENOY, 2006, *International Journal of Nuclear Engineering and Design*, Vol. 236, pp. 1481-1489. Copyright 2006 by Elsevier.

- Delineate systems and system boundaries
- Delineate systems and system boundaries
- Specify model assumption and specify conditions for the failure of the system
- Construct fault trees
- Collection of failure data for each component
- Analyze model, generate cut sets, optimize the result and perform checks as needed.

The SAPHIRE model developed for the SI plant has been used to calculate the plant failure frequency or the number of hours the plant will be out of service due to component failures within a specified mission time. Different ways to improve the reliability of the plant were also identified during this analysis.

A. The SAPHIRE Model Development for SI Plant

To develop the SAPHIRE model, the fault tree top event for the coupled chemical reaction was first identified. The complete SAPHIRE model that includes all three sections of the SI hydrogen production process was then developed in several steps. In the first step, models for each of the three main reaction sections of the SI process were developed assuming single components for each of the functions identified in the flow sheets. In the second step, these models were modified to include multiple components to perform each different function, according to the number of component for each function provided in the earlier referenced GA report.

The complete SI based hydrogen production plant consists of four individual plants. Each plant provides one fourth of total hydrogen production capacity of the plant, and utilizes all the heat from one 600 MWt MHR. Therefore, a total of four MHRs are used to provide heat to four separate hydrogen production plants. At the beginning of this work, the flow sheet development for each individual section of the plant was not completed to the level needed for the development of SAPHIRE model. Therefore, some

assumptions were made in the initial development stages of the SAPHIRE model. Based on those assumptions, the failure modes of the system were defined.

In addition, since the number, type and capacity of individual parallel components listed in the General Atomics report are developed for cost estimating purposes only, and do not necessarily represent the final system design required to meet system reliability and availability requirements, adjustments are made to the number of parallel components to provide consistency across individual sections.

Since there are four completely independent hydrogen production plants connected with each MHR, the total numbers of components in the entire system are selected to be divisible by four. Therefore, as an example, if 40 components are identified to perform a particular function, 10 of these components are associated with one MHR supplying heat to one hydrogen plant that provides one-fourth of the total hydrogen production.

For some cases, this assumption results in more than one component at a single location for a single function. The number of component provided for a single function, therefore, varies from one to ten for a single independent plant providing one-fourth of the total hydrogen production capacity. From the available information in the SI process flow sheets, it is sometimes difficult to predict the effect of the failure of some of the component on the whole process. In case we have multiple components for a single function at a single location, total capacity of these equipments is greater than the required capacity for the relevant function. Therefore, one of the decisions is made during the SAPHIRE model development is that the failure of one parallel component does not necessarily result in a system failure. As a result, the total capacity of some components operating in parallel is 25% more than the required total capacity. Therefore, as an example, with five components in parallel, failure of one component does not lead to a system failure, but the simultaneous failure of two or more parallel components may cause either failure or degradation in the system performance. This approach allows for a degree of redundancy while at the same time preserving the numbers of components specified in the earlier referenced GA Report.

Many discussions with researcher form GA/INL working on the development and modification of these hydrogen production plants have been performed to resolve those confusions that arose during this model development. An alternative model also has been developed and analyzed considering number of every component or equipment is one instead of 5 or 10. So a comparative study is possible to figure out how the probability of failure for the complete H_2 process plant changes if one large component is replaced by corresponding several small components.

Since the flow sheet development and modification was not complete at the beginning of this model development and further modification was continued simultaneously with the development of this SAPHIRE model, any modification that has been done for flow sheet or for those components by the time of this analysis has been included in this model. The developed SAPHIRE models at the first and second steps were used as the basis for the present final model development but those initial and intermediate models are not included for this final analysis.

The initial model was used to optimize the size and specification of many components. As the development of the final flow sheets progressed, a refined SAPHIRE model was developed in the third and final steps for a representative SI plant having a hydrogen production capacity equal to one fourth of the total hydrogen production capacity. Figure 32 shows the master fault tree for the SI thermochemical plant.

The master fault tree has four transfer gates, each connected to house events with an AND gate. The very first transfer gate corresponds to the product hydrogen purification process. The other three transfer gates of this fault tree link to the individual fault trees for each of the chemical reaction sections in the SI process (i.e., the Bunsen reaction section, the H_2SO_4 decomposition section, and the HI decomposition section).

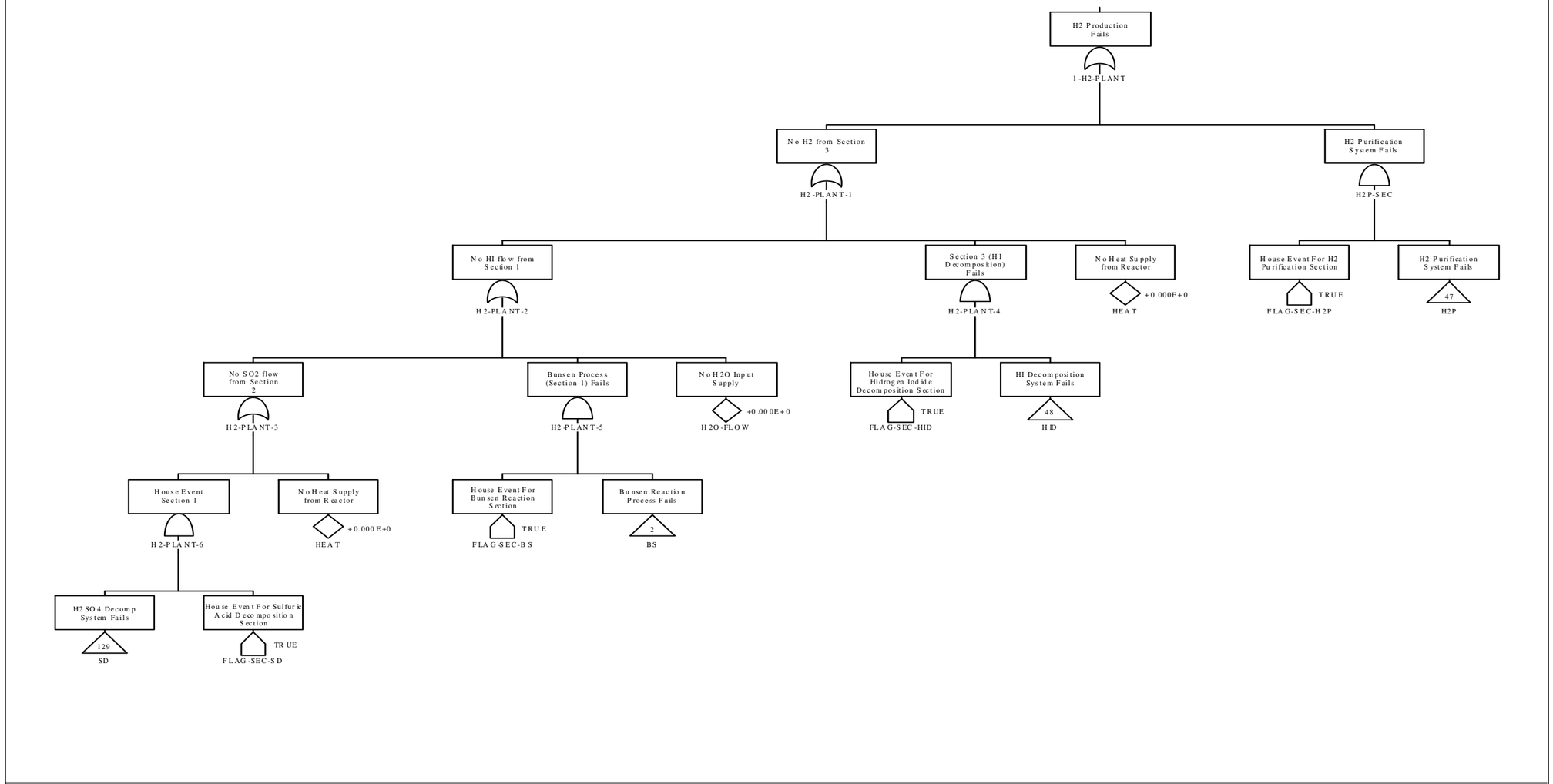

Fig. 32. Master fault tree model for SI thermochemical plant.

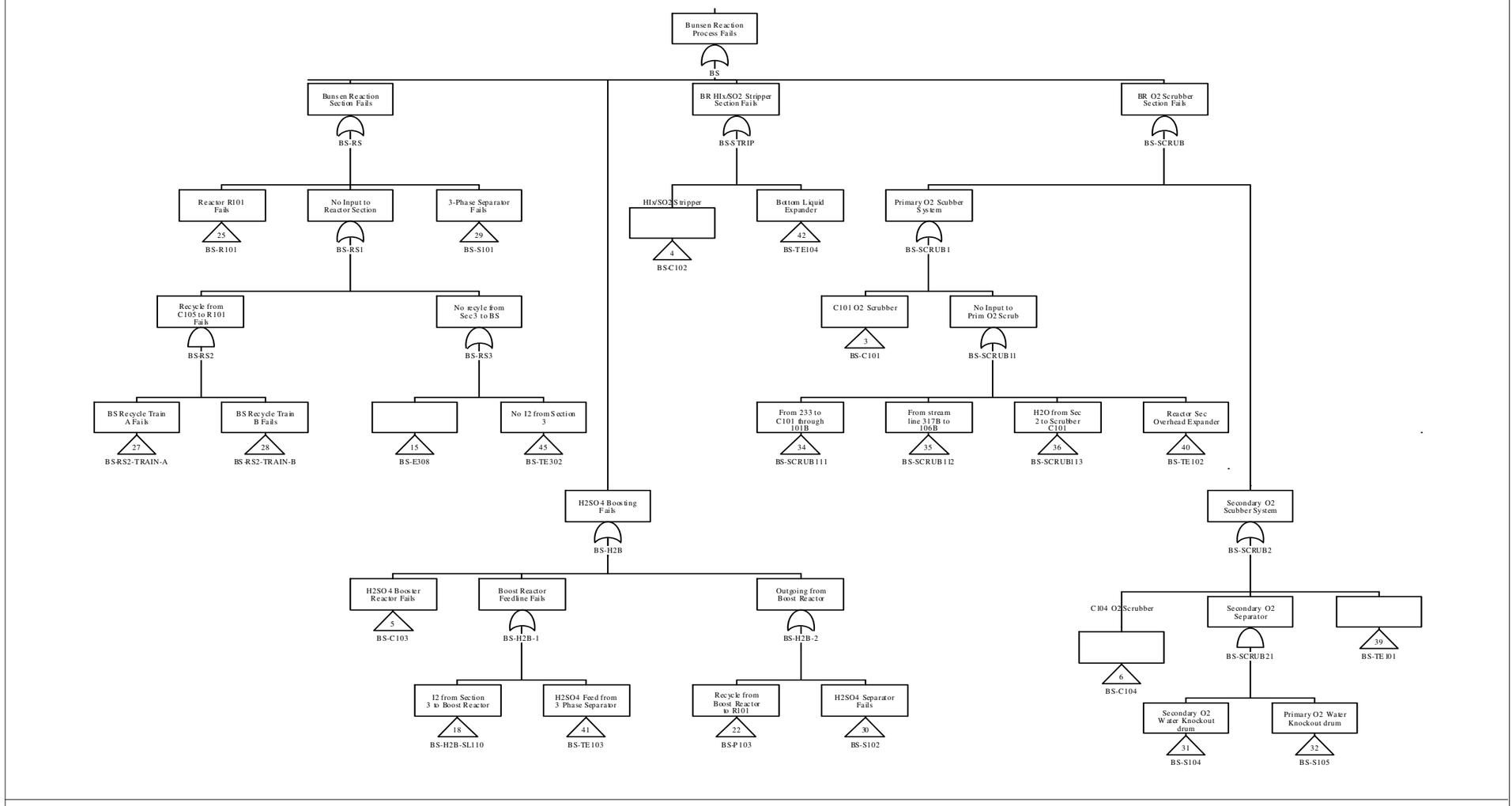

BS - Bunsen Reaction Process Fails 2006/05/10 Page 2

Fig. 33. Fault tree for Bunsen reaction process.

In the next step, the fault trees for all three sections of chemical reactions were developed. Figure 33 shows the fault tree for the Bunsen reaction process. The transfer gate in the master fault tree which corresponds to the Bunsen reaction process has the same name as the top event for the Bunsen reaction fault tree.

The master fault tree, when linked to the individual fault tree for each of the three separate chemical reactions, provides the basis for evaluating and improving overall plant reliability, and assessing plant availability based on component failure rates and mission times. The system configuration, flow sheet and specifications for each of the components are also obtained from the referenced GA report.

The fault tree model for the Bunsen reaction process has 22 transfer gates, but unlike the master fault tree, these transfer gates are not connected to house events by an AND gate. Each of the transfer gates corresponds to another fault tree or sub tree. Therefore, to explain the Bunsen reaction process elaborately, each of these extended fault tree and sub tree need to be added and explained which is not reasonable considering the total space requirement and the existence of complexity to represent such an entire system in a report. The fault tree models for hydrogen iodide decomposition section and for the sulfuric acid decomposition section also has many transfer gates. Each of the transfer gates correspond to another fault tree or sub tree. A sub tree may have a transfer gate again and so on.

The complete SI process and HTE process are represented by the extended fault tree with all the sub trees included. The complete model for the sulfur iodine based thermochemical plant consists of 27 fault trees, 115 sub-trees and 274 basic events. The Fault Tree models for Bunsen reaction section were discussed here as an example for the rest of the system. The complete SAPHIRE models for the SI plant which includes the Bunsen reaction section, hydrogen iodide decomposition section and sulfuric acid decomposition section are provided to GA/INL.

The complete SAPHIRE model consists of several sub sections. The boundaries for each sub-section are defined as part of the overall model development effort. These modeling boundaries used for the SAPHIRE analyses do not necessarily correspond to

the boundaries of the three sections in the SI process (i.e., Bunsen, HI decomposition, and Sulfuric Acid decomposition sections). The basis for establishing the modeling boundaries is system dependency on components for failure.

The SAPHIRE model for Bunsen process included all equipment associated with the Bunsen process (Section 1) flow sheet. It also includes some components from H_2SO_4 decomposition (Section 2) and HI decomposition (Section 3) flow sheets. The basis for selection of system modeling boundaries is the significance of the failure of a particular component on each section. For example, failure of component TE303 in the HI decomposition section affects the Bunsen reaction process much more than it does the HI decomposition process. Similarly, components TE301, TE302, TE303, E307, E308, E309 and C303 in the HI decomposition section are modeled as part of the Bunsen reaction process because their failure would have the greatest impact on that section. For the same reasons, components TE201, E209, E210, E211, E213 and P203 in the H_2SO_4 decomposition (Section 2) flow sheet are included in the Bunsen reaction process model.

The SAPHIRE model is developed to provide the maximum modeling flexibility for the future users of this model. The house events in the master fault tree are provided to allow users to analyze each of the sections in the process flow sheets separately or together. In addition, through the 'Generate' option in the SAPHIRE code, various sections of the SI plant can be analyzed separately or together. Using 'Generate' the following modeling options can be exercised:

- The complete SI plant
- The complete SI plant except hydrogen iodide section
- The complete SI plant except Bunsen reaction section
- The complete SI plant except sulfuric acid decomposition
- Hydrogen iodide section only
- Bunsen reaction section only
- Sulfuric acid decomposition plant only

B. Data Collection and Selection for Component of SI Plant

Following development of the SAPHIRE, five data sources (mentioned in the previous chapter) are evaluated to collect failure data for each major component. The failure data considered for this analysis included critical failures and degraded failures. Incipient failures, however, are not considered. The collection and comparison of data from these five sources for each of the components in the SI based hydrogen production plant is included in Appendix A.

C. Calculation for SI Plant

Table XII shows the cut sets results for the SI based thermochemical plant. From a total of 1857 cut sets, the first 22 cut sets shown in the table account for about 94% of total failures. Column 4 of the table shows the failure contribution for each of the components defined in the GA flow sheets, and column 3 represent the percentage contribution for each of the component failures to the total failure rate of the system. Column 2 is the cumulative failure contributions of components. These results show that the unavailability of the SI based thermochemical plant for a one year mission time is 0.02212, i.e., during a year the total number of hours the plant will be out of service due to component failures and repair time is about 193 hours or about 8 days.

As expected, as shown on Table XII, rotating or dynamic equipment like turbines, pumps, etc., have the highest failure rates and are the highest contributors to the overall system failure rate. These results indicate that the total failure probability of the SI plant is considerably higher than that expected for the economic nuclear hydrogen production using this plant. Therefore, further improvements in the SI hydrogen production plant reliability are needed. Different ways to improve the reliability of the plant are also identified during this analysis.

TABLE XII Cut Set for SI Based Hydrogen Production Plant

Sort/Slice Cut Set Report

Project : SI_PLANT Fault Tree: SI-PLANT
Min Cut Upper Bound: 2.212E-002 Units: Not Specified

Cut No.	% Total	% Cut Set	Prob./Frequency	Cut Sets
1	14.11	14.11	3.120E-003	TE101, Turbine/Expander
2	23.32	9.21	2.035E-003	TE103, Turbine/Expander
3	32.53	9.21	2.035E-003	TE104, Turbine/Expander
4	41.74	9.21	2.035E-003	TE201, Turbine/Expander
5	50.94	9.21	2.035E-003	TE301, Turbine/Expander
6	60.15	9.21	2.035E-003	TE302, Turbine/Expander
7	69.36	9.21	2.035E-003	TE303, Turbine/Expander
8	72.08	2.72	5.995E-004	P302, Pump
9	74.79	2.72	5.995E-004	P203, Pump
10	77.14	2.35	5.181E-004	TE102, Turbine/Expander
11	79.04	1.91	4.201E-004	C201-A
12	80.49	1.44	3.183E-004	S201
13	81.93	1.44	3.183E-004	S202
14	83.38	1.44	3.183E-004	S203
15	84.82	1.44	3.183E-004	S205
16	86.27	1.44	3.183E-004	E202-F1
17	87.71	1.44	3.183E-004	E202-F2
18	89.15	1.44	3.183E-004	E202-F3
19	90.60	1.44	3.183E-004	E202-F4
20	91.74	1.15	2.522E-004	S204
21	92.80	1.06	2.330E-004	S101
22	93.81	1.01	2.226E-004	S102

To reduce the overall system failure probability, additional redundancies need to be incorporated into the hydrogen production plant design, particularly for those components that are large contributors to the overall system failure probability. Therefore, different redundancies and design improvements and enhancements for the SI plant were continued using the SAPHIRE code to optimize the plant design and achieve higher hydrogen production efficiencies.

TABLE XIII Cut Set for SI Based Plant with Redundancies for Seven Number of Components

Sort/Slice Cut Set Report

Project : SI_PLANT Fault Tree: S-I-PLANT
Min Cut Upper Bound: 8.547E-003 Units: Not Specified

Cut No.	% Total	% Cut Set	Prob./Frequency	Cut Sets
1	7.02	7.02	5.995E-004	P302-A
2	14.04	7.02	5.995E-004	P203-A
3	20.11	6.07	5.181E-004	TE102-A
4	25.03	4.92	4.201E-004	C201-A
5	28.76	3.73	3.183E-004	S201
6	32.49	3.73	3.183E-004	S202
7	36.22	3.73	3.183E-004	S203
8	39.95	3.73	3.183E-004	S205
9	43.68	3.73	3.183E-004	E202-F1
10	47.41	3.73	3.183E-004	E202-F2
11	51.14	3.73	3.183E-004	E202-F3
12	54.86	3.73	3.183E-004	E202-F4

From column 4 of Table XII, it is apparent that the first seven components are responsible for about 70% of the total system failures. The next three components also have somewhat higher contributions to the overall system failure rate compared to the remaining components in the table. Therefore, redundancies for components are incorporated into the SAPHIRE model in two steps. In the first step, redundancies for first seven components of the above table are incorporated into the SAPHIRE model. Table XIII shows the resulting cut sets with these seven redundancies. In this table, only the first twelve cut sets out of a total of 1864 cut sets are shown.

The unavailability of the plant with these seven redundancies is 0.008547 for a mission time of one year. Therefore, the plant is likely to be out of service due to component failure and repair for an accumulated time of about 74 hours (a little more than three days) in a year. With redundancies included for the first eleven components, shown in Table XIV, the overall system unavailability is reduced to 0.009. It can be seen from the table that, first 12 components have failure probability close to each other and may not be reasonable to use further component redundancy to improve the system reliability more.

A single model is developed with the capability to perform all of the calculations described above. The model is developed in such a way that during a code run, the user can specify whether the model will be run without redundancy or with a specific number of redundancies. A separate calculation for each of the main chemical reaction sections is also possible with this model. For example a separate calculation for the Bunsen reaction process will give a total of 513 cut sets. Similar calculations for the hydrogen iodide and sulfuric acid decomposition sections are also possible to separately evaluate with this final developed model.

TABLE XIV Cut Set for SI Plant with Redundancies for Eleven Numbers of Components

Sort/Slice Cut Set Report

Project : SI_PLANT Fault Tree: SI-PLANT
Min Cut Upper Bound: 6.638E-003 Units: Not Specified

Cut No.	% Total	% Cut Set	Prob./Frequency	Cut Sets
1	4.80	4.80	3.183E-004	S201
2	9.60	4.80	3.183E-004	S202
3	14.40	4.80	3.183E-004	S203
4	19.20	4.80	3.183E-004	S205
5	24.00	4.80	3.183E-004	E202-F1
6	28.80	4.80	3.183E-004	E202-F2
7	33.60	4.80	3.183E-004	E202-F3
8	38.40	4.80	3.183E-004	E202-F4
9	43.11	4.71	3.120E-004	TE101-CCF
10	46.91	3.80	2.522E-004	S204
11	50.43	3.52	2.330E-004	S101
12	53.78	3.36	2.226E-004	S102

To verify the results of this modeling effort, additional calculations such as the minimum cut set upper bound approximation, min/max quantification, importance analysis, etc., were performed to check for inconsistencies in the analyses. Results from those calculations are not included here considering the goal and mission of these studies. However, the results of a fault tree uncertainty analysis without any redundancy are presented in Figure 34. This uncertainty analysis is based on Monte Carlo sampling, with uncertainty data for each component provided to the SAPHIRE model. Figure 34 shows the plot of probability distribution including relevant statistical values; a trial run of 5000 was used for this uncertainty analysis.

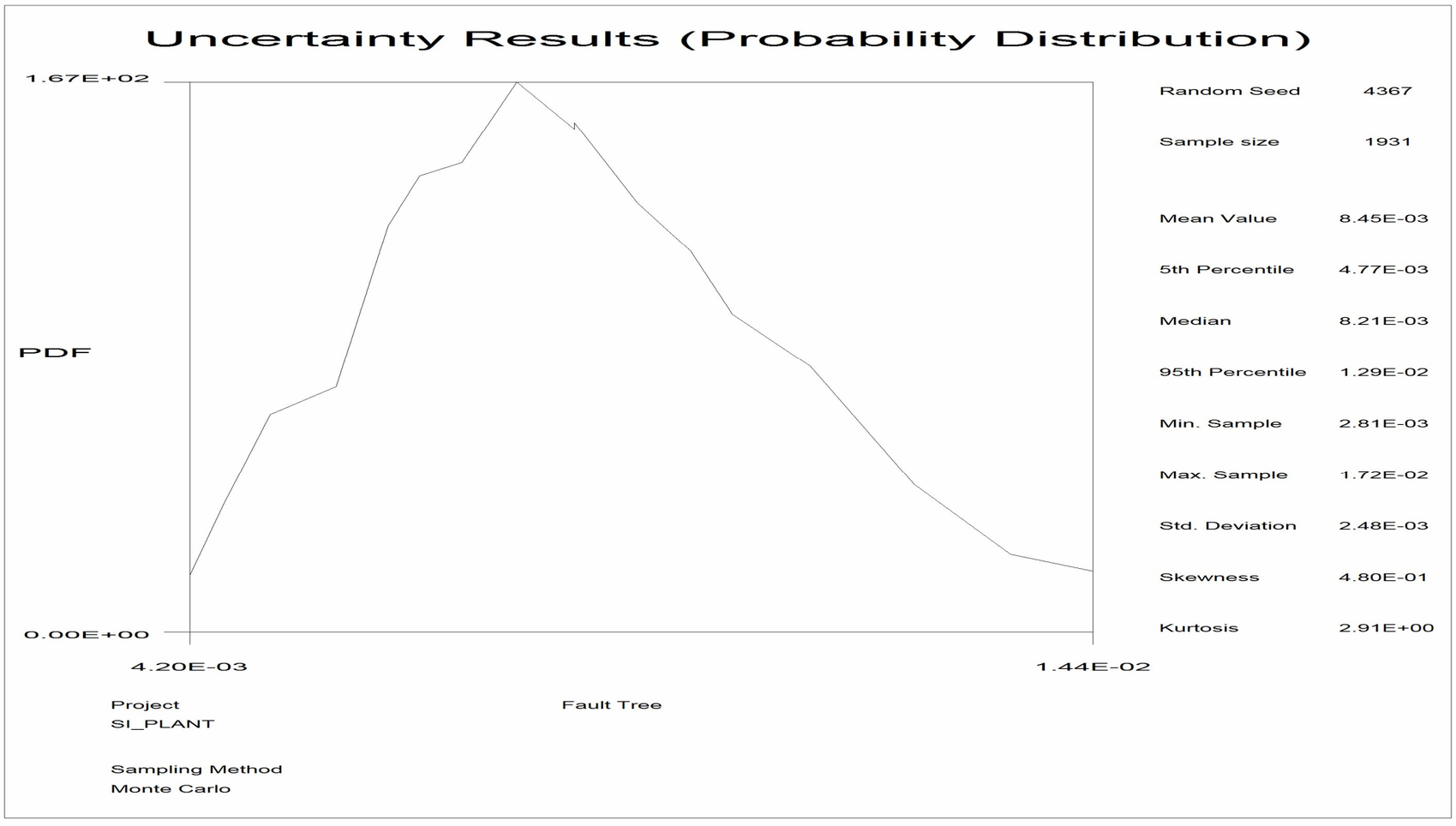

Fig. 34. Uncertainty analysis: Probability distribution for SI plant model.

CHAPTER IX

SAPHIRE ANALYSIS OF HTE PLANT

The development of the Probabilistic Risk Analysis (PRA) model for the High Temperature Electrolysis (HTE) process is important in order to perform reliability, availability and maintainability studies, and economic analyses of the HTE based nuclear hydrogen production process. This work is one component of a complete PRA model for the entire nuclear hydrogen production process that should ultimately be developed. This chapter will discuss the development of PRA model, reliability and availability studies performed, improvements to system reliability and optimization of the plant design for the HTE based nuclear hydrogen production process. The SAPHIRE model includes the HTE plant and the Brayton cycle power conversion system.

The fault tree model for the HTE based nuclear hydrogen production plant is first developed and then the reliability and availability of the system are assessed. The availability includes the estimation of the expected number of total hours or days the plants will be out-of-service due to component failures during a specified mission time. For most cases the mission time is a year. These studies also evaluate component redundancies to improve and optimize the plant design for improved economics and reliable operation of nuclear hydrogen production process. The HTE based hydrogen production plant also has a number of closed loop component dependencies similar to those in the SI based plant. Therefore, the closed loop dependencies in the HTE plant schematic need to be modeled as equivalent open loop dependencies in the SAPHIRE model.

A brief discussion of the HTE plant was included in Chapter I. The component information, stream line constituents, temperatures, pressures and all other necessary information for the SAPHIRE model are taken from the information generated by the HYSYS process analysis code at INL. The most recent flow sheet information from the HYSYS code is incorporated into the SAPHIRE model as the design evolved.

A. The SAPHIRE Model Development for HTE Plant

The SAPHIRE model for the HTE plant is developed by evaluating the schematic of the HTE plant and selecting the top event for the fault tree. The entire HTE based hydrogen production process plant is then broken down into several sub sections, and the sub-section boundaries are defined. The master fault tree for this model is shown in Figure 35. The extensions to the master fault tree that consist of other fault trees and sub-trees for the HTE subsections are not shown here but have been handed over to GA/INL which consists of the complete SAPHIRE model. The SAPHIRE model for the HTE based hydrogen production plant has been developed to provide the maximum possible analysis flexibility. There will be an option to perform SAPHIRE analyses with or without the MHR included. The SAPHIRE model is also capable of analyzing the system by either including or excluding the Brayton Cycle Power Conversion System (BC-PCS). In addition, during a run, the user can specify any particular redundancy that he or she chooses to consider in the analyses.

The system configuration, flow sheet and information about the component are obtained from the result of conceptual design for the High Temperature Electrolysis process using HYSYS at INL. Three transfer gates used in the main fault tree correspond to heat transfer section, hydrogen production section and make-up water plus oxygen section as shown and discussed briefly in Chapter I.

B. Data Analysis for the Components of HTE Plant

A combination of critical and degradation failure rates for each of the major components, mean repair time and their uncertainty are studied. Complete tables for these data are shown in Appendix B. Five data sources as mentioned in Chapter VII have been evaluated for this purpose.

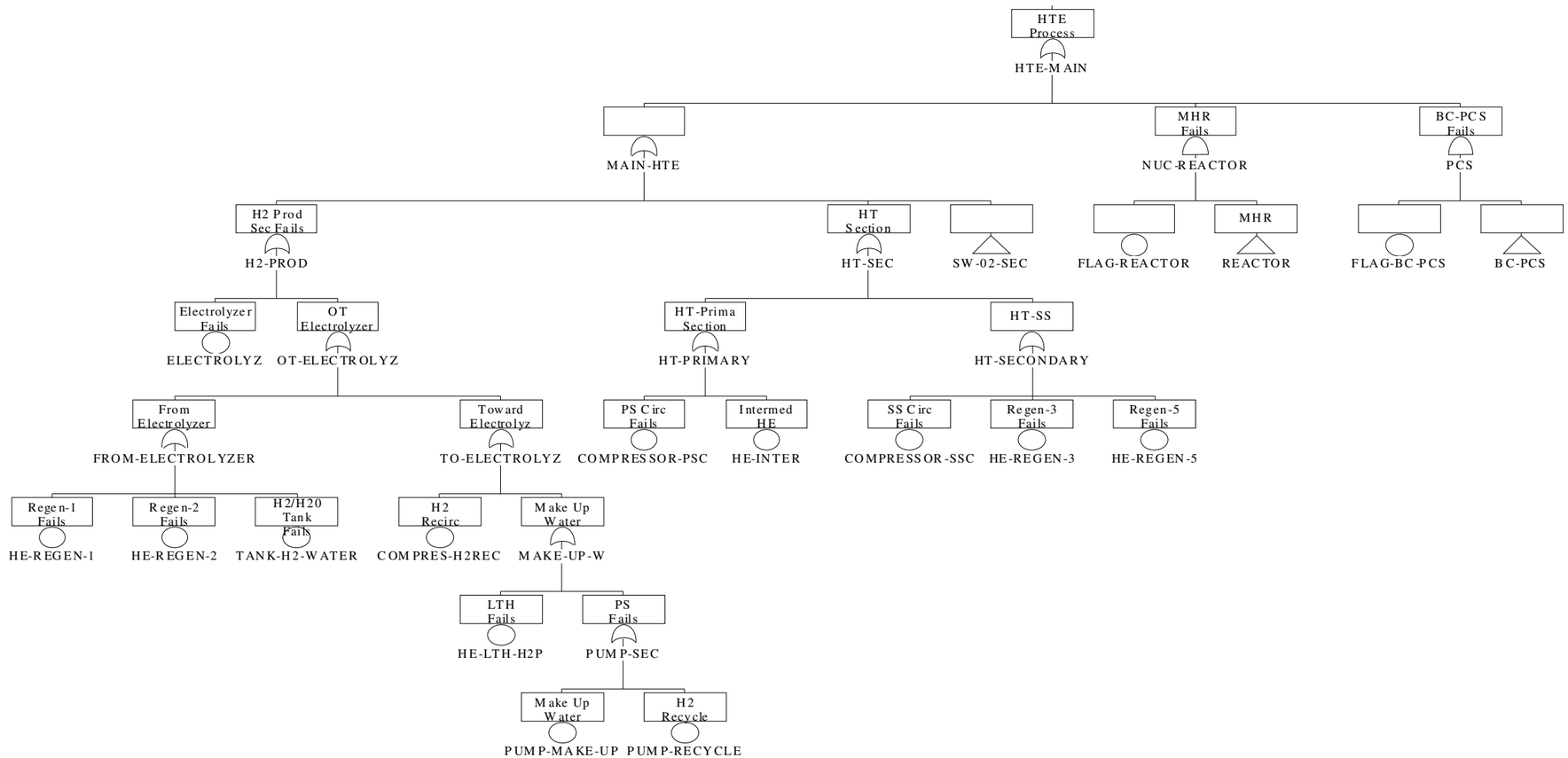

Fig. 35. Main fault tree for the HTE process.

No failure data for the electrolyzer (which is the major component of the HTE process) is found in any of the available data sources. However, according to CERAMATEC (the provider of the electrolysis cells being developed at the INL), the expected mean time between failures for each cell is approximately 50,000 hours. The corresponding failure rate for the electrolyzer is derived from this expected mean time between failures. The electrolyzer is expected to experience 0.5% degradation in 1000 hours. If it is assumed that failure of 25% of the cells constitutes total failure of the Electrolysis stack, then including 25% more cells than required along with the option to replace cells during operation would result in a highly reliable electrolyzer design. Since no additional information is available, this assumption is made and corresponding failure rate derived from the mean failure time is used as the failure rate for the Electrolysis stack in the SAPHIRE analysis. Although the above assumptions are made to simplify the analysis of the HTE process, this sort of approach may be taken in actual practice to achieve high reliability of the HTE plant design.

C. Calculation for HTE Plant

The fault tree analysis provides information on overall system reliability. The fault tree analysis also shows the contribution of each of the components to the overall failure rate of the system, the way the system reliability can be improved, and the fractional improvement of system reliability corresponding to individual component redundancies. The SAPHIRE model for this plant is developed in such a way that, it calculates the failure probability of the plant due to component failures and considers the plant as unavailable or out of service during the mean repair time of the failed components unless redundancies are included.

Although more detailed information on risk reduction/increase and the uncertainly of results are generated and can be provided, only the cut set report, i.e., the different ways the plant can fail, are presented here.

Table XV shows the first 10 cut sets from a total of 25 cut sets generated for the HTE plant by the SAPHIRE analysis for a mission time of one year. The first 6 cut sets of this table are higher contributor for the system failure and are responsible for about 88% of the total failure of the plant. This result indicates that the unavailability of the plant within a year is 0.02661, i.e., the accumulated time the HTE plant is likely to be out of service due to component failures and component repair time is about 233.1 hours or about 10 days. The table shows the component names and their corresponding failure contribution to the total system failure rate.

TABLE XV Cut Set for HTE Plant Including BC-PCS and No Redundancy

Sort/Slice Cut Set Report

Project: HTE_PLANT Fault Tree: HTE-MAIN

Min Cut Upper Bound: 2.661E-002

Cut No.	% Total	% Cut Set	Prob./Frequency	Cut Sets
1	30.71	30.71	8.172E-003	TURBINE
2	44.59	13.88	3.692E-003	COMPRESSOR-HP
3	58.47	13.88	3.692E-003	COMPRESSOR-LP
4	68.28	9.81	2.609E-003	COMPRESSOR-H2REC-1
5	78.09	9.81	2.609E-003	COMPRESSOR-PSC-1
6	87.90	9.81	2.609E-003	COMPRESSOR-SSC-1
7	89.85	1.96	5.188E-004	EXPAN-O2-STEAM
8	91.58	1.73	4.585E-004	PUMP-MAKE-UP
9	93.31	1.73	4.585E-004	PUMP-RECYCLE
10	95.04	1.73	4.585E-004	PUMP-SW

These results show that components in the BC-PCS, especially rotating components like the turbine, compressors, etc., are the largest contributors to the overall system failure rate. In reality the whole BC-PCS will be within a single housing, and individual components are not likely to be replaced. As a result, redundancy is not feasible for BC-PCS or for any of its major component. Therefore, our focus for this analysis is on the rest of the components in the HTE plant. Therefore, the SAPHIRE model for the HTE plant was then run without taking into consideration the BC-PCS. The results of this analysis are presented in Table XVI, which shows the 10 cut sets that are responsible for about 90% of the total system failure probability. In this case the main contributors to the system failures are the three compressors: H_2-re-circulator, primary side circulator, and secondary side circulator.

TABLE XVI Cut Set for HTE Plant without Any Redundancy

Sort/Slice Cut Set Report

Project : HTE_PLANT Fault Tree: HTE-MAIN

Min Cut Upper Bound: 1.093E-2 Units: Not Specified

Cut No.	% Total	% Cut Set	Prob./Frequency	Cut Sets
1	23.88	23.88	2.609E-003	COMPRESSOR-H2REC-1
2	47.75	23.88	2.609E-003	COMPRESSOR-PSC-1
3	71.63	23.88	2.609E-003	COMPRESSOR-SSC-1
4	76.38	4.75	5.188E-004	EXPAN-O2-STEAM
5	80.58	4.20	4.585E-004	PUMP-MAKE-UP
6	84.78	4.20	4.585E-004	PUMP-RECYCLE
7	88.98	4.20	4.585E-004	PUMP-SW
8	91.39	2.40	2.620E-004	TANK-H2-WATER
9	93.79	2.40	2.620E-004	TANK-V100
10	95.93	2.14	2.333E-004	TANK-H20-O2

Table XVI shows the first 10 cut sets from a total of 19 cut sets generated for the HTE plant using the SAPHIRE model for a mission time of one year. The unavailability of the plant during a year in this case is 0.01093, i.e., the accumulated time the HTE plant is likely to be out of service due to component failures and component repair time is about ~96 hours or about ~4 days. The third column of the table shows the failure contribution for each component. It shows where we have to use component redundancy to improve the system reliability and how much the system reliability will be improved by each redundancy. The first two and three components of above table account for about 48% and 72% respectively of total system failure.

This calculation shows that the unavailability or outage of the HTE plant is less than both the MHR and the BC-PCS. The availability of the combination of MHR and the BC-PCS is about 90%. Even though the reliability of the HTE based hydrogen production plant is higher than both the MHR and BC-PCS, this reliability is advised for further improvement by adding component redundancies to minimize the probability of failed components in the HTE plant shutting down the entire system. This redundancy is incorporated to ensure that any possible failure of the HTE based nuclear hydrogen production process would happen due to failure of the component from either MHR or the BC-PCS but not due to failure of the HTE plant or its component. To reduce the system failure probability due to component failures in the HTE plant, the redundancies for the first three components in the above table are incorporated into the SAPHIRE model. As mentioned before, the user can include or exclude these redundancies for components during execution of the SAPHIRE model.

Table XVII shows the unavailability of the plant with the three component redundancies. For this case, the calculated outage of the plant for a mission time of one year is 0.003947, i.e., ~35 hours. Therefore, these redundancies could be incorporated into the plant design to achieve higher reliabilities for the nuclear hydrogen production process.

As was done for the SI process, additional analyses, including minimum cut set upper bound approximation, min/max quantification, importance analysis, etc., are

performed to check for inconsistencies in the analyses. Results from these analyses are not included here, but the results of a fault tree uncertainty analysis are presented in Figure 36. This uncertainty analysis is based on Monte Carlo sampling, with uncertainty data for each component provided to the SAPHIRE model. Figure 36 shows the plot of the probability distribution and relevant statistical values for the analysis of the HTE plant.

TABLE XVII Cut Set for HTE Plant Only with Three Redundancies

Sort/Slice Cut Set Report

Project : HTE_PLANT Fault Tree: HTE-MAIN

Min Cut Upper Bound: 3.947E-003 Units: Not Specified

Cut No	% Total	% Cut Set	Prob./Frequency	Cut Sets
1	13.15	13.15	5.188E-004	EXPAN-O2-STEAM
2	24.77	11.62	4.585E-004	PUMP-MAKE-UP
3	36.39	11.62	4.585E-004	PUMP-RECYCLE
4	48.01	11.62	4.585E-004	PUMP-SW
5	54.65	6.64	2.620E-004	TANK-H2-WATER
6	61.29	6.64	2.620E-004	TANK-V100
7	67.91	6.61	2.609E-004	COMPRESSOR-H2REC-CCF
8	74.52	6.61	2.609E-004	COMPRESSOR-PSC-CCF
9	81.14	6.61	2.609E-004	COMPRESSOR-SSC-CCF
10	87.05	5.91	2.333E-004	TANK-H20-O2

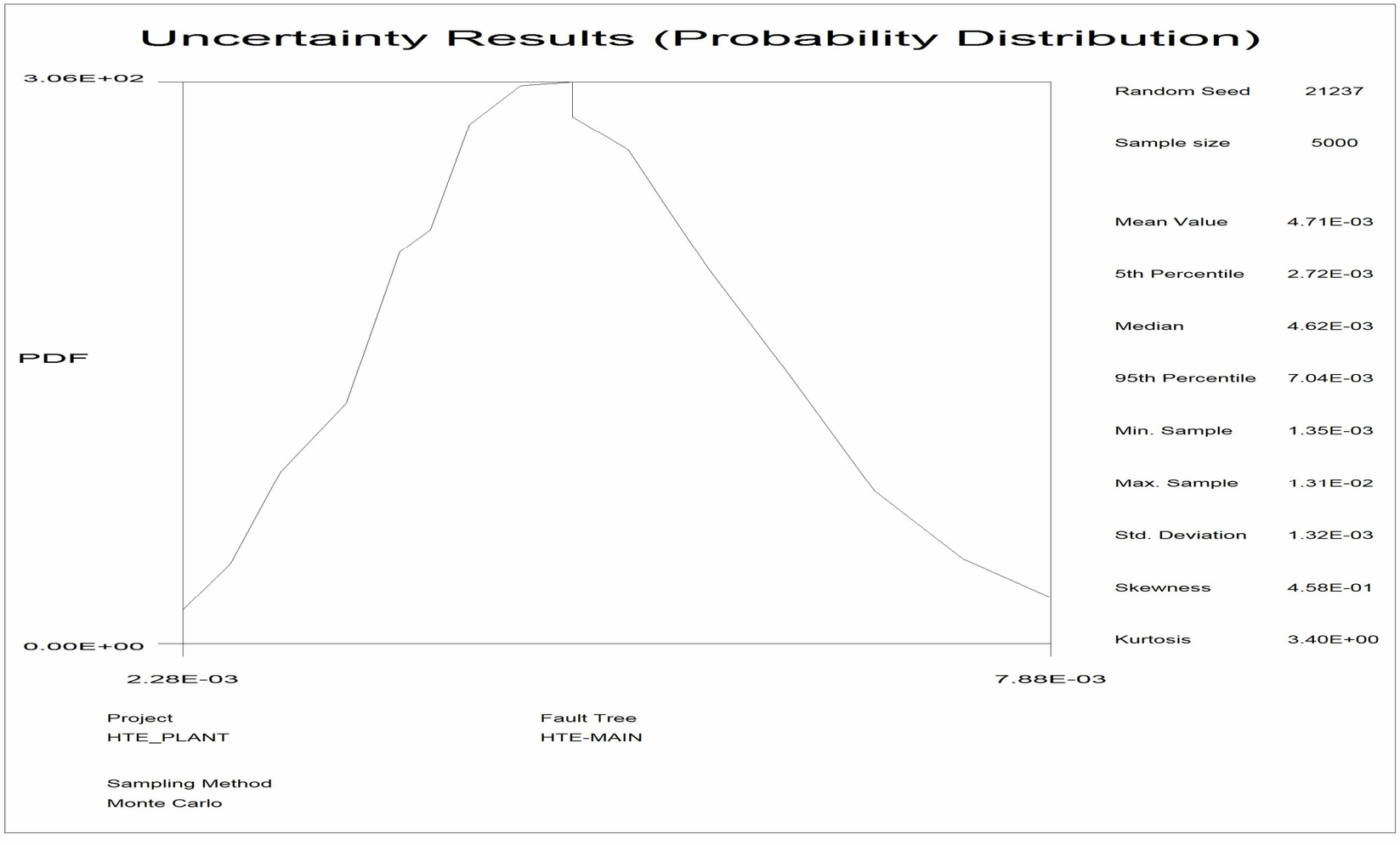

Fig. 36. Uncertainty analysis: Probability distribution for HTE plant model.

CHAPTER X

SUMMARY

Design modifications for a MHR for higher temperature operation and the reliability studies for the nuclear hydrogen production processes have been performed. An alternative coolant path through the permanent side reflector has been developed and evaluated. In addition, a new graphite block (fuel element) reactor core design has been evaluated and optimized. Using the alternative coolant scheme through PSR and the new core design together, the vessel temperature during steady-state operation has been reduced to about 350 ^{0}C, which is comparable to the vessel temperature in a LWR.

The MHR with inlet and outlet temperatures of 590 ^{0}C and 950 ^{0}C, respectively had a calculated peak vessel temperature of 541 ^{0}C. With the alternative configuration for the coolant inlet flow through the PSR, the calculated vessel temperature during steady-state operation is reduced to ~421 ^{0}C. With the new graphite block (fuel element) core design the coolant inlet temperature is reduced to 482 ^{0}C. This reduced inlet temperature together with the alternative coolant scheme result a further reduction in the calculated vessel temperature to 350 ^{0}C.

The reduced steady state reactor vessel temperature allows the MHR to operate at the higher coolant outlet temperatures which is required for efficient hydrogen production. In the original design of the MHR, 9Cr-1Mo-V was prescribed as the vessel material for the reactor vessel which is too costly compared to the vessel material of LWR. In addition, the fabrication of reactor vessel for MHR with high temperature material like 9Cr-1Mo-V and with the current size is not likely to be possible with the world's existing facility. Therefore, it was necessary to reduce the vessel operating temperature or the vessel size to be consistent with the current existing facilities. Therefore, the reduction of vessel temperature will result in a significant reduction in the cost for the reactor vessel material and for the reactor design. In addition, due to this reduced vessel temperature the vessel can be made in any reasonable size.

During the design of the new inlet coolant passage, all limiting criteria are found to be within acceptable range. The amount of graphite removal is 10% of outer reflector which is well below the maximum limit of 20%. The pressure drop for the final design is ~60 KPa which is well below the maximum allowable limit of ~90 KPa. The inlet coolant velocity is found to be consistent with the coolant velocity in the reactor core. The peak fuel temperature and peak vessel temperature of the reactor during both LPCC and HPCC transients are found to be within acceptable limits.

For the modification of reactor core design, the numbers of fissile and fertile particles are conserved in the final design. The dimensions of fuel rod, coolant hole, web thickness etc. in the final design are within design limit. The peak fuel temperature is maintained within acceptable limit.

The new block design has a smaller hydraulic diameter, but due to the reduced inlet temperature, the mass flow rate through the reactor core is reduced from 324 kg/sec to 249.3 kg/sec, resulting in a pressure drop comparable to that of the current GT-MHR design.

For the alternative coolant configuration, about ~10% of the graphite from the outer reflector (which is about ~5% graphite heat capacity for the entire core) is removed to accommodate the new coolant path. The removal of graphite may affect the neutron leakage from the reactor, neutron dose to the reactor vessel, criticality of the reactor, etc. Evaluation of those effects is beyond the scope of these studies and should be addressed in future work. At this conceptual design stage, the limits on the amount of graphite removal and acceptable inlet coolant flow velocities are based in large measure on previous experience and engineering judgment. More detailed assessments should be performed to proceed from this conceptual design stage to the preliminary and final design stages.

With the new core deign the allowable ΔT across the reactor core is increased from 350 ^{0}C to ~468 ^{0}C. This increased ΔT across the reactor core results a reduced peak vessel temperature of ~350 ^{0}C – 360 ^{0}C at normal operating condition. Any possible

adverse influence of this higher ΔT across the reactor core to the flow stability or reactor performance, need to be addressed.

To modify and evaluate the new reactor core design, the reactor core which already has the new coolant configuration through permanent side reflector has been used. The calculation for the core design modification with the original coolant configuration through the annular path between reactor core barrel and reactor vessel wall is not included.

Two key parameters for these studies are core bypass flow and power distribution. Calculations show that for up to 15% core bypass flow, the PVT can be reduce to ~350 ^{0}C. If the bypass flow is about 20% then a portion of fuel may have temperatures above 1250 ^{0}C depending on the core power distribution. A detailed study of core bypass flow and precise power distributions consistent with the reactor core layout are recommended.

The above calculations assume no bypass or leakage of the core coolant flow through the annular path between the core barrel and reactor vessel wall. Since even a small leak of helium through this annular path significantly affects the calculated vessel wall temperatures, preventing this leakage could be a major design requirement. Preventing of any possible leakage of inlet helium through the original coolant path needs to be addressed in future to avoid any excessive temperature rise of the reactor vessel during normal operation.

SAPHIRE models for probabilistic risk analysis and for reliability/availability studies of the nuclear hydrogen production plants have been developed and evaluated. The Fault Tree models for both the SI and HTE based nuclear hydrogen production processes have been developed. These models have been used to evaluate the reliability and availability of the plants. The required redundancies are made to improve the system reliability and to optimize plant design. With several redundancies, the reliability of the plants found to be within acceptable levels.

System reliability is determined based on equipment reliability which is determined based on component reliability. Failure data for each of the equipment is

used for this analysis, but the developed model can be extended up to component reliability. For these analyses five data sources have been used to collect failure data for the process equipment. Access to more data bases in future might help to get more relevant data for equipment and components.

The common cause failure probabilities (as well as the alpha and beta factors) are determined based on the thumb rule for this analysis. A detailed study for exact alpha and beta factor and for common cause failure probability for each redundant component may be performed in the future. The cost for these redundancies might be addressed. In addition, the developed model does not develop its own maintenance schedule likely to follow the same maintenance schedule of the MHR.

Some sections of the hydrogen production plant(s) are not included in the flow sheet yet, such as the water treatment plant, product hydrogen purification plant, etc. Therefore, failure of these support systems was not considered in this analysis. When more detailed information on these support systems becomes available, these systems could be included in the current model as part of future developmental design efforts.

REFERENCES

1. L. C. BROWN, G. E. BESENBRUCH, R. D. LENTSCH, K. R. SCHULTZ, J. F. FUNK, P. S. PICKARD, A. C. MARSHAL, S. K. SHOWALTER, "High Efficiency Generation of Hydrogen Fuels Using Nuclear Power," GA-A24285, General Atomics, San Diego, CA (2003).
2. M. B. RICHARD, A. S. SHENOY, K. R. SCHULTZ, L. C. BROWN, E. A. HARVEGO, M. G. MCKELLAR, J. P.COUPEY, S. M. M. REZA, F. OKAMOTO and N. HANDA, "H2-MHR Conceptual Designs Based on the Sulfur-Iodine Process and High Temperature Electrolysis," *International Journal of Nuclear Hydrogen Production and Application,* **1**, 36 (2006).
3. P. E. MACDONALD, P. D.BAYLESS, H. D.GAUGAR, R. L. MOORE, A. M. OUGOUAG, R.L. SANT, J.W. STERBENTZ and W.K.TERRY, "NGNP Preliminary Point Design-Results of the Initial Neutronics and Thermal-Hydraulic Assessment," INEEL/EXT-03-00870, Idaho National Laboratory , Idaho Falls, ID (2003).
4. INTERNATIONAL ATOMIC ENERGY AGENCY, "Hydrogen as an Energy Carrier and its Production by Nuclear Power," TECDOC-1085, Vienna (1999).
5. C. W. FORSBERG and K.L. PEDDICORD, "Why Hydrogen Production from Nuclear Power? (Is Nuclear Energy Compatible with Hydrogen Production?)," *American Institute of Chemical Engineers Spring National Meeting*, New Orleans, LA (March 2002).
6. A. C. MARSHAL, "An Assessment of Reactor Types for Thermo Chemical Hydrogen Production," SAND2002-0513, Sandia National Laboratory, Albuquerque, NM and Livermore, CA (2002).
7. NATIONAL ACADEMY OF SCIENCES, NATIONAL RESEARCH COUNCIL, "The Hydrogen Economy: Opportunities, Costs, Barriers and R&D Needs," National Research Council Report, Washington DC (2004).

8. M. B. RICHARD, A. S. SHENOY, K. R. SCHULTZ, L. C. BROWN, F. OKAMOTO, and Y. KISO, "The H2-MHR: Nuclear Hydrogen Production Using the Modular Helium Reactor," *Proc. International Congress on Advances in Nuclear Power Plants (ICAPP)*, Seoul, Korea, May 15-19, 2005.
9. Energy Group of General Atomics, San Diego, CA (Personal Communication)
10. GENERAL ATOMICS, "Gas Turbine-Modular Helium Reactor (GT-MHR) Conceptual Design Report," GA-910720, General Atomics, San Diego, CA (1996).
11. M. B. RICHARDS, A. S. SHENOY, E. A.HARVEGO, M. G. MCKELLAR, K. L. PEDDICORD, S.M.M.REZA and J.P.COUPEY, "H2-MHR Pre-Conceptual Design Report: HTE Based Plant," GA A25402, General Atomics, Idaho National Laboratory and Texas A&M University (2006).
12. E. A. HARVEGO, S. M. M. REZA, M. B. RICHARDS, A. S. SHENOY, "An Evaluation of Reactor Cooling and Coupled Hydrogen Production Processes Using Modular Helium Reactor," *International Journal of Nuclear Engineering and Design,* **236**, 14-16, (2006).
13. E. A. HARVEGO, S. M. M. REZA, M. B. RICHARDS, A. S. SHENOY, "Hydrogen Production using the Modular Helium Reactor," *Proc. 13th International Conference on Nuclear Engineering, (ICONE-13)*, Beijing, China, May 16-20, 2005.
14. "RELAP-3D© Code Manual," RELAP-3D© Code Development Team, Idaho National Laboratory (1999).
15. "RELAP5-3D/ATHENA© Code Manual," RELAP5-3D/ATHENA© Code Development Team, Idaho National Laboratory (2005).
16. S. M. M. REZA, E. A. HARVEGO, M. B. RICHARDS, A. S. SHENOY, K. L. PEDDICORD, "Design of an Alternative Coolant Inlet Flow Configuration for the Modular Helium Reactor," *Proc. International Congress on Advances in Nuclear Power Plants (ICAPP)*, Reno, NV, June 4-8, 2006.

17. KEVIN T. CLARNO, "Development of a RELAP5-3D Three-Dimensional Model of a VVER-1000 Nuclear Power Plant for Analysis of a Large-Break Loss-of-Coolant Accident," M.S. Thesis, Texas A&M University (August 2001).
18. M. B. RICHARDS, A. S. SHENOY, K. SCHULTZ, L. BROWN, E. A. HARVEGO, M. G. MCKELLAR, F. OKAMOTO, N. HANDA, J. P. COUPEY, S.M.M. REZA, "Conceptual Design for MHR-Based Hydrogen Production Systems," *Proc. 7th International Conference on Nuclear Energy Systems for Future Generation and Global Sustainability (GLOBAL)*, Tsukuba, Japan, October 9-13, 2005.
19. R. KAPERNICK, "POKE User's Manual," CEGA-002928, General Atomics, San Diego, CA (1993).
20. "Fuel Design Data Manual," GA-901866 (ISSUE F), General Atomics, San Diego, CA (1987).
21. C. B. DAVIS and G. L. HAWKES, "Thermal Hydraulic Analysis of the LS-VHTR," *Proc. International Congress on Advances in Nuclear Power Plants (ICAPP)*, Reno, NV, June 4-8, 2006.
22. H. KUMAMOTO and E. J. HENLEY, *Probabilistic Risk Assessment and Management for Engineers and Scientists,* 2nd Edition, IEEE Inc., New York (1996).
23. "SAPHIRE Code Manual," SAPHIRE Code Development Team, Idaho National Laboratory, Idaho Falls, ID (2005).
24. *Offshore Reliability Data (OReDA),* SINTEF INDUSTRIAL MANAGEMENT, 4th Edition, OREDA Participants, Trondheim, Sweden (2002).
25. H. PROCACCIA, S. P. ARSENIS, and P. AUFORT, *European Industry Reliability Data Bank (EIReDA),* 3rd Edition, Crete University Press, European Commission Joint Research Center, Crete, Greece (1998).
26. *Guidelines for Process Equipment Reliability Data with Data Tables,* American Institute of Chemical Engineers (AIChE), Center for Chemical Process Safety (CCPS) of the AIChE, New York (1989).

27. THE ATV OFFICE, STUDSVIK AB, *T-Book: The Reliability Data of Components in Nordic Nuclear Power Plants,* 3rd Edition, The ATV Office, Vattenfall AB, Vallingby, Sweden (1992).
28. T. R. MOSS, *The Reliability Data Handbook,* 1st Edition, ASME Press, New York (2005).
29. F.M. MARSHALL, D.M. RASMUSON, A. MOSLEH, "Common Cause Failure Parameter Estimations," NUREG/CR-5497, INEEL/EXT-97-01328, Idaho National Laboratory, Idaho Falls, ID (1998).
30. F.M. MARSHALL, A. MOSLEH, D.M. RASMUSON, "Common-Cause Failure Database and Analysis System: Data Collection and Event Coding," NUREG/CR-6268, INEEL/EXT-97-00696, Idaho National Laboratory, Idaho Falls, ID (1998).

APPENDIX A

DATA FOR COMPONENTS OF SI PLANT

Check valve

Item Description	Data Source	Type	Mean Failure Rate $\times 10^6$				Error Function/Standard Deviation $\times 10^6$				Mean Repair Time (hrs)
			Critical	Degrade	Incipient	All Modes	Critical	Degrade	Incipient	All Modes	
Three check valve used before each Flash separator, Type of valves is unknown.	OREDA-P600	CV, Chemical Injection	---	---	---	0.28	---	---	---	0.39	---
			---	---	---	0.29	---	---	---	0.41	---
	EIReDA P93	CV-Water	---	---	---	0.22	---	---	---	3E+6	15.0
			---	---	---	---	---	---	---	---	---
	T-book P123-4	CV	---	---	---	0.98*	---	---	---	---	---
			---	---	---	---	---	---	---	---	---
	CCPS P198	CV-Non-Operated	---	---	---	3.18	---	---	---	---	---
			---	---	---	---	---	---	---	---	---
	T R Moss P256		---	---	---	2.0	---	---	---	---	---
			---	---	---	---	---	---	---	---	---

*Fail to open = 2.8×10^{-7}, Fail to close = 7×10^{-7}, Total failure is 9.8×10^{-7}

Heat Exchanger

Item Description	Data Source	Fluid	Mean Failure Rate $\times 10^6$				Error Function/Standard Deviation $\times 10^6$				Repair time (hrs) Crit/Deg/ Inc →All Modes
			Critical	Degrade	Incipient	All Modes	Critical	Degrade	Incipient	All Modes	
Heat Exchanger, Shell-tube, product/helium, E202-2, E202-3, E202-4, E204, E205, E206, E207, E215, E306, E309 [E-HEL-PRO]	OREDA-P409	Gas-water/glycol	4.25 4.44	4.51 4.67	54.12 56.77	63.03 66.0	5.77 6.07	4.39 4.57	58.29 61.68	56.57 60.09	11.0 ---
	OREDA-P405	Gas/water	00 00	17.56 28.52	175.62 270.98	189.47 299.50	00 00	13.45 28.51	41.47 203.60	63.01 245.26	7.7 (mh) ---
	EIReDA-P44	Water/ Dematerialized water	0.2 ---	--- ---	--- ---	0.2 ---	--- ---	--- ---	--- ---	10E+6 ---	25 ---
	T-book	---	---	---	---	---	---	---	---	---	---
	CCPS-P182	Any	31.1 ---	25.8 ---	--- ---	56.9 ---	--- ---	--- ---	--- ---	--- ---	--- ---
	T R Moss P-255	Any	--- ---	--- ---	--- ---	32.7 ---	--- ---	--- ---	--- ---	--- ---	--- ---
Heat Exchanger, Shell-tube, water/product, R101, E102, E201, E208, E209, E210, E211, E212, E213, E214, [E-PRO-PRO-W]	OREDA-P413	water/ glycol	00 00	00 00	10.19 10.63	10.19 10.63	00 00	00 00	10.19 10.63	10.19 10.63	17.5 ---
	EIReDA-P44	Water/ Dematerialize water	0.2 ---	--- ---	--- ---	0.2 ---	--- ---	--- ---	--- ---	10E+6 ---	25 ---
	T-book	---	---	---	---	---	---	---	---	---	---
	CCPS-P182	Any	31.1 ---	25.8 ---	--- ---	56.9 ---	--- ---	--- ---	--- ---	--- ---	--- ---
	T R Moss P-255	Any	--- ---	--- ---	--- ---	32.7 ---	--- ---	--- ---	--- ---	--- ---	--- ---
Heat Exchanger, Shell-tube, product/product, E202-1, E203, E301, E302, E303, E304, E305, E307, E308, [E-PRO-PRO-W]	OREDA-P413	water/ glycol	00 00	00 00	10.19 10.63	10.19 10.63	00 00	00 00	10.19 10.63	10.19 10.63	17.5 ---
	EIReDA-P44	Water/ Dematerialized water	0.2 ---	--- ---	--- ---	0.2 ---	--- ---	--- ---	--- ---	10E+6 ---	25 ---
	T-book	---	---	---	---	---	---	---	---	---	---
	CCPS-P182	Any	31.1 ---	25.8 ---	--- ---	56.9 ---	--- ---	--- ---	--- ---	--- ---	--- ---
	T R Moss P-255	Any	--- ---	--- ---	--- ---	32.7 ---	--- ---	--- ---	--- ---	--- ---	--- ---

Power Recovery Devices: Turbine/liquid Expander

Item Description	Data Source	Power/ Purpose	Mean Failure Rate $\times 10^6$				Error Function/Standard Deviation $\times 10^6$				Repair time (hrs)
			Critical	Degrade	Incipient	All Modes	Critical	Degrade	Incipient	All Modes	All Modes
Gas Turbine, TE101 [GT], 5987 shaft hp.	OREDA-P129	--/Gas	354.75 553.77	266.17 369.56	569.36 1359.67	1199.23 2398.21	312.92 577.96	189.13 276.08	569.36 932.68	808.20 1648.61	17.7 ---
	OREDA-P136	-1 MW /Gas (Aero-derivative)	363.52 590.62	236.55 364.69	575.67 936.50	1186.51 1909.61	373.99 767.34	196.70 352.71	455.61 968.51	1186.51 1909.61	14.7 ---
	OREDA-P143	-1 MW /Gas	364.05 364.41	123.31 123.44	120.91 120.99	601.1 601.54	48.51 48.56	107.57 107.77	50.62 50.80	182.47 183.26	19.7 ---
	OREDA-P144	3-10 MW /Gas	202.53 257.67	141.27 181.76	563.46 732.87	955.76 1216.9	65.71 103.68	38.89 50.31	31.69 35.56	102.33 198.36	5.1 (9.3C)
	EIReDA-P86	Any/Steam, drives generator	3200 ---	--- ---	--- ---	3200 ---	2.3E+6 ---	--- ---	--- ---	2.3E+6 ---	13 ---
	T-book P192-3	Standby, No data for Running	--- ---	--- ---	--- ---	**4.6 ---	--- ---	--- ---	--- ---	--- ---	3 ---
	CCPS	---	---	---	---	---	---	---	---	---	---
	T R Moss P-254	---	--- ---	--- ---	--- ---	*1235.8 ---	--- ---	--- ---	--- ---	--- ---	--- ---
Turbine-Expander, Oxygen mixed with some other liquid, TE102 [GT1], 135 shaft hp	OREDA-P280	Any/Combined	57.08 57.08	00 00	171.23 171.23	228.31 228.31	57.08 57.08	00 00	171.23 171.23	228.31 228.31	--- ---
	OREDA-P281	Gas Processing	85.59 101.91	114.11 135.89	162.54 208.65	374.56 469.46	18.68 21.98	21.56 25.38	124.20 176.84	81.64 163.41	32.4 (mh)
	EIReDA-P86	Any/Steam, drives generator	3200 ---	--- ---	--- ---	3200 ---	2.3E+6 ---	--- ---	--- ---	2.3E+6 ---	13 ---
	T-book P192-3	Standby, No data for Running	--- ---	--- ---	--- ---	**4.6 ---	--- ---	--- ---	--- ---	--- ---	3 ---
	CCPS	---	---	---	---	---	---	---	---	---	---
	T R Moss P-254	Gas Turbine	--- ---	--- ---	--- ---	*1235.8 ---	--- ---	--- ---	--- ---	--- ---	--- ---
Turbine-Liquid Expander, TE103A, TE103B, TE103C, TE201, TE301, TE302, TE303 [LE1]	OREDA-P272	Any/ Expander	72.61 81.9	91.82 115.65	302.06 326.31	459.16 510.39	27.31 38.41	54.01 21.33	259.49 276.13	204.5 217.9	32.4 (73.4) (mh)
	EIReDA	---	---	---	---	---	---	---	---	---	---
	T-book	---	---	---	---	---	---	---	---	---	---
	CCPS	---	---	---	---	---	---	---	---	---	---
	T R Moss P-254	Steam Turbine	--- ---	--- ---	--- ---	29 ---	--- ---	--- ---	--- ---	--- ---	--- ---

*(4212+3550+1667+1484+865+525+491+320+240+205+35)÷11=1235.8

**(7+2.2))÷2=4.6

Pumps

Item Description	Data Source	Power /Fluid	Mean Failure Rate ×10^6				Error Function/Standard Deviation ×10^6				MRT (hrs)
			Critical	Degrade	Incipient	All Modes	Critical	Degrade	Incipient	All Modes	
Centrifugal Pump, (Chemical), 52hp-250hp: P102, P103, P104 and P301, 200-1500hp: P101 and P201, 2752hp: P202, 6952hp: P204. [CENT-PUMP-CH]	OREDA-P358	Any/Chemical	*2.28 **2.31	6.84 6.93	1.14 1.15	10.27 10.39	2.28 2.31	6.84 6.93	1.14 1.15	10.27 10.39	8.0 9.0
	OREDA-P359	Any/Combined	00 00	00 00	13.53 18.26	13.53 18.26	00 00	00 00	13.53 18.26	13.53 18.26	1.5 ---
	EIReDA-P56	<200kw/Water	200 ---	--- ---	--- ---	200 ---	--- ---	--- ---	--- ---	2E+6 ---	20 ---
	EIReDA-P54	1500-4500kw /water	4 ---	--- ---	--- ---	4 ---	--- ---	--- ---	--- ---	2.1E+6 ---	14 ---
	T-book	---	---	---	---	---	---	---	---	---	---
	CCPS-P193	Any/Any	104 ---	24 ---	--- ---	128 ---	--- ---	--- ---	--- ---	--- ---	--- ---
	T R Moss P-254	Any	--- ---	--- ---	--- ---	99† ---	--- ---	--- ---	--- ---	--- ---	--- ---
Centrifugal Pump, (Water), 44hp (P203 and P302) [CENT-PUMP-W]	OREDA-P372	Any/Water	24.0 27.59	11.89 14.2	26.26 30.77	64.59 75.36	19.4 21.8	11.89 9.31	32.63 38.08	59.93 69.38	31.4 52.5C
	OREDA-P361	Any/Cooling Systems	9.51 16.65	00 00	00 00	9.51 16.65	9.51 16.65	00 00	00 00	9.51 16.65	4 (mh) ---
	OREDA-P360	Any/Condensate processing	18.01 25.95	7.61 11.70	5.19 9.93	30.01 47.21	12.22 18.82	6.98 13.23	8.51 15.91	15.99 41.34	17.6 (37D) ---
	OREDA-P359	Any/Combined	00 00	00 00	13.53 18.26	13.53 18.26	00 00	00 00	13.53 18.26	13.53 18.26	1.5 ---
	EIReDA-P56	<200hp/W	200 ---	--- ---	--- ---	200 ---	--- ---	--- ---	--- ---	2E+6 ---	20 ---
	T-book P81-84	40-60 Kg/s Horizontal	--- ---	--- ---	--- ---	23.0 ---	--- ---	--- ---	--- ---	--- ---	10 ---
		75-150 Kg/s Horizontal	--- ---	--- ---	--- ---	97 ---	--- ---	--- ---	--- ---	--- ---	16 ---
		130-200 Kg/s Horizontal	--- ---	--- ---	--- ---	11 ---	--- ---	--- ---	--- ---	--- ---	12 ---
	CCPS-P193	Any/Any	104 ---	24 ---	--- ---	128 ---	--- ---	--- ---	--- ---	--- ---	--- ---
	T R Moss P-254	Any	--- ---	--- ---	--- ---	99† ---	--- ---	--- ---	--- ---	--- ---	--- ---

*First Line: Data for Calendar Time, **Second Line: Data for Operational Time
†(250+194+88+32+22+8)÷6=99

Vessel/Tanks

Item Description	Data Source	Purpose/ Size	Mean Failure Rate $\times 10^6$				Error Function/Standard Deviation $\times 10^6$				MRT (hrs)
			Critical	Degrade	Incipient	All Modes	Critical	Degrade	Incipient	All Modes	
Distillation Column, C201 (0.07 bar, ~146 m^3), C301 (22 bar, 276 m^3) [DIST-COLUMN]	OREDA-P437	Dist. Col (100-300)m^3	00 ---	28.5 28.74	199.5 201.15	228.0 229.89	00 ---	28.5 28.74	199.5 201.15	228.0 229.89	46.8 (mh) --
	EIReDA	---	---	---	---	---	---	---	---	---	---
	T-book	---	---	---	---	---	---	---	---	---	---
	CCPS	---	---	---	---	---	---	---	---	---	---
	T R Moss	---	---	---	---	---	---	---	---	---	---
Flash Drum, S102 (~3 m^3)	OREDA-P444	Flash Drum (1-10)m^3	11.57 11.12	30.90 30.32	122.34 114.49	172.46 165.31	23.58 22.87	59.01 57.02	225.09 217.76	326.72 316.38	5.3 ---
S201 (~55 m^3), S202 (~52 m^3), S203 (~35 m^3), S205 (~18 m^3),	OREDA-P446	Flash Drum (10-50)m^3	28.16 29.30	25.08 26.54	234.55 239.34	301.67 308.13	42.65 42.51	21.68 20.37	447.86 456.73	509.09 516.28	6.1 (8.5C, 29.8D)
	OREDA-P447	Flash Drum (50-100)m^3	00 00	00 00	24.4 25.50	24.4 25.50	00 00	00 00	28.83 30.06	28.83 30.06	1.5 ---
	EIReDA-P82	Feed water storage tank	0.21 ---	--- ---	--- ---	0.21 ---	10 ---	--- ---	--- ---	--- ---	16.8 ---
	T-book	---	---	---	---	---	---	---	---	---	---
	CCPS-P205	Metal vessel-pressurized	0.0109 ---	0.0636 ---	--- ---	0.0745 ---	--- ---	--- ---	--- ---	--- ---	--- ---
	T R Moss	---	---	---	---	---	---	---	---	---	---
Scrubber, C101 (~34 m^3), C102 (~340 m^3), C104 (~45 m^3), C302 (~4 m^3), C303 (~5.5 m^3)	OREDA-P462	Scrubber (1-10) m^3	27.83 28.99	22.31 23.10	105.96 110.01	151.67 157.17	42.83 44.63	34.14 34.03	88.32 88.28	141.58 142.63	9.7 ---
	OREDA-P464	Scrubber (10-50) m^3	00 00	5.55 5.75	25.93 27.00	30.69 32.00	00 00	6.73 7.08	27.26 29.07	34.11 36.27	24.2 (mh) ---
	EIReDA-P82	Feed water storage tank	0.21 ---	--- ---	--- ---	0.21 ---	10 ---	--- ---	--- ---	--- ---	16.8 ---
	T-book	---	---	---	---	---	---	---	---	---	---
	CCPS-P205	Metal vessel-pressurized	0.0109 ---	0.0636 ---	--- ---	0.0745 ---	--- ---	--- ---	--- ---	--- ---	--- ---
	T R Moss P-255	Scrubber	--- ---	--- ---	--- ---	16.0 ---	--- ---	--- ---	--- ---	--- ---	--- ---

Vessel/Tanks (Continued)

Item Description	Data Source	Purpose/ Size	Mean Failure Rate $\times 10^6$				Error Function/Standard Deviation $\times 10^6$				MRT (hrs)
			Critical	Degrade	Incipient	All Modes	Critical	Degrade	Incipient	All Modes	
Separator: S101 (~50 m^3), S104 (~2.5 m^3), S105 (~1 m^3), S204, S301 (~1.5 m^3)	OREDA-P470	Separator (1-10)m^3	10.69 28.83	94.50 182.94	136.00 285.56	250.41 499.14	7.5 23.87	52.23 137.33	76.86 205.39	132.28 359.14	2.4 ---
	OREDA-P472	Separator (10-50)m^3	17.87 18.24	79.24 81.45	328.25 336.66	425.82 436.81	20.23 20.53	115.33 119.44	485.49 499.41	607.44 626.13	2.4 ---
	EIReDA-P82	Feed water storage tank	0.21 ---	--- ---	--- ---	0.21 ---	10 ---	--- ---	--- ---	--- ---	16.8 ---
	T-book	---	---	---	---	---	---	---	---	---	---
	CCPS-P205	Metal vessel-pressurized	0.0109 ---	0.0636 ---	--- ---	0.0745 ---	--- ---	--- ---	--- ---	--- ---	--- ---
	T R Moss P-255	Separator	--- ---	--- ---	--- ---	91.3 ---	--- ---	--- ---	--- ---	--- ---	--- ---
Reactor: , C103 (~11 m^3, C105 (~185 m^3	OREDA-P416	Vessel	24.45 28.93	24.66 46.92	132.17 175.51	185.04 255.91	31.26 37.87	45.37 68.13	257.74 308.37	326.82 394.06	7.0 ---
	EIReDA-P82	Feed water storage tank	0.21 ---	--- ---	--- ---	0.21 ---	10 ---	--- ---	--- ---	--- ---	16.8 ---
	T-book	---	---	---	---	---	---	---	---	---	---
	CCPS P205	Metal vessel-pressurized	0.0109 ---	0.0636 ---	--- ---	0.0745 ---	--- ---	--- ---	--- ---	--- ---	--- ---
	T R Moss P255	Reactor	--- ---	--- ---	--- ---	3.3 ---	--- ---	--- ---	--- ---	--- ---	--- ---

APPENDIX B

DATA FOR COMPONENTS OF HTE PLANT

Compressors

Item Description	Data Source	Power	Mean Failure Rate $\times 10^6$				Error Function/Standard Deviation $\times 10^6$				Mean Repair Time (hrs)	Population/ Installation /No of Demand
			Critical	Degrade	Incipient	All Modes	Critical	Degrade	Incipient	All Modes		
Centrifugal, Turbine Driven, HPC-102MW, LPC-98MW,	OREDA-P86	---	73.49 107.71	149.69 232.74	236.67 391.87	564.28 878.17	21.92 37.79	135.8 236.44	215.10 401.18	305.35 615.17	18.7	22/8/2469
	EIReDA	---	---	---	---	---	---	---	---	---	---	---
	T-book	---	---	---	---	--	---	---	---	---	---	---
	CCPS	---	---	---	---	--	---	---	---	---	---	---
	T R Moss P-254	--- Tur/Elec	--- ---	--- ---	--- ---	1678 ---	--- ---	--- ---	--- ---	--- ---	---	3/---/---
Centrifugal, Electric Driven, PSC-1071kw, SSC-880kw, H2-Rec-8kw	OREDA-P79	0.1-1 MW	151.76 256.43	74.98 115.01	344.86 643.71	579.49 1047.2	117.91 262.19	30.06 89.52	363.13 773.08	544.05 1177.9	13.8 31.4D	5/3/1299
	OREDA-P81	1-3 MW	179.76 205.57	157.62 187.43	661.08 744.21	991.89 1129.0	184.69 206.86	33.34 56.17	604.93 651.89	823.08 890.57	9.1 (15D)	6/5/815
	EIReDA-P26	360 KW	93 ---	--- ---	--- ---	93 ---	--- ---	--- ---	--- ---	10E+6 ---	21	2/1/---
	T-book	---	---	---	---	--	---	---	---	---	---	---
	CCPS-P189	Any	2470.0 ---	--- ---	--- ---	2470.0 ---	--- ---	--- ---	--- ---	--- ---	---	---/---/---
	T R Moss P-254	--- Tur/Elec	--- ---	--- ---	--- ---	1678 ---	--- ---	--- ---	--- ---	--- ---	---	3/---/---

*(2694+1700+640)÷3=1678

Electrolyzer

Item Description	Data Source	Mean Failure Rate $\times 10^6$				Error Function/Standard Deviation $\times 10^6$				Mean Repair Time (hrs)	Population/ Installation/ No of Demand
		Critical	Degrade	Incipient	All Modes	Critical	Degrade	Incipient	All Modes		
Electrolyzer	OREDA	---	---	---	---	---	---	---	---	---	---
	ElReDA	---	---	---	---	---	---	---	---	---	---
	T-book	---	---	---	---	---	---	---	---	---	---
	CCPS	---	---	---	---	---	---	---	---	---	---
	T R Moss	---	---	---	---	---	---	---	---	---	---
	CERAMATEC *	2	---	---	2	---	---	---	---	---	---

*This data was collected by telephone from CERAMATEC:

Generators

Item Description	Data Source	Power /Purpose	Mean Failure Rate ×10^6				Error Function/Standard Deviation ×10^6				Mean Repair Time (hrs)	Population/ Installation/ No of Demand
			Critical	Degrade	Incipient	All Modes	Critical	Degrade	Incipient	All Modes		
Turbine Driven, ~300 MW	OREDA-P321	Any/ Main	83.61 98.74	50.08 57.68	70.87 76.24	215.80 240.24	21.05 41.87	35.82 39.26	66.43 68.79	140.99 145.46	14.2	8/3/166
	OREDA-P330	20-30 KVA /Main	57.67 75.99	105.59 123.98	180.80 238.48	348.04 437.81	37.63 38.30	118.04 139.09	103.70 119.38	178.85 162.76	31.7	12/5/2691
	EIReDA P190	900 MW /Main	20 ---	--- ---	--- ---	20 ---	4E+6 ---	--- ---	--- ---	4E+6 ---	192	1/1/--
	EIReDA P190	1300 MW /Main	15 ---	--- ---	--- ---	15 ---	10E+6 ---	--- ---	--- ---	10E+6 ---	500	1/1/--
	T-book	---	---	---	---	--	---	---	---	---	---	---
	CCPS	---	---	---	---	--	---	---	---	---	---	---
	T R Moss P-254	---/---	1667 ---	--- ---	--- ---	1667 ---	--- ---	--- ---	--- ---	--- ---	---	1/1/--

Heat Exchangers

Item Description	Data Source	Fluid	Mean Failure Rate ×10^6				Error Function/Standard Deviation ×10^6				Mean Repair Time (hrs)	Population/ Installation /No of Demand
			Critical	Degrade	Incipient	All Modes	Critical	Degrade	Incipient	All Modes		
Heat Exchanger, Shell-Tube, helium/ helium IHE,	OREDA -P406	Gas/Gas	--- ---	--- ---	--- ---	11.84 12.82	--- ---	--- ---	--- ---	16.75 18.13	---	2/1/21720
	EIReDA	---	---	---	---	---	---	---	---	---	---	---
	T-book	---	---	---	---	---	---	---	---	---	---	---
	CCPS-P182	Any	31.1 ---	25.8 ---	--- ---	56.9 ---	--- ---	--- ---	--- ---	--- ---	---	---
	T R Moss P-255	Any	--- ---	--- ---	--- ---	32.7 ---	--- ---	--- ---	--- ---	--- ---	---	1/1/---
Heat Exchanger, Shell-Tube, Helium/ water Regenerator -3 and 5	OREDA -P405	Gas/ Water	00 00	17.56 28.52	175.62 270.98	189.5 299.5	00 00	13.45 28.51	41.47 203.6	63.01 245.26	7.7 (mh)	6/2/---
	OREDA -P404	Gas/ Condensate	00 00	00 00	114.16 114.16	114.16 114.16	00 00	00 00	114.16 114.16	114.16 114.16	5.0 (mh)	1/1/---
	EIReDA	---	---	---	---	---	---	---	---	---	---	---
	T-book	---	---	---	---	---	---	---	---	---	---	---
	CCPS-P182	Any	31.1 ---	25.8 ---	--- ---	56.9 ---	--- ---	--- ---	--- ---	--- ---	---	---
	T R Moss P-255	Any	--- ---	--- ---	--- ---	32.7 ---	--- ---	--- ---	--- ---	--- ---	---	1/1/---
Heat Exchanger, Shell-tube, water/water Recuperator, Regenerator -1, 2, 6, and 7	OREDA -P413	water/ glycol-water/ glycol	00 00	00 00	10.19 10.63	10.19 10.63	00 00	00 00	10.19 10.63	10.19 10.63	17.5	4/1/---
	EIReDA -P42	W/DW, 30/220C 7/155 bar	1.0 ---	--- ---	--- ---	1.0 ---	--- ---	--- ---	--- ---	10E+6 ---	25	2/1/---
	EIReDA -P44	DW/DW, 200/300C 155 bar	0.2 ---	--- ---	--- ---	0.2 ---	--- ---	--- ---	--- ---	10E+6 ---	25	9/1/33430
	EIReDA -P46	DW, 50/220C 7/50 bar	1.27 ---	--- ---	--- ---	1.27 ---	--- ---	--- ---	--- ---	10E+6 ---	72	2/1/---
	T-book	---	---	---	---	---	---	---	---	---	---	---
	CCPS-P182	Any	31.1 ---	25.8 ---	--- ---	56.9 ---	--- ---	--- ---	--- ---	--- ---	---	---
	T R Moss P-255	Any	--- ---	--- ---	--- ---	32.7 ---	--- ---	--- ---	--- ---	--- ---	---	1/1/---

Pumps

Item Description	Data Source	Power/Purpose/Mode	Mean Failure Rate $\times 10^6$				Error Function/Standard Deviation $\times 10^6$				Mean Repair Time (hrs)	Population/ Installation /No of Demand
			Critical	Degrade	Incipient	All Modes	Critical	Degrade	Incipient	All Modes		
Centrifugal Pump, (Water) SWP-94 KW, MWP-138 KW, RP-1 KW	OREDA-P372	Any/Water/Running	24.0 27.59	11.89 14.2	26.26 30.77	64.59 75.36	19.4 21.8	11.89 9.31	32.63 38.08	59.93 69.38	31.4 52.5C	24/6/1590
	OREDA-P361	Any/Cooling system/Running	9.51 16.65	00 00	00 00	9.51 16.65	9.51 16.65	00 00	00 00	9.51 16.65	4 (mh)	6/1/150
	OREDA-P359	Any/Combined/Running	00 00	00 00	13.53 18.26	13.53 18.26	00 00	00 00	13.53 18.26	13.53 18.26	1.5	3/1/---
	EIReDA-P56	<200 hp/W	37.4†† ---	--- ---	--- ---	37.4†† ---	--- ---	--- ---	--- ---	3E+6 ---	20	---
	EIReDA-P58	28/75 KW/Running	11.7 ---	--- ---	--- ---	11.7 ---	--- ---	--- ---	--- ---	10E+6 ---	18	2/1/32360
	T-book P81	40-60 Kg/s Horizontal/Running	--- ---	--- ---	--- ---	23.0 ---	--- ---	--- ---	--- ---	--- ---	10	30/---/---
	CCPS-P193	Any/Any/Running	104 ---	24 ---	--- ---	128 ---	--- ---	--- ---	--- ---	--- ---	---	---
	T R Moss P-254	Any/Any/Running	--- ---	--- ---	--- ---	99† ---	--- ---	--- ---	--- ---	--- ---	---	6/---/---

*First Line: Data for Calendar Time

**Second Line: Data for Operational Time

†(250+194+88+32+22+8)÷6=99

††37.4: This pump was used only in case of accident and the failure rate is 200E-6 and EF is 3, sample and reliability parameter are estimated by expert judgment. Failure rate of drain pump on feed water system is 37.4E-6 and EF is 3

Power Recovery Devices: Turbine/Liquid Expander

Item Description	Data Source	Power/ Purpose	Mean Failure Rate $\times 10^6$				Error Function/Standard Deviation $\times 10^6$				Mean Repair Time (hrs)	Population /Installation /No of Demand
			Critical	Degrade	Incipient	All Modes	Critical	Degrade	Incipient	All Modes		
Gas Turbine, 511.5 MW	OREDA-P129	Any /Gas	354.75 553.77	266.17 369.56	569.36 1359.67	1199.2 2398.2	312.92 577.96	189.1 276.1	619.28 893.14	880.20 1648.61	17.7 (27C)	84/23/11096
	OREDA-P148	20-40 MW /Gas	373.37 756.82	272.44 462.24	660.98 1233.57	1326.0 2477.5	491.76 1136.9	205.9 396.6	591.14 1366.7	1247.64 2858.08	15.2 (23.7C)	15/5/3512
	EIReDA-P86	Any/Steam, Drives Aux-Generator	3200 ---	--- ---	--- ---	3200 ---	2.3E+6 ---	--- ---	--- ---	2.3E+6 ---	13	2/1/358
	T-book P192-3	Standby, No data for Running	--- ---	--- ---	--- ---	**4.6 ---	--- ---	--- ---	--- ---	--- ---	3	---
	CCPS	---	---	---	---	---	---	---	---	---	---	---
	T R Moss P-254	Gas	--- ---	--- ---	--- ---	*1236 ---	--- ---	--- ---	--- ---	--- ---	---	11/---/---
O2/Steam Expander, 9.356 MW	OREDA-P280	Any/ Combined	57.08 57.08	00 00	171.23 171.23	228.31 228.31	57.08 57.08	00 00	171.23 171.23	228.31 228.31	---	1/1/---
	OREDA-P281	Gas Processing	85.59 101.91	114.11 135.89	162.54 208.65	374.56 469.46	18.68 21.98	21.56 25.38	124.20 176.84	81.64 163.41	32.4 (mh)	8/2/---
	EIReDA-P86	Any/Steam, drives generator	3200 ---	--- ---	--- ---	3200 ---	2.3E+6 ---	--- ---	--- ---	2.3E+6 ---	13	2/1/358
	T-book	---	---	---	---	---	---	---	---	---	---	---
	CCPS	---	---	---	---	---	---	---	---	---	---	---
	T R Moss	---	---	---	---	---	---	---	---	---	---	---

*(4212+3550+1667+1484+865+525+491+320+240+205+35)÷11=1236

**(7+2.2)÷2=4.6

Vessel: Knockout Tanks

Item Description	Data Source	Purpose /Size	Mean Failure Rate $\times 10^6$				Error Function/Standard Deviation $\times 10^6$				Mean Repair Time (hrs)	Population/ Installation /No of Demand
			Critical	Degrade	Incipient	All Modes	Critical	Degrade	Incipient	All Modes		
Knockout Tank i.e. Separator	OREDA -P470	Separator (1-10)m^3	10.69 28.83	94.50 182.94	136.00 285.56	250.41 499.14	7.5 23.87	52.23 137.33	76.86 205.39	132.28 359.14	2.4	50/5/---
	OREDA -P472	Separator (10-50)m^3	17.87 18.24	79.24 81.45	328.25 336.66	425.82 436.81	20.23 20.53	115.33 119.44	485.49 499.41	607.44 626.13	2.4	11/7/---
	EIReDA -P82	Feed water storage tank	0.21 ---	--- ---	--- ---	0.21 ---	10 ---	--- ---	--- ---	--- ---	16.8	---/---/36
	T-book	---	---	---	---	---	---	---	---	---		---
	CCPS-P205	Metal vessel-pressurized	0.0109 ---	0.0636 ---	--- ---	0.0745 ---	--- ---	--- ---	--- ---	--- ---		---
	T R Moss P-255	Separator	--- ---	--- ---	--- ---	91.3 ---	--- ---	--- ---	--- ---	--- ---		1/1/---

VITA

S.M. Mohsin Reza, son of Mrs. Monwara Begum and the late Tosir Uddin Sarker, was born in Rajshahi, Bangladesh. After completing his first 10 years of education he continued his study at Rajshahi Polytechnic Institute (Bangladesh) and received his Diploma-in Engineering degree in electrical engineering in March 1989. He then attended Dhaka University of Engineering and Technology (DUET), Gazipur, Bangladesh, and received his Bachelor of Science in electrical and electronic engineering in March 1994, with a focus on electrical control systems. He started his career at the Bangladesh Power Development Board (BPDB) and worked there until March 1996. In March 1996, he was employed by the Bangladesh Atomic Energy Commission (BAEC). During his career at BAEC, Mr. Reza worked at a Radioactive Beach-Mineral Separating Plant at Cox's Bazar, and then at the Institute of Nuclear Science and Technology, Savar, Dhaka. At the end of his career at BAEC, he was posted to TRIGA MARK-II Research Reactor, the only reactor facility in Bangladesh. He then joined the Nuclear Engineering Department of Texas A&M University in the fall of 2000 for his graduate studies. He received his Master of Science degree in nuclear engineering in December 2002. The title of the thesis for his Master of Science program was 'Simulation of Subcooled Boiling at Low Pressure Conditions with RELAP-3D Computer Program'. He continued his graduate studies and received his Ph.D. in nuclear engineering in May 2007. He may be contacted through his postal address at: Department of Nuclear Engineering, Texas A&M University, 129 Zachry Engineering Center, TX 77843-3133 or through email at rezasmm@hotmail.com.